THESIS

COMPARATIVE ANALYSIS OF REMOTE SENSING PLATFORMS FOR ASSESSING MAIZE CROP BIOPHYSICAL CHARACTERISTICS AND EVAPOTRANSPIRATION ESTIMATION

Submitted by:

Zaid Al-Majali

Department of Civil and Environmental Engineering

In partial fulfillment of the requirements

For the Degree of Master of Science

Colorado State University

Fort Collins, Colorado

Summer 2024

Master's Committee:

Advisor: José L. Chávez

Frances Davenport

Jessica O'Connel

ABSTRACT

COMPARATIVE ANALYSIS OF REMOTE SENSING PLATFORMS FOR ASSESSING MAIZE CROP BIOPHYSICAL CHARACTERISTICS AND EVAPOTRANSPIRATION ESTIMATION

The rapid growth in population, climate variability, and decreasing water resources necessitate innovative agricultural practices to ensure food security and resource conservation. This study investigates the effectiveness of various multispectral imagery from remote sensing (RS) platforms (such as Unmanned Aircraft Systems (UAS), PlanetDove microsatellites, Sentinel-2, Landsat 8/9, and proximal MSR-5) in the appropriate estimation of crop biophysical characteristics (CBPCs) and actual crop evapotranspiration (ETa) for maize fields in northeastern Colorado. The research aimed at evaluating the accuracy of vegetation indices (VIs) derived from different sources of RS data in estimating key CBPCs, including leaf area index (LAI), crop height (Hc), and fractional cover (Fc), as well as the ETa. Field experiments were conducted at the USDA-ARS Limited Irrigation Research Farm in Greeley, Colorado, in 2022. Different irrigation strategies were used to assess the maize's water use response. Surface reflectance data was collected using the MSR-5 sensor, and observed LAI, Hc, and Fc values served as ground truth for validating remote sensing estimates. The study applied various statistical analyses to compare the performance of different remote sensing platforms and models. Results indicate that higher-resolution platforms, particularly UAS, provided higher accuracy in estimating VIs and CBPCs than other satellite platforms. The study also highlights the influence of environmental conditions on the accuracy of remote sensing models, with locally calibrated models outperforming those developed in dissimilar conditions. The findings underscore the potential of

advanced remote sensing technologies in enhancing precision agriculture practices and optimizing water resource management.

ACKNOWLEDGMENTS

This thesis would only have become real with many people's warm help and support. I want to send my sincere appreciation to all of them. Foremost, I would like to present this endeavor to God for the wisdom, good health, and strength he granted me to achieve this research. I am deeply grateful for the encouragement from my family, which motivated me to complete this research.

I am highly indebted to my advisor, Dr. Jose Chavez, for his constant supervision and guidance and for imparting his expertise and knowledge to enrich me with the needed information and support to complete this research.

DEDICATION

I dedicate this research to my beloved family. My mother, your prayers and gladness, my father, your encouragement, and affection.

TABLE OF CONTENTS

LIST OF TABLES

LIST OF FIGURES

Chapter 1: Introduction

1.1 Background

The urgency of rapid population growth, climate variability, and dwindling water resources necessitates immediate and innovative approaches to enhance agricultural productivity while conserving natural resources. These pressing challenges underscore the critical need for sustainable farming practices that optimize resource use efficiency, mitigate environmental impact, and ensure food security for present and future generations (FAO, 2017). Agriculture, as the primary consumer of water among all water uses, with irrigated agriculture utilizing about 70% of the world's available water resources (Galán-Martín et al., 2017), is at the forefront of these challenges.

Improved irrigation water management is essential in ensuring water and irrigation sustainability. Optimizing water use efficiency through techniques like drip irrigation or precision irrigation conserves water resources and minimizes water loss. These techniques enhance crop productivity, support environmental conservation by reducing soil erosion and groundwater depletion, and help farmers adapt to changing climate conditions. Additionally, efficient irrigation practices lead to economic savings and contribute to the long-term sustainability of the agricultural systems, benefiting both present and future generations.

Remote Sensing (RS) has emerged as a crucial tool in contemporary agricultural research, particularly in addressing water resource challenges. Its practical applications, such as facilitating the estimation of crop biophysical characteristics (CBPC) and actual crop Evapotranspiration (ETa), as indicated by Shanmugapriya et al. (2019), enable more efficient

irrigation water management and promise advancements in accuracy. These advancements are key to effectively addressing water resource challenges across diverse locations worldwide that vary in climate or topography. The accuracy of the RS-based algorithms in estimating CBPCs is crucial, with key variables such as Leaf area index (LAI), Crop Height (Hc), and Fractional vegetation Cover (Fc) playing a central role in providing a quantitative measure of the vegetation health, structure, and distribution. These variables are fundamental in understanding the sophisticated dynamics of water use by crops, and their understanding enables informed decisions regarding water use applications by farmers, researchers, and policymakers, as indicated by Sishodia et al. (2020). In agricultural research, the study of CBPCs using RS has gained significance due to its implications for sustainable farming and natural resource management (Thenkabail et al., 2018; Wardlow & Egbert, 2008).

1.2 Literature Review

Remote Sensing plays a pivotal role in estimating CBPCs and ETa, as it allows for multispectral image data collection while also providing frequent updates on changing crop conditions, offering high spatial and temporal resolutions for more detailed monitoring of these spatial variabilities. Accurate estimation of ETa and CBPCs is crucial in appropriately estimating the water budget and provides a better understanding of water management in irrigated and rainfed crop fields. Remote Sensing products also indicate crop health, development, and growth, aiding in assessing crop development stages, predicting yields, and identifying stress factors (Karthikeyan et al., 2020). Proper spatially distributed ETa estimates can be used to better manage irrigation decisions (schedules), prevent water wastage, and sustainably use water resources, making the proper ETa estimates a valuable tool in regions prone to drought or facing water scarcity challenges, as indicated by Moran et al. (1997).

Remote Sensing technologies offer numerous advantages when studying CBPCs and ETa. First, they allow for large-scale and near real-time monitoring of agricultural areas, providing comprehensive spatial and temporal data, aiding in detecting changes over time, and assessing crop conditions in time and space. Secondly, remote sensing techniques provide a non-invasive means of multispectral data collection, reducing the need for extensive fieldwork and physical measurements and resulting in a cost-effective tool. The RS techniques save time and resources and enhance the accuracy and frequency of data collection, leading to more reliable insights and predictions, Wardlow et al. (2007).

Moreover, RS facilitates the integration of multispectral and multitemporal images, enabling complex analyses and modeling of crop behavior and water dynamics, which enhances the understanding of ecosystem processes. RS data can also be used to assess the effectiveness of precision agriculture techniques and monitor changes in land cover, supporting informed strategies for sustainable farming and water resource management.

Different RS platforms have been used to estimate CBPCs and ETa. The importance of choosing the proper platforms emerged dramatically to enhance the estimations of CBPCs, ETa, and other important factors related to crop growth and management. Remote sensing multispectral data can directly estimate vegetation indices (VIs) and simple ratios, which are used in models to estimate vegetation fractional cover, crop yield, and the physical properties of the vegetation, such as leaf area index and crop height.

Remote sensing advanced agricultural practices to meet the escalating demands for food, fibers, and raw materials by providing repetitive information on crop status throughout the season, catering to diverse scales and stakeholders (Sishodia et al., 2020). Over the past two decades, there has been a substantial surge in the utilization of remote sensing technologies, with

a predominant focus on satellite platforms such as Landsat and Sentinel. Additionally, Unmanned Aerial Systems (UAS) technologies, as highlighted by Khanal et al. (2020), have significantly contributed to agricultural monitoring studies.

Vegetation indices represent mathematical formulations derived from the remote sensing-derived surface reflectance images acquired across multiple spectral bands. Also, Vegetation indices are numerical measures derived from surface reflectance values in different spectral bands, providing valuable information about vegetation status (Basso et al., 2004). These indices have been extensively applied in remote sensing practices within the vegetation domain, particularly utilizing diverse airborne satellite platforms. Vegetation Indices are integral components for quantitative and qualitative assessments of vegetation characteristics, including vegetation fractional cover, vigor, and growth dynamics. Additionally, the utility of vegetation indices extends beyond these vegetation characteristics, encompassing a huge number of applications in the crop field, as mentioned by Xue and Su (2017).

The Normalized Difference Vegetation Index (NDVI), a widely applied vegetation index, is calculated from the difference between vegetation reflectance in the near-infrared (NIR) and red (RED) bands (Rouse et al., 1974). High NDVI values indicate healthy and vigorous vegetation, while low values may suggest stress, short or sparse vegetation cover. Numerous studies have demonstrated the effectiveness of NDVI in monitoring crop health and growth. Huete (1988) developed the Soil Adjusted Vegetation Index (SAVI), an enhancement of NDVI, designed to minimize soil background influences. It incorporates a soil-adjustment factor (L) to improve sensitivity to vegetation changes. Another VI is the Optimized Soil Adjusted Vegetation Index (OSAVI) developed by Rondeaux et al. (1996), which is also an index used to adjust the spectral indices so the soil variations do not influence the measurements of vegetation. The

OSAVI was found to be valuable in areas with varying soil types, contributing to more accurate assessments of vegetation conditions. Gao (1996) found The Normalized Difference Water Index (NDWI) helpful because it is allegedly more sensitive to changes occurring in the liquid water content of the vegetation canopies.

Various remote sensing platforms offer unique advantages in the application of vegetation indices. UAS platforms, for instance, provide very high spatial resolutions and flexibility in multispectral data acquisition. Anderson and Gaston (2013) explored using VIs from UAS imagery to monitor and provide detailed information about crop health at fine spatial scales for precision agriculture practices. Microsatellites, such as PlanetDove, provide frequent revisit times and global coverage (Skakun et al., 2021); they also investigated crop yields using VIs derived from microsatellite data. Satellite platforms, on the other hand, offer broader coverage and continuity. VIs derived from Sentinel-2 and LandSat 8-9 data have been employed in regional and global studies, such as the study by Zhu and Woodcock (2014) that assessed crop health, land cover changes, and the effect of environmental factors on vegetation.

In the context of irrigation water management (IWM), the utilization of RS, VIs, CBPC, and ETa can substantially enhance operational efficiency and resource conservation. For instance, studies by Kamble et al. (2013) demonstrate the effectiveness of using satellite-based RS data to optimize irrigation scheduling. By integrating RS-derived vegetation indices like NDVI and surface temperature measurements, more accurate crop growth monitoring and water requirements lead to informed irrigation decisions (Chavez et al., 2024). In parallel, the analysis of ETa through RS-based methods offers real-time insights into crop water use dynamics (Saadi et al., 2018). Researchers can quantify ETa at field scales by analyzing RS multispectral image data, allowing for adaptive irrigation strategies that conserve water. Baret and Guyot (1991)

emphasized that the accuracy of VIs is influenced by sensor calibration. They included the importance of accurate sensor calibration to ensure consistent and reliable vegetation index values across RS platforms.

Anderson et al. (2004) provided multiple regression equations to estimate maize and soybean Hc and LAI using OSAVI and NDWI indices as VI-based inputs for the functions developed. The study by Anderson et al. (2004) mainly aimed at comparing the utility of different RS images in upscaling a set of ground-based measurements of LAI, Hc, and vegetation water content that have been collected through the NASA Soil Moisture Experiment of 2002 (SMEX02) in the Walnut Creek Watershed near Ames, Iowa, USA. They collected the vegetation indices from 1.5-meter resolution aircraft and 30-meter Landsat satellite images. The LAI estimation function had a coefficient of determination (R^2), which is a statistical measure that represents the proportion of the variance for a dependent variable that is explained by an independent variable in a regression model, ranging from 0.76 to 0.85, and the crop height Hc estimation function R^2 ranged from 0.84 to 0.93. This study developed functions using ground-based measurements, radiometry, plant samples, and RS VIs and compared high-resolution aircraft with Landsat imagery for upscaling ground-based measurements of canopy properties. Also, Anderson et al. (2004) research highlights that different RS platforms provide different VI values for the same observed crops, showing the importance of developing different calibration equations for estimating CBPCs.

Yang et al. (2015) also used VIs for estimating LAI, Hc, and Fc values, using NDVI as a main VI. They tested the performance of these functions using in-situ observed data; the R^2 was 0.82 for the Hc function, 0.75 for the LAI function, and 0.77 for the Fc function. They used the RS based on six Advanced Spaceborne Thermal Emission and Reflection Radiometer (ASTER)

images acquired during the Multi-Scale Observation Experiment on Evapotranspiration 2012 (MUSOEXE-12) campaign. The ASTER satellite images have a spatial resolution of 15 meters for both the visible and near-infrared bands, 90 meters for the thermal bands, and 30 meters for the shortwave infrared bands, and the resulting Hc, LAI, and Fc were used in order to estimate RS-based ETa and determine the ETa model's performance and limitations. Mourad et al. (2020) conducted research to estimate distributed LAI values using SAVI, NDVI, the Enhanced Vegetation Index 2 (EVI2), and Sentinel-2 Leaf Area Index (SeLI) indices values derived from Harmonized Landsat, Sentinel-2 (HLS) surface reflectance images. The abovementioned VIs were used to estimate the LAI for different types of crops in semi-arid irrigated landscapes, and one general regression equation was used for each VI. The R^2 and the Root Mean Square Error (RMSE) for estimating LAI using NDVI-based models were 0.51 and 1.07 m^2/m^2, respectively, and 0.61 and 0.97 m^2/m^2 for SAVI-based models. The studies by (Anderson et al., 2004; Yang et al., 2015; Mourad et al., 2020) touch on the importance of accurate crop characterization for estimating ETa and how different RS platforms and different VIs can impact the accuracy of CBPCs and ETa modeling for maize, considering factors like sensor spatial resolution, spectral bands, and VI choices.

The recent work by Costa-Filho et al. (2021) developed an empirical exponential model to estimate the maize Hc, which resulted in an R^2 of 0.91. This function, which was dependent on LAI in-situ measurements and evaluated at the same site as the current study, was based on different irrigation strategies, where the east and west fields shifted irrigation treatments to full irrigation and deficit irrigation each year between 2017 and 2019. The Hc variable modeling was an essential and dependent variable in the Costa-Filho et al. (2021) study, which also estimated the roughness length for momentum transfer (Zom), the zero-plane displacement height (do), and

other aerodynamic variables that have been used in estimating the sensible heat flux and surface water evaporation fluxes. Arslan et al. (2022) also used functions dependent on LAI and NDVI to estimate maize Hc. They used Sentinel-1 Synthetic Aperture Radar (SAR) and Sentinel-2 optical satellite images as the VIs source, resulting in an R^2 for the LAI and NDVI-based functions exceeding 0.90. The studies by Costa-Filho et al. (2021) and Arslan et al. (2022) have achieved high R^2 values for Hc estimations, showing an improvement in Hc estimation models. Also, both studies showed different ranges in Hc estimates; Hc estimation models by Arslan et al. (2022) indicated higher maize Hc, showing how different site area conditions can vary the estimates of Hc.

Other studies included the estimation of Hc using VIs were done by (Khaliq et al., 2018; Jeong & Park, 2021). Khaliq et al. (2018) researched the relationship between the VIs and the maize Hc in Carpi, Emilia-Romagna, Italy. They included NDVI, Green Normalized Difference Vegetation Index (GNDVI), and Ratio Vegetation Index (RVI) collected from atmospheric corrected Sentinel-2 multispectral satellite images, which resulted in an R^2 of the NDVI-based function of 0.63. They also applied Pearson Correlation to assess the linear correlation between the VIs and Hc, showing a high correlation between maize Hc and VIs. Jeong and Park (2021) also used linear regression models to estimate the Hc using NDVI collected from UAV images for six maize fields during maize's reproductive and vegetative stages of maize in South Korea. The Hc-NDVI function R^2 during the vegetative stage was 0.93, and for the reproductive stage, it was 0.66. Both Khaliq et al. (2018) and Jeong & Park (2021) studies emphasized the importance of local-scale studies for accurately estimating crop characteristics and measuring the maize Hc within humid and fully irrigated areas. Also, both studies used higher reflectance image resolution, resulting in higher R^2.

Regarding the estimation of LAI, Bastiaanssen et al. (1998) provided an overall regression function to estimate the LAI for multiple crop types using SAVI. However, this LAI model has some range limitations, where the SAVI value should be less than 0.69 for the LAI model to achieve a reliable result. An enhancement of VI-based models to estimate LAI was done by Vina et al. (2011), which provided functions based on multiple VIs and simple ratios to determine maize and soybean crops' green Leaf Area Index (gLAI). They used an NDVI-based function with their observations, resulting in a gLAI model that had an RMSE of 1.176 m^2/m^2. The VIs in the Vina et al. (2011) study were estimated using simulated reflectance bands from the Moderate Resolution Imaging Spectrometer (MODIS) and the Medium Resolution Imaging Spectrometer (MERIS). Also, Nguy-Robertson et al. (2012) provided multiple functions based on simple VI ratio, NDVI, SAVI, and many other VIs to estimate the maize gLAI. They performed their study for eight crop growing seasons, including 24 irrigated and rainfed maize and soybean fields. The R^2 and RMSE of the NDVI-based function used to estimate the gLAI were 0.87 and 0.64 m^2/m^2, respectively. The R^2 and RMSE were 0.81 and 0.78 m^2/m^2 for the SAVI-based model used to estimate gLAI, respectively. Nguy-Robertson et al. (2012) study aims to test different VIs in estimating gLAI and then develop some combined VIs highly sensitive to gLAI, which have a range of 0-6.5 m^2/m^2 for maize. Both studies by (Nguy-Robertson et al., 2012; Vina et al., 2011) incorporated multiple VIs to estimate LAI, aiming to improve the LAI estimation accuracy. From both studies, the RMSE has been different from each LAI estimation model based on different VIs. Results from both studies also show how the soil background can impact the estimation of CBPCs.

The use of higher resolution multispectral reflectance data to estimate LAI was done by Liu et al. (2011), where they conducted a comprehensive study using Landsat-5/7 images to

estimate the NDVI and OSAVI and their relationship with the LAI over multiple growing seasons of wheat, maize, and soybean fields. They then compared the LAI measurements with ground-observed data, providing a robust validation of their results. The R^2 and RMSE of their developed NDVI-based and OSAVI-based LAI function were 0.68 and 0.71 m^2/m^2, respectively, and 0.67 and 0.76 m^2/m^2, respectively. Also, Chavez et al. (2009) modeled LAI; they used an exponential function to estimate LAI for maize and sorghum under dry and irrigated systems, in an advective environment in Texas, using OSAVI. They utilized OSAVI as the RS VI input obtained from surface reflectance values from the Utah State University (USU) airborne digital multispectral system and used ground-based measurements with an EXOTECH handheld multispectral sensor. They conducted the research in Bushland, Texas, USA, at the USDA-ARS Conservational and Production Research Laboratory (CPRL), which is in a highly advective environment, demonstrating the importance of accounting for regional variations in RS-based vegetation assessments. Also, Jayasree et al. (2013) estimated the maize LAI based on NDVI collected from a multiband ground truth radiometer in Rajendranagar, Hyderabad, India, for two years. The LAI model based on NDVI resulted in an R^2 of 0.85 and an RMSE of 0.221 m^2/m^2. Studies by Liu et al. (2011), Chavez et al. (2009), and Jayasree et al. (2013) show how the selection of higher spectral image resolution may result in higher accuracy of LAI estimates, compared to studies by Nguy-Robertson et al. (2012) and Vina et al. (2011) who used medium-/low-resolution spectral image data.

Regarding the estimation of Fc, Johnson and Trout (2012) estimated Fc using data from 18 different crops and applied a linear function depending on NDVI obtained from surface reflectance measurements obtained from Landsat-5 satellite images on 11 different dates. This research was done in the San Joaquin Valley, California, and the functions used to estimate Fc

resulted with an R^2 of 0.96 and an RMSE of 6.2%. Gitelson (2013) also used an NDVI-based model, as well as the Enhanced Vegetation Index 2 (EVI2) and green NDVI to estimate the Fc. The NDVI exponential function used to estimate Fc resulted in an R^2 of 0.90. The study by Gitelson (2013) was conducted in Lincoln, Nebraska, and the surface reflectance values were collected between 2002 and 2006 and obtained from a hyperspectral radiometer. Studies by Johnson and Trout (2012) and Gitelson (2013) showed high R^2, finding a good relationship between NDVI and Fc.

Neale et al. (1989) estimated the basal crop coefficient (Kcb), which is related to the transpiration of the plant and is calculated as the ratio of the ETa to the reference evapotranspiration (ETr), for periods of dry surface conditions, for maize for two sites in Colorado, Greely and Fruita. They used models based on NDVI derived from surface reflectance values obtained with Landsat 5 satellite images. Bausch (1993) also used VIs using SAVI values to estimate Kcb in the then existing Agricultural Engineering Research Center, at Colorado State University, for two maize fields using Landsat 5 satellite reflectance data. Further, Kcb functions were estimated by González-Piqueras et al. (2004), where they estimated the Kcb using linear functions based on multiple VIs, such as NDVI, SAVI, OSAVI, and the Modified Soil Adjusted Vegetation Index (MSAVI), allowing to investigate the influence of soil background effects. The research by González-Piqueras et al. (2004) was done for maize fields in Barrax, Spain, using RS surface reflectance data from Landsat 5 satellite, showing high R^2 values ranging from 0.94 to 0.95.

Singh and Irmak (2009) also estimated the Kcb using a linear model based on NDVI obtained from Landsat-7 satellite surface reflectance data; the fitted Kcr function has an R^2 of 0.84. This research was conducted in Southcentral Nebraska and was done for maize, soybean,

sorghum, and alfalfa crops. A different approach was done by Trout and DeJonge (2018) to parameterize an alfalfa-base maize reflectance crop coefficient (Kcb) by using the Fc model developed by Johnson and Trout (2012), which is a function of NDVI. They used field data collected at the United States Department of Agriculture, Agricultural Research Service (USDA-ARS), Limited Irrigation Research Farm (LIRF), near Greely, Colorado, USA, from 2008 to 2013. The Kcb in their study was calculated for the entire cropping season, and a linear function model was developed to estimate Kcb, which resulted with an R^2 value of 0.91. Trout and DeJonge's (2018) linear function showed a good relationship between the Fc and Kcb.

1.3 Hypothesis and objectives

Remote sensing multispectral images have become indispensable tools for estimating CBPCs and ETa, enabling efficient and comprehensive monitoring of agricultural landscapes. The advancement of remote sensing platforms, particularly UAS, offers the potential for higher-resolution multispectral data acquisition, which can significantly impact the accuracy of vegetation indices VIs and subsequent estimates of CBPCs and ETa, consequently on proper agricultural water management. Previous studies have demonstrated that the spatial and spectral resolution of remote sensing imagery plays a critical role in the accuracy of crop monitoring and modeling. For instance, higher-resolution UAS platforms have shown promise in providing detailed and accurate assessments of CBPCs. Higher resolution suggests that the quality and granularity of data acquired through UAS may lead to enhanced performance in estimating VIs and related parameters compared to traditional satellite platforms.

The first hypothesis, which posits that higher-resolution RS multispectral data platforms will yield more accurate estimates of VIs, subsequently enhancing the accuracy of CBPCs and ETa assessments, is being tested to achieve the research goal of contributing to the optimal

utilization of remote sensing technologies for agricultural water use monitoring. This hypothesis is based on the understanding that finer spatial details captured by higher-resolution images can capture variations in crop conditions and spectral signatures, which are crucial for accurate CBPCs and ETa estimations.

The second hypothesis suggests that models developed and validated under similar site conditions to our study area will exhibit higher accuracy than those implemented in dissimilar, humid areas. This hypothesis is supported by the concept that environmental conditions, such as humidity, can significantly influence the relationship between VIs and CBPCs/ETa. Therefore, models calibrated and validated in comparable environmental settings are expected to demonstrate better performance and generalizability within this study region.

By testing these hypotheses, this research aims to contribute valuable insights into the optimal utilization of remote sensing technologies for agricultural crops and their water use monitoring, emphasizing the importance of spatial resolution and environmental context in improving the accuracy of CBPCs and ETa estimates. The outcomes of this study are expected to inform precision agriculture practices and water resource management strategies in regions characterized by similar environmental conditions.

The thesis research's main goal is to determine how products from different RS platforms (sensors) affect the estimation of crop biophysical characteristics and ETa for maize in northeastern Colorado. Then, the main objectives of the study are to:

1- Assess the accuracy of VI derived from various RS platforms.
2- Estimate and evaluate CBPCs such as Hc, LAI, and Fc inputting VIs derived from different RS platforms, in different selected functions.

3- Estimate and evaluate Kcb and ETa algorithms using the CBPCs and VIs from the previous objectives and independent measurements of crop water use.

Chapter 2: Methodology

2.1 Site description

The experiment was conducted at the United States Department of Agriculture, Agricultural Research Service (USDA-ARS), Limited Irrigation Research Facility (LIRF) located in Greeley, Colorado, in 2022, and it focused on evaluating the impact of different irrigation strategies on maize production. The study utilized drip irrigation systems in two different fields within the facility. In the eastern field, a deficit irrigation approach was implemented, subjecting the field to water stress conditions during the growth stages of the maize. The aim was to assess how maize plants responded to limited water availability and to study the effects on yield and water use efficiency. Conversely, the western field was managed with a fully irrigated practice to maintain optimal soil moisture levels throughout the growing season. This served as a comparative reference to evaluate the performance of maize under favorable irrigation conditions. The dates and the amount of irrigation water used for each field are shown in Table 1.

Table 1: Dates and amount of applied irrigation

Date	Irrigation amount (mm)	
	Full Irrigation Field	Deficit Irrigation Field
07-Jun	66.2	-
08-Jun	-	69.2
22-Jun	67.8	-
09-Jul	73.5	-
14-Jul	-	52.7
15-Jul	-	27.7
21-Jul	86.3	-
28-Jul	-	59.9
11-Aug	-	65.1
18-Aug	128.2	-
01-Sep	91.3	-
Total	513.2	274.6

The fields were situated at approximately Latitude 40.4470 N and Longitude -104.3696 W, with an elevation of around 1425 meters above mean sea level. Each of these fields has a rectangular shape with ~ 190 m x 110 m dimensions. Figure 1 illustrates the precise location of the study area within the LIRF, while Figure 2 provides a top view of the study area.

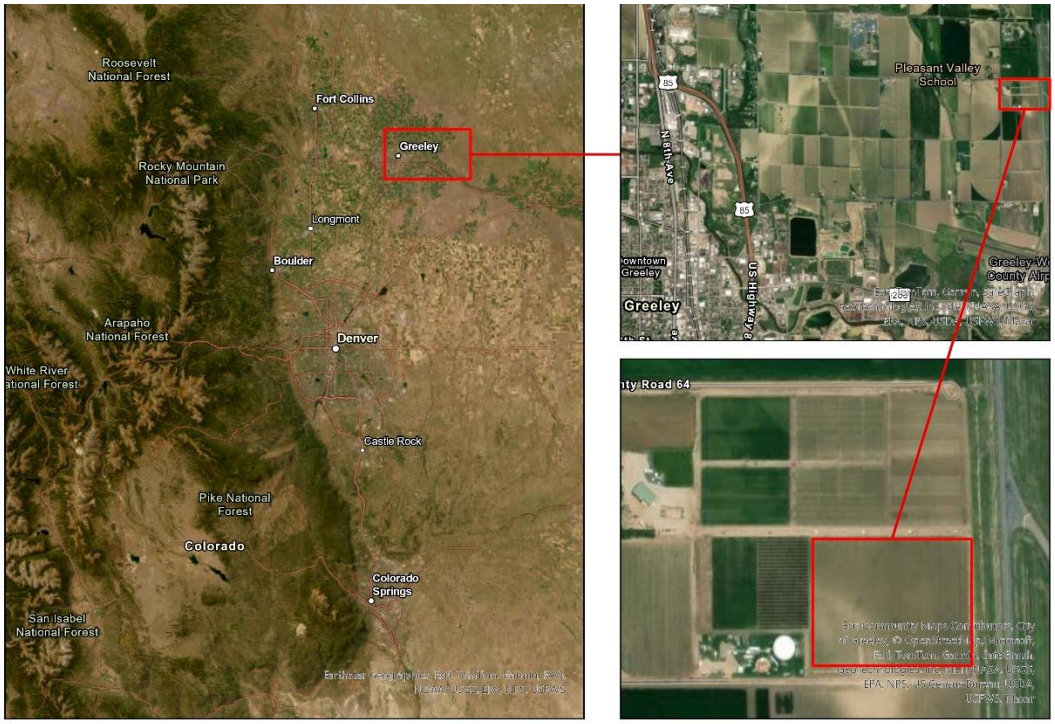

Figure 1: Location Map of the study area near Greeley, Co

Figure 2: Closed up of the two fields used in the study at LIRF

2.2 Instruments

Proximal surface reflectance measurements were obtained using a portable multispectral radiometer (MSR5, CropScan Inc., Rochester, MN, USA) radiometer at various stations throughout the maize growth season. The MSR5 radiometer is a compact handheld device that was mounted on a telescopic pole for nadir-looking measurements above the canopy. Each MSR5 radiometer measurement, over a ground sampling area, footprint is equivalent to a 1-meter-diameter circle. This passive sensor relies on natural sunlight and replicates Landsat-5 spectral bandwidths across the visible and near-infrared spectrum. During this study, MSR5 based surface reflectance readings were obtained at 44 different stations, 10 meters apart, within the study fields, as shown in Figure 3.

Figure 3: Location of the stations for MSR-5 based target reflectance readings

The LAI2200C plant canopy analyzer, (Li-Cor, Inc., Lincoln, NE, USA) was used to measure LAI values. It achieves this by measuring radiation above and below the plant canopy and applying a theoretical relationship between leaf area and canopy transmittance. The optical sensor of this device consists of five detectors arranged in concentric rings, each detecting radiation below 490 nm from different portions of the sky. Canopy transmittance is calculated by comparing readings below the canopy to those above it for each detector ring. The leaf area estimate assumes that foliage elements are randomly distributed within the canopy. Figure 4 shows the LAI measurement collected throughout the crop growth period in 2022.

The crop height was measured in situ, directly within the field where the crops were growing. The measurements involved physically going to the location and using measurement tools (tapes) to assess the height of the crops within their natural environment. This in situ measurement ensured accurate and real-time data collection, reflecting the actual conditions of the crop at the time of measurement. Figure 5 shows the measured Hc for the full and deficit irrigation fields. Table 2 shows the dates where LAI, Hc, and MSR-5 reflectance data were measured.

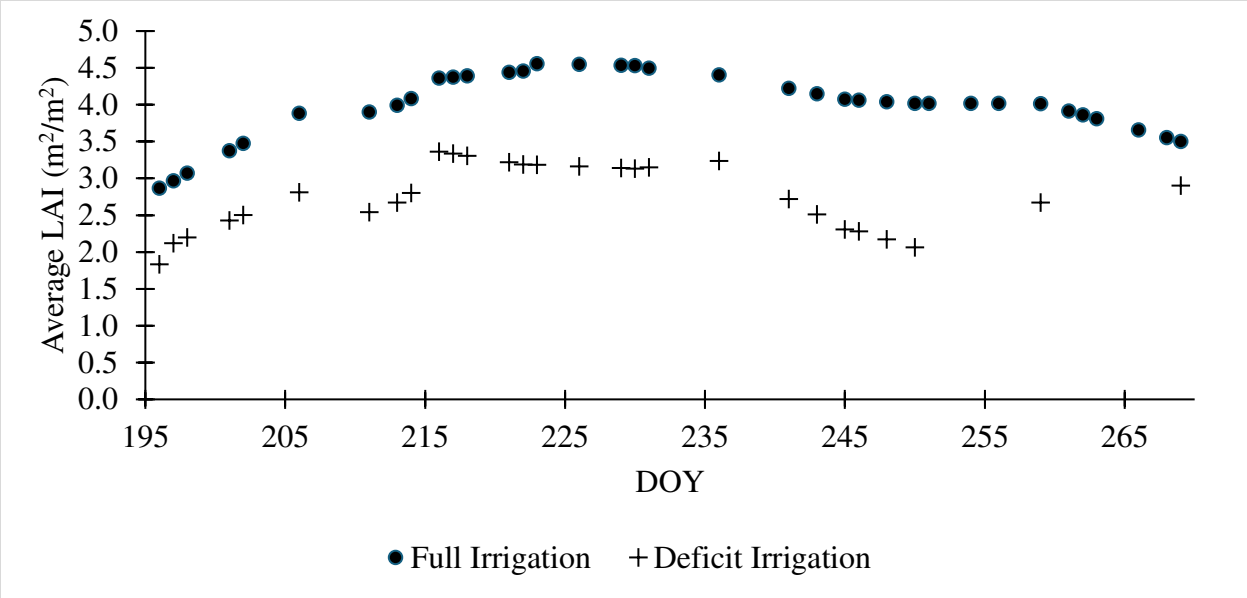

Figure 4: Observed maize LAI values

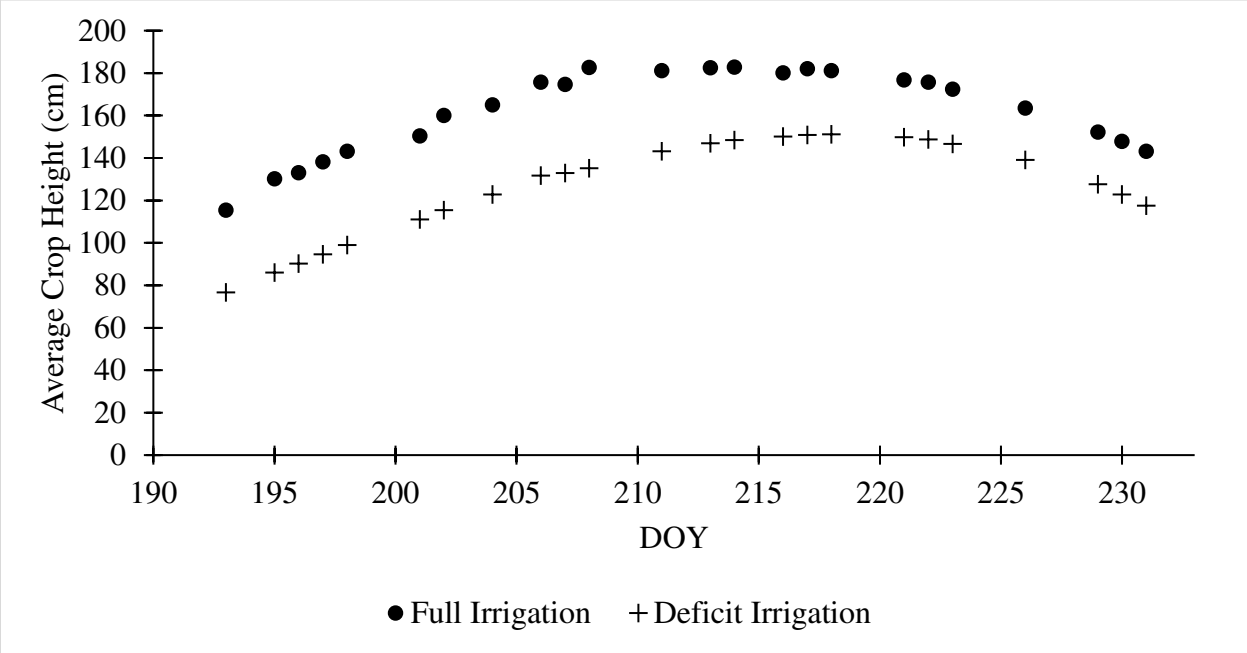

Figure 5: Observed crop height values

Table 2: Dates for each site measurement

Date	MSR-5 reflectance data	LAI2200C For LAI measurement	Tape measure of crop height
7/14/2022	X		X
7/15/2022		X	
7/16/2022	X		
7/18/2022	X		
7/20/2022	X		X
7/23/2022			X
7/25/2022		X	X
7/27/2022	X	X	X
8/04/2022		X	X
8/05/2022	X		
8/10/2022	X	X	X
8/18/2022	X	X	
8/24/2022	X	X	
9/02/2022	X	X	
9/07/2022	X	X	
9/16/2022	X	X	
9/26/2022	X		

Weather conditions for the site area, and daily and hourly alfalfa reference evapotranspiration (ETr) data were obtained from the COAGMET weather station Greeley 04 (GLY04), situated at the LIRF site. The station is positioned at a latitude of 40.449 and longitude of -104.6380, northwest of the two study area fields on a grass field. Daily in-situ maize ETa data were measured using an atmometer (Model E, ETgage, Loveland, CO, USA) that works as an evapotranspiration simulator. The atmometer used in this study used a Polyvinyl chloride (PVC) pipe placed around one meter above the ground. The PVC pipe is filled with distilled water, and

water used information can be read by measuring the water drop daily. Atmometers consist of a porous, wet, ceramic cup placed on top of a cylindrical water reservoir. The ceramic cup is covered with a green canvas, simulating the canopy of maize (resistance). Distilled water is poured into the cylindrical reservoir, which evaporates from the cup and is pulled through a suction tube extending to the bottom of the reservoir. A special membrane underneath the fabric keeps rainwater from seeping into the cup. This atmometer (ETgage) was placed in the fully irrigated field only. Studies performed by Gleason et al. (2013), using a large monolithic precision weighing lysimeter, validated the use of an ETgage atmometer under conditions commonly found in Colorado.

As for the Fc observations, the data were collected using the shadow sampling method, or also known as the meter-stick method. This method uses a meter-long stick that is placed on the land surface perpendicular to the crop rows' direction. The length of the shadow on the stick is measured, and the ratio of the shadow length to the total length of the stick is the Fc, as indicated by Adams and Arkin (1997). Figure 6 shows the observed Fc data.

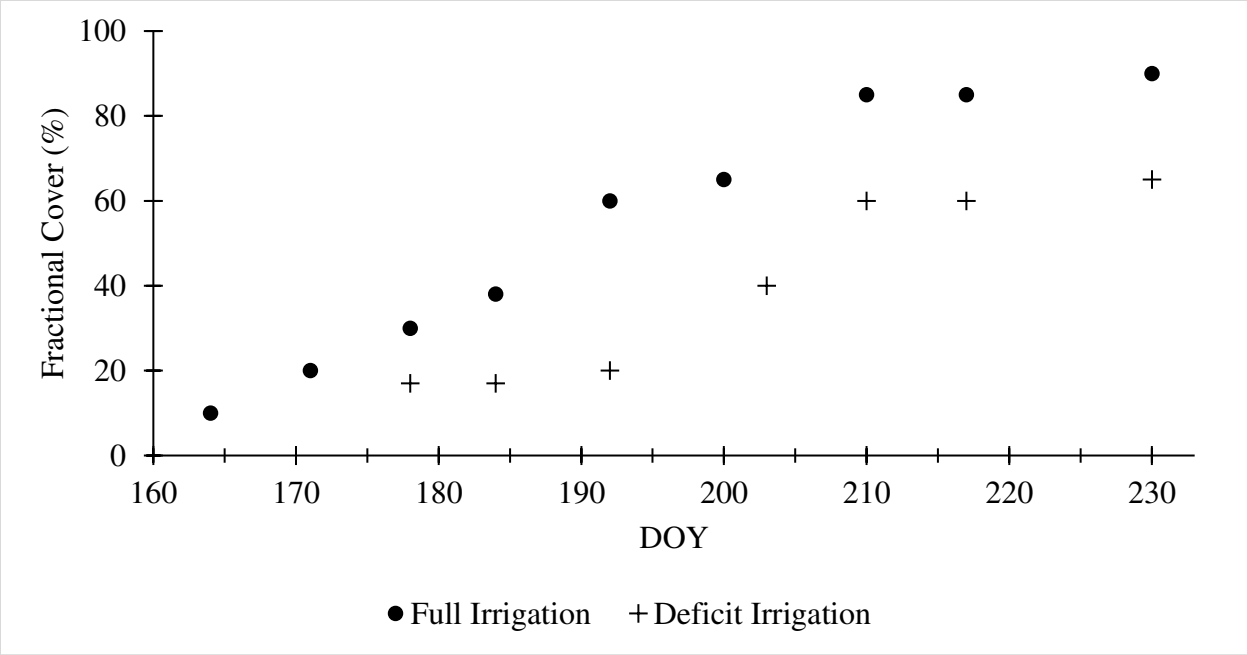

Figure 6: Observed fractional vegetation cover values

2.3 Remote Sensing data

As the main goal of this study is to compare and evaluate the performance of different RS platforms in estimating VIs, CBPCs, and ETa, this section introduces each of these platforms and provides some of their properties. The following are the RS platforms used in this study:

1- Unmanned Aircraft Systems (UAS): The UAS in this study uses a drone system to provide a multispectral image for the crop fields; it uses a calibrated reflectance panel using MicaSense RedEdge-MX multispectral camera (MicaSense Inc., Seattle, WA, USA), with five bands, including the visible and NIR bands. It has a very high resolution and can be flown anytime. The UAS in this study was scheduled to fly four times, as shown in Table 3, and was flying 120 meters above the two fields. The UAS, commonly known as drones, have revolutionized agricultural remote sensing due to their flexibility

and affordability. Figure 7 shows the MicaSense RedEdge-MX multispectral camera spectral responses for each band.

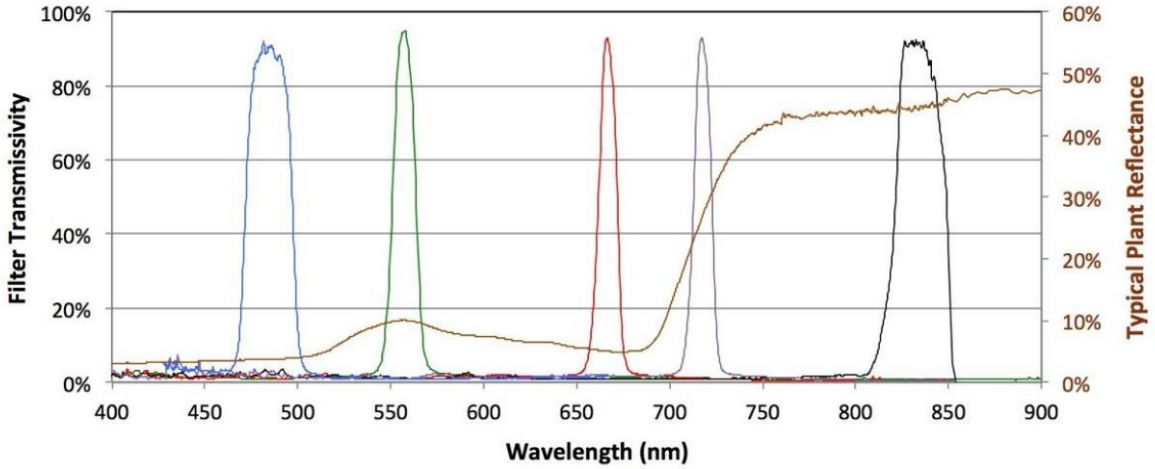

Figure 7: MicaSense RedEdge-MX multispectral camera spectral responses (Micasense, 2015)

2- PlanetScope Dove micro-satellite: It provides high-resolution images with high temporal resolution. Planet Dove, operated by Planet Labs (Planet Labs, Inc., San Fransisco, CA, USA), is a low-cost commercial satellite constellation (150+) designed for frequent and global Earth imaging. The Dove satellites capture multispectral imagery at a spatial resolution (3 m) suitable for monitoring agricultural landscapes. The advantage of Planet Dove imagery lies in its high revisit rate (daily) and ability to provide consistent and up-to-date information on crop changes. The Planet surface reflectance images are pre-processed and calibrated with a factor of 10,000. Atmospheric corrections use MODIS data and the 6SV2.1 radiative transfer model (Planet team, 2017) to remove the effect of gases and aerosol concentrations and their changes in the altitude between the camera sensor in the space and the landscape. However, they exclude effects like stray light and haze from the correction process. Geometric corrections use sensor telemetry, ground control points, and digital elevation models to have a harmonized imagery version that

meets the Sentinel-2 standards. Figure 8 shows the spectral responses for the RED and NIR bands used in this study for the Planet platform (Vanhellemont, 2019).

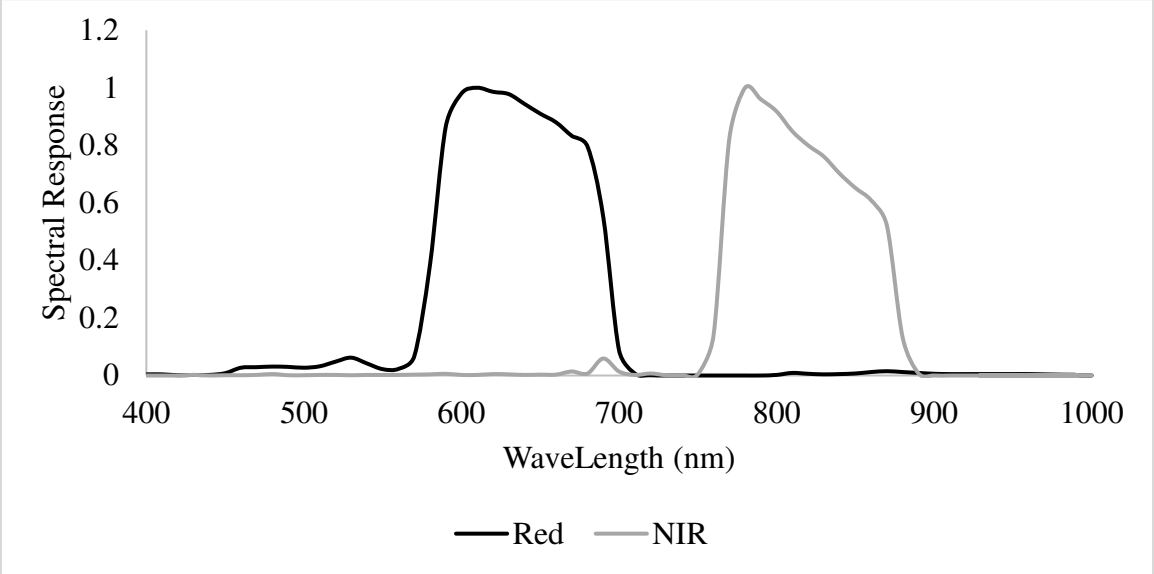

Figure 8: PlanetScope sensor spectral responses

3- Sentinel-2 Satellite: Sentinel satellites are part of the European Space Agency's (ESA) Copernicus program, offering a series of Earth observation missions. Sentinel-2 has two satellites (Sentinel-2A and Sentnel-2B), and both provide multispectral images of the Earth's landscape. The radiometric resolution of the Sentinel-2 image is 16 bits after post-processing the images by the ESA from 12 bits. To provide surface reflectance images, the sentinel-2 images are pre-processed and calibrated through a calibration factor of 10,000; the ESA (Sen2Cor) developed an algorithm to process the atmospheric corrections. Figure 9 shows the spectral response for the RED and NIR bands for the Sentinel-2 platform (ESA, 2017).

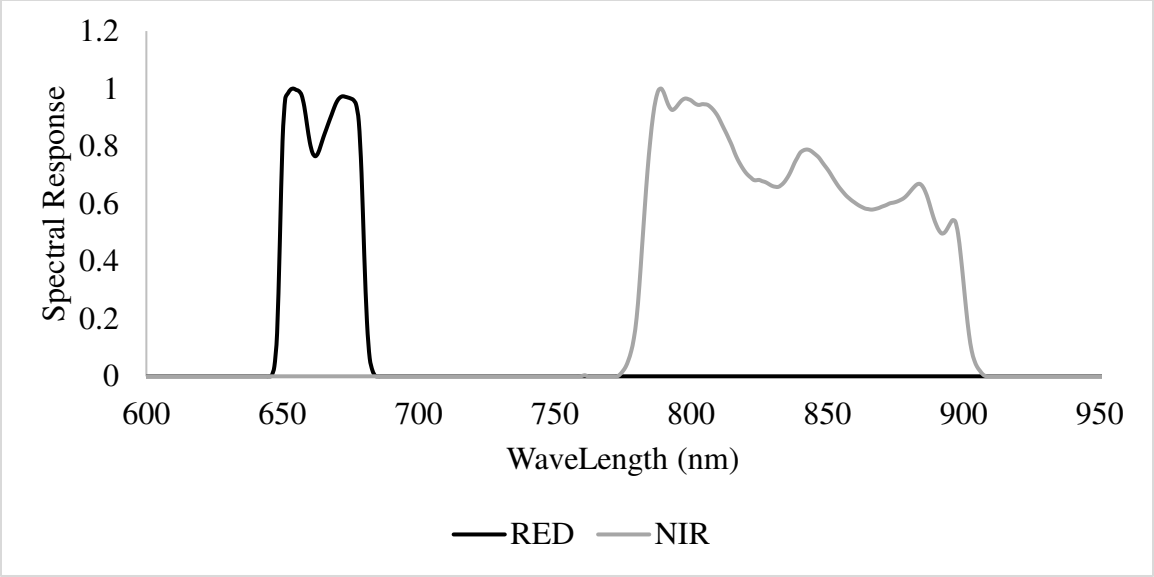

Figure 9: Sentinel-2 spectral responses

4- LandSat 8/9: It is a spaceborne RS platform operated by NASA and the USGS, providing the longest continuous global record of Earth's surface imagery. Landsat satellites take images of the landscapes using the Operational Land Manager (OLI), which provides short-wave multispectral data, and the Thermal Infrared Sensors (TISS), which uses a camera to measure the long-wave infrared thermal radiation images. The radiometric resolution of Landsat imagery is 16 bits, converted from 12 bits after USGS/NASA post-process data. Linear calibration coefficients are used to convert the digital number (DN) to surface reflectance data. Figure 10 shows the Landsat RED and NIR band's spectral responses (Acharya and Yang, 2015).

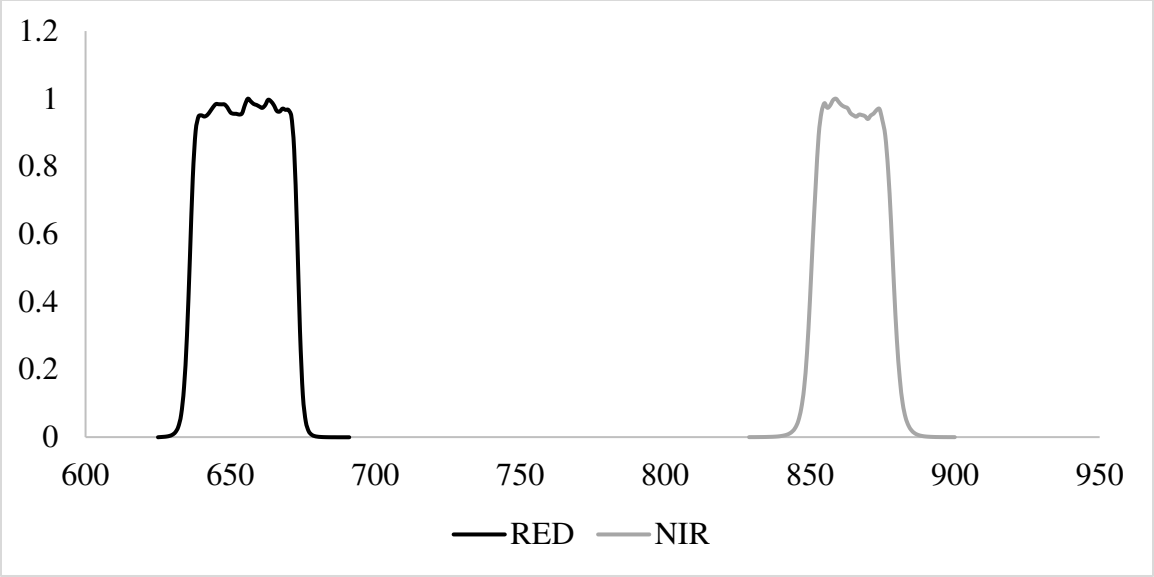

Figure 10: Landsat spectral responses

Additionally, MSR-5 data were also included in this study, detailed separately in the previous section. Table 3 shows the dates each satellite's images were used in this study. Table 4 shows the properties of each satellite and the used bands with their wavelengths. Figure 11 to Figure 14 show the true color (RGB) images with the corresponding AOI for the UAS, Planet, Sentinel-2, and Landsat RS platforms, respectively.

Table 3: Image acquisition date used for each remote sensing platform in this study

RS Platform	Dates of images taken (in 2022)
UAS	Jul/21, Jul/25, Aug/18, Sep/07
Planet	Jul/12, Jul/16, Jul/17, Jul/27, Jul/30, Aug/01, Aug/04, Aug/5, Aug/11, Aug/18, Aug/24, Sep/2, Sep/7, Sep/11, Sep/26
Sentinel-2	Jul/07, Jul/11, Jul/15, Jul/17, Jul/20, Jul/30, Aug/01, Aug/04, Aug/06, Aug/09, Aug/11, Aug/19, Aug/23, Aug/29, Aug/31, Sep/03, Sep/5, Sep/8, Sep/13, Sep/18, Sep/20, Sep/23, Sep/25, Sep/28
Landsat	Jul/08, Jul/09, Jul/16, Jul/17, Jul/25, Aug/01, Aug/02, Aug/10, Aug/17, Aug/18, Sep/02, Sep/03, Sep/11, Sep/18, Sep/19, Sep/27

Table 4: Remote sensing platforms characteristics

RS Platform	Spatial Resolution	Temporal Resolution	Used Bands	Central Wavelength (nm)	Band Width (nm)
UAS	0.03 meter	-	Red	668	14
			NIR	842	57
Planet	3 meters	1 day	Band 6 (Red)	666	80
			Band 8 (NIR)	867	80
Sentinel-2	10 to 60 meters	10 days	Band 4 (Red)	665	31
			Band 8 (NIR)	833	106
Landsat8/9	30 to 100 meters	16 days	Band 4 (Red)	655	30
			Band 5 (NIR)	870	30
			Band 7 (SWIR-2)	2200	30
MSR-5	1 meter	-	Red	660	60
			NIR	830	140

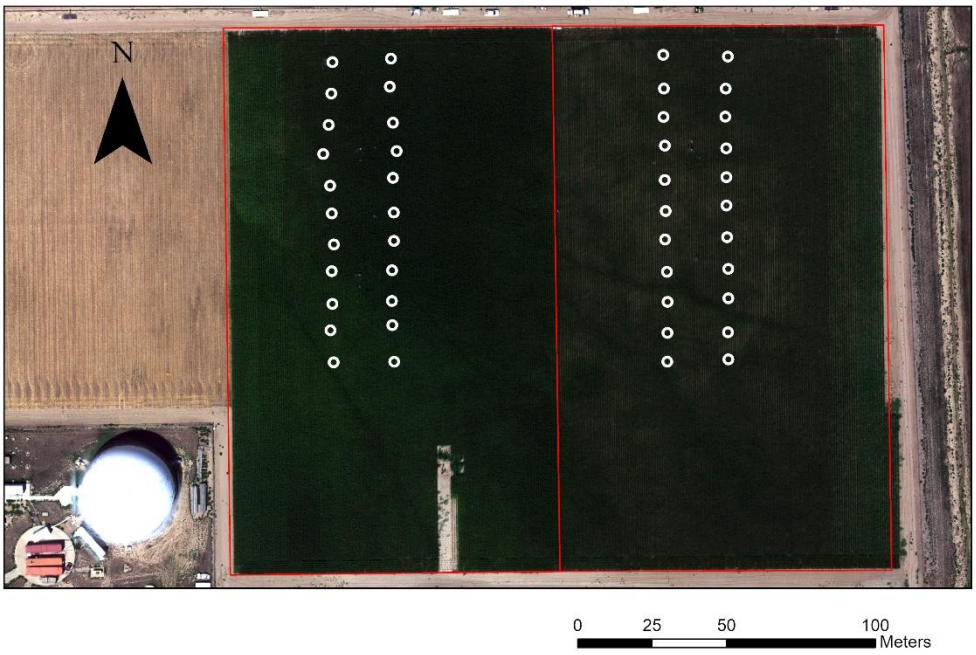

Figure 11: UAS true image with the corresponding AOIs

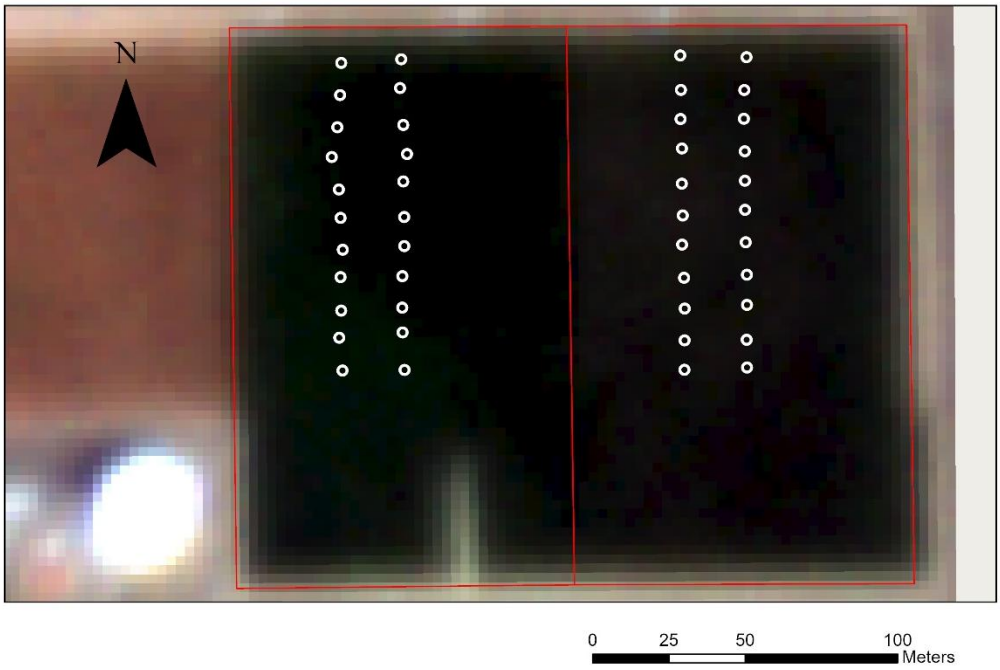

Figure 12: Planet true-color image with the corresponding AOIs

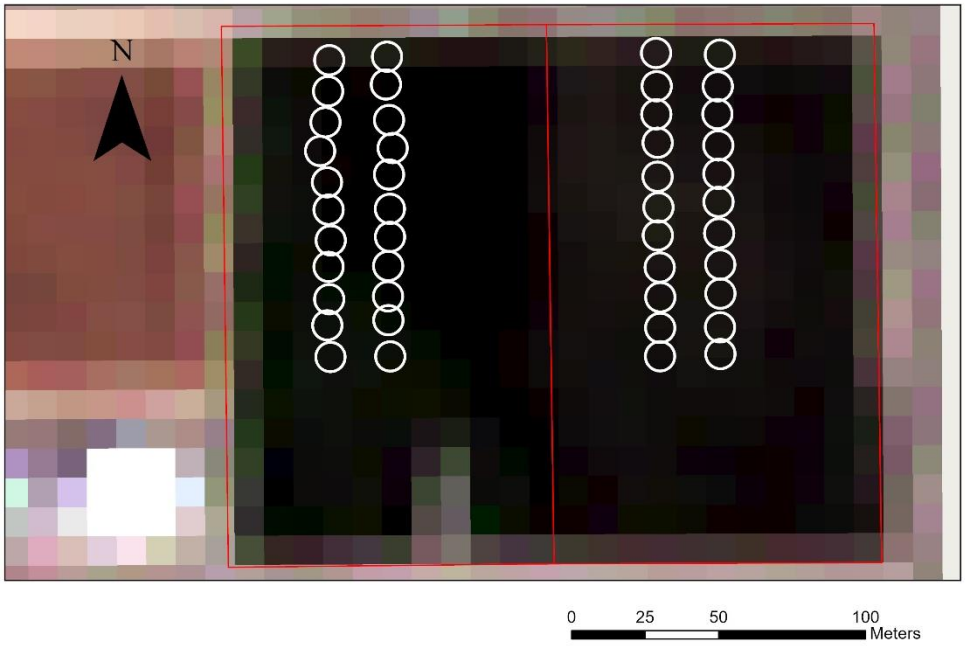

Figure 13: Sentinel-2 true-color image with the corresponding AOIs

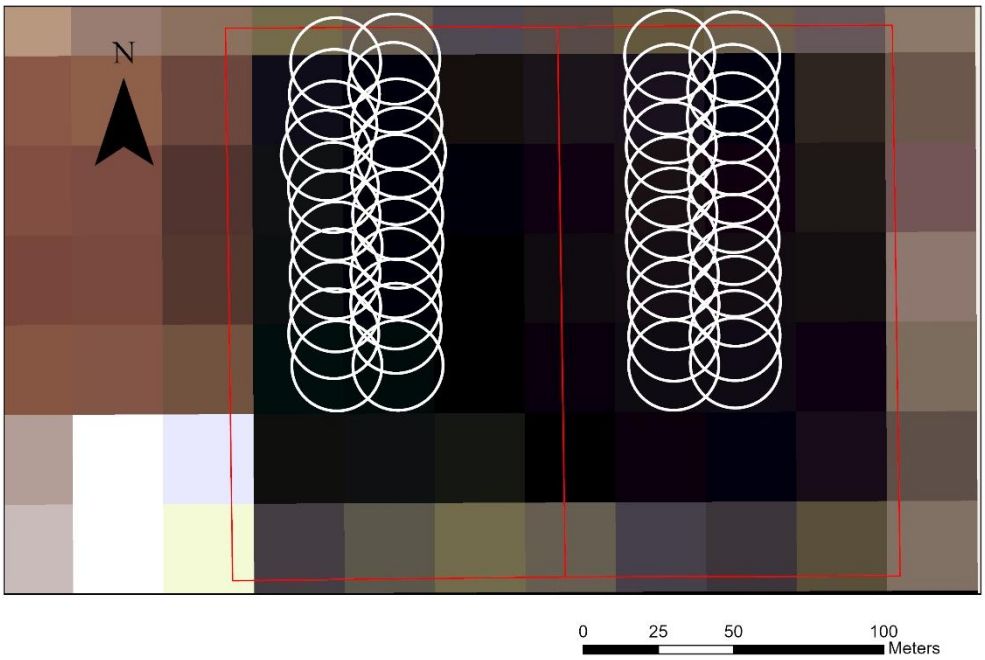

Figure 14: Landsat true-color image with the corresponding AOIs

2.4 Determination of Vegetation Indices

Four different RS-platforms were used in this study to determine the VIs throughout the maize growth stages. For each DOY specified in Table 2, NDVI, SAVI, and OSAVI were estimated based on Red and NIR reflectance data. NDWI was estimated in addition to the abovementioned VIs for the Landsat satellite platform. These VIs can be estimated using the following Equations 1 to 4:

$$\mathrm{NDVI} = \frac{\mathrm{NIR}-\mathrm{RED}}{\mathrm{NIR}+\mathrm{Red}} \tag{1}$$

$$\mathrm{SAVI} = (1+\mathrm{L})\frac{\mathrm{NIR}-\mathrm{RED}}{\mathrm{NIR}+\mathrm{Red}+\mathrm{L}}, \mathrm{L}=0.5 \tag{2}$$

$$\mathrm{OSAVI} = (1+\mathrm{L})\frac{\mathrm{NIR}-\mathrm{RED}}{\mathrm{NIR}+\mathrm{Red}+\mathrm{L}}, \mathrm{L}=0.16 \tag{3}$$

$$\mathrm{NDWI} = \frac{\mathrm{NIR}-(\mathrm{SWIR}-2)}{\mathrm{NIR}+(\mathrm{SWIR}-2)} \tag{4}$$

Where NIR represents the target reflectance in the near-infrared band, RED is the reflectance in the red band, and SWIR-2 is the Short-wave infrared reflectance. The L factor in Equation 2 and Equation 3 is the adjustment factor that has been used to minimize the interference caused by the soil background to the reflectance values from vegetated surfaces. The estimation of the L factor is based on crop densities; for intermediate crop density L=0.5, and for high crop density L=0.16.

The reflectance of the light for the maize surface was obtained using RED, NIR, and the Mid-Infrared (MIR) bands over 44 different stations, 22 stations in the fully irrigated field and 22 stations in the deficit irrigation field. Using ArcGIS Pro (ESRI, Redlands, CA, USA), circles or polygons representing an Areas of Interest (AOI) were determined with a specific diameter of influence for each station. For the UAS and Planet images, an AOI diameter of 3 meters was used; for Sentinel-2, a 10-meter AOI diameter was used; and for Landsat images, a 30-meter AOI diameter was used. Each AOI was centered at the MSR-5 site coordinates. These different AOI diameters were set to capture the surface reflectance from the area of a pixel of interest.

After a comprehensive collection of the reflectance data for each RS platform and each station throughout the dates mentioned in Table 2, these reflectance data were used to estimate the VIs. These VIs were compared to the MSR-5 surface reflectance-based VIs data to evaluate the performance of each RS platform throughout the entire maize growth season.

2.5 Estimation of crop biophysical characteristics

The LAI, Hc, and Fc were estimated using different functions that are based on different VIs. The CBPCs were estimated for each of the 44 stations. Several VI-based functions/models were tested for this study to estimate CBPCs. The selection criteria of CBPC calculation

functions were based on using models that incorporated different site conditions, different RS platforms for measuring reflectance data, and various VI-based models. Firstly, site conditions variability may significantly impact the performance of VIs and RS platforms in estimating CBPCs. Secondly, different RS platforms (satellites, airborne, or proximal sensors) have varying spatial and spectral resolutions, which may influence the sensitivity and accuracy of VIs in estimating CBPCs. Additionally, different VIs respond differently to variations in CBPCs. Therefore, selecting different functions that align with the sensitivity and formulation of different VIs allows for a comprehensive evaluation of how these indices estimate CBPCs across diverse conditions and sensor types. The selected LAI functions are shown in Table 5 below.

Table 5: Selected models for LAI estimation

Model-VI	Function	n	R^2	RMSE (m^2/m^2)	Reference
NDVI	$(VI + 1.1)(1 + 0.01 * e^{5.72*VI})$	425	0.51	1.07	Mourad et al. (2020)
NDVI	$0.2092 * e^{3.3554*VI}$	68	0.85	0.22	Jayasree et al. (2013)
NDVI	$\log_{0.6}[(0.943 - VI)/0.731]$	423	0.87	0.64	Nguy-Robertson et al. (2012)
SAVI	$-[(1.49 * \ln VI) + 2.71]/\ln VI$	423	0.81	0.78	
NDVI	$[\ln \frac{1}{1-(\frac{VI-0.2064}{0.7298})}]/0.6159$	261	-	1.18	Vina et al. (2011)
NDVI	$-\frac{[\ln 1.007*(1-(1.036*VI))]}{0.719}$	47	0.78	0.66	Liu et al. (2012)
OSAVI	$-\frac{[\ln 1.123*(1-(1.155*VI))]}{0.562}$	47	0.83	0.59	
NDVI	$6.32 * VI^{1.51}$	204	0.75	-	Yang et al. (2015)
SAVI	$-\frac{\ln\frac{0.69-VI}{0.59}}{0.91}$	-	-	-	Bastiaanssen (1998)
OSAVI	$0.263 * e^{3.813*VI}$	-	-	-	Chavez et al. (2009)
NDWI	$(2.88 * VI + 1.14) * (1 + 0.104 * e^{4.1*VI})$	69	0.76	0.66	Anderson et al. (2004)
OSAVI	$(4 * VI - 0.8) * (1 + 0.00000473 * e^{15.64*VI})$	60	0.85	0.58	

This study evaluated various models for the estimation of Hc and Fc. Moreover, some of the Hc models were based on the observed LAI estimation. Table 6 summarizes the detailed functions and corresponding performance metrics of the crop height estimation models. Table 7

shows detailed information about Fc functions. The CBPCs' functions were compared to the observed data mentioned in Section 2.2.

Table 6: Selected Models for Crop Height estimation

Model-Based	Function	n	R^2	RMSE (m)	Reference
LAI	$\frac{LAI+0.3919}{1.44}$	11	0.91	-	Arslan et al. (2022)
NDVI	$\frac{VI-0.0285}{0.34}$	11	0.95	-	
NDVI	$0.283 * VI - 0.0277$	360	0.93	0.41	Jeong and Park (2021)
NDVI	$3.4086 * VI^{1.643}$	207	0.82	-	Yang et al. (2015)
LAI	$(0.697 * e^{0.236*LAI}) - (3.42 * e^{-3.177*LAI})$	-	0.91	-	Costa-Filho et al. (2021)
OSAVI	$(1.86 * VI - 0.8) * (1 + 0.000000482 * e^{17.69*VI})$	64	0.93	0.27	Anderson et al. (2004)
NDWI	$(1.2 * VI + 0.6) * (1 + 0.04 * e^{5.3*VI})$	74	0.92	0.2	
NDVI	$\frac{VI-0.25}{0.21}$	43	0.63	-	Khaliq et al. (2018)

Table 7: Selected Models for Fc estimation

VI-Based	Function	n	R^2	RMSE %	Reference
NDVI	$1.26 * VI - 0.18$	74	0.96	6.20	Johnson and Trout (2012)
NDVI	$1 - (\frac{0.82-VI}{0.74})^{0.696}$	204	0.75	-	Yang et al. (2015)
NDVI	$-[\ln\left(1 - \left(\frac{VI}{0.93}\right)\right)]/3$	347	0.90	5.84	Gitelson (2013)

2.6 Estimation of crop coefficients and ET

Multiple linear models based on Fc and VIs were used to estimate basal crop coefficients (Kcb). Table 8 shows the selected models used to estimate Kcb. The estimated coefficients were then used to estimate the daily maize actual evapotranspiration (ETa) using Equation 5.

$$\mathrm{ETa} = \mathrm{Kcbx} * \mathrm{ETr} \quad (5)$$

Where Kcbx is the reflectance-based crop coefficient estimated by the x function shown in Table 8, and ETr is the daily reference evapotranspiration observed by COAGMET weather station in Greeley 04 (GLY04).

The estimated daily ETa was compared to the daily ETgage estimated using in-situ measurements for the full irrigation field, shown in detail in section 2.2.

Table 8: Selected models to estimate Kcb

Model-Based	Function	n	R^2	RMSE	Reference
Fc	$(1.1 * \mathrm{Fc}) + 0.17$	60	0.93	-	Trout and DeJonge (2018)
NDVI	$(1.181 * \mathrm{NDVI}) - 0.026$	-	-	-	Neale et al. (1989)
SAVI	$(1.416 * \mathrm{SAVI}) + 0.017$	-	-	-	Bausch (1993)
NDVI	$(1.2358 * \mathrm{NDVI}) + 0.0245$	55	0.94	-	González-Piqueras et al. (2004)
NDVI	$(1.308 * \mathrm{NDVI}) + 0.027$	63	0.84	-	Singh and Irmak (2009)

2.7 Balanced Analysis

To ensure a balanced analysis, new comparative study of the different RS platforms was carried out by selecting of a subset of data acquired with the various platforms coinciding as closely as possible in overpass time. Given that there were only four UAS flights, the other platforms were matched with the dates of data acquisition of those of the UAS flights. The UAS dates were July 21, July 25, August 18, and September 7, as these were the days when data from UAS were available. Table 9 presents the specific dates selected for each platform to ensure temporal alignment. The selected dates in Table 9 were used for the analysis to provide a clearer comparison of the results across different RS platforms. By focusing on these dates, we minimized the temporal discrepancies that could affect the accuracy of the comparative analysis.

Table 9: Dates of images chose for the balanced analysis

RS Platform	Dates of images for the balanced analysis
UAS	Jul/21, Jul/25, Aug/18, Sep/07
PlanetDove	Jul/17, Jul/27, Aug/18, Sep/07
Landsat	Jul/17, Jul/25, Aug/18, Sep/11
Sentinel-2	Jul/20, Jul/30, Aug/19, Sep/8
MSR-5	Jul/20, Jul27, Aug/18, Sep/07

To further balance the study and provide a comprehensive analysis, the data were separated into two distinct subsets representing early and late crop growth stages. This separation allows for the evaluation of the performance of the RS platforms and models across different developmental phases of the maize crop. The early growth stage was defined as the period from the beginning of the season until the end of July, while the late growth stage was defined as the

period from the beginning of August until the end of the season. This approach ensures that the analysis covers different growth cycles of the maize crop and provides insights into how each RS platform performs at different stages.

2.8 Statistical analysis, models performance, and sensitivity analysis

A One-way sensitivity analysis was done for all CBPCs and Kcb functions to assess the impacts of uncertainties of independent variables (VIs) on the output results of CBPCs and ETa estimates. The sensitivity analysis varied the value of the variable (i.e, VIs, Fc, and LAI) in 2.5% (2.5% increase and 2.5 decrease) and 5% (5% increase and 5% decrease) increments. Any increase in VI values should yield a value less than or equal to one; since the values of the indices range between -1 and 1, any VI values larger than one were excluded. Also, an increase in Fc values should obtain an Fc value less than the expected maximum maize Fc of 85% (or 0.85), and any change in Fc values that results in an Fc values higher than 85% were excluded. As for the LAI changes, the values should not exceed 5.5 m^2/m^2, and any values exceeding 5.5 m^2/m^2 were excluded.

To evaluate the performance of the VIs and the selected CBPCs and ETa models, we utilized the Mean Bias Error (MBE), the Normalized MBE (MBE%), the Root Mean Square Error (RMSE), and the RMSE%. The MBE, MBE%, RMSE, and RMSE% are shown in Equations 6 to 9, respectively.

$$\mathrm{MBE} = \frac{\sum \mathrm{Pi} - \mathrm{Oi}}{\mathrm{n}} \tag{6}$$

$$\mathrm{MBE\%} = \frac{\mathrm{MBE}}{\bar{\mathrm{O}}} * 100\% \tag{7}$$

$$\mathrm{RMSE} = \sqrt[2]{\frac{\sum(\mathrm{Pi} - \mathrm{Oi})^2}{\mathrm{n}}} \tag{8}$$

$$\text{RMSE\%} = \frac{\text{MBE}}{\bar{O}} * 100\% \quad (9)$$

Where Pi is the predicted value provided by the models, Oi is observed value, n is the number of observations (sample size), and $\bar{O}$ is the average value of the observed data.

The MBE helps assess prediction bias, where positive MBE values indicate overestimation and negative MBE values indicate an underestimation of the models compared to the observed data. The RMSE provides a measure of the overall prediction error. Lower values suggest better predictive accuracy relative to the scale of the actual values, while high RMSE values show that the model has high error. These metrics are commonly used in evaluating the performance of predictive models and are frequently employed to assess the effectiveness of predictive models. Jamieson et al. (1991) proposed the following categories based on RMSE% to evaluate the performance of the models:

- RMSE% ≤ 10%: Excellent performance
- 10% < RMSE% ≤ 20%: Good performance
- 20% < RMSE% ≤ 30%: Fair performance
- RMSE% > 30%: Poor performance

Before testing the function results, the data were subjected to a Median Absolute Deviation Analysis (MADA) to detect and remove outliers from the error analysis (Leys et al., 2013). The MADA was used in this study to replace the method used to remove the outliers based on using the mean and standard deviation. The MAD was calculated using the following equation:

$$\text{MAD} = \text{b} * \text{Mi}(|\text{xi} - \text{Mj}(\text{xj})|) \quad (10)$$

$$\text{b} = \begin{cases} 1.4826, & \text{Normally distributed data} \\ 1/\text{Q}(0.75), & \text{Unnormally distributed data} \end{cases} \quad (11)$$

Where ‘b’ is a constant linked to the normality of the data, ‘Mi’ is the median of the new series that will be resulted by applying in between the brackets, ‘xi’ is each individual value of the series, ‘Mj(xj)’ is the median of the original series. The process of this analysis is by subtracting each of the values of the original series with the median value of the original series, then find the median value of the new series, that resulted from the subtracting, and then multiplying the new median value with the constant ‘b’, finding the MAD value.

After having the MAD value, the outliers can be detected using the following:

$$\mathrm{M} - 3 * \mathrm{MAD} < \mathrm{xi} < \mathrm{M} + 3 * \mathrm{MAD}$$

All values greater than M+3*MAD and smaller than M-3*MAD were excluded from the analysis. The use of (3*MAD) is suggested to be very conservative by Miller (1991) instead of using (2.5*MAD) or (2*MAD).

Chapter 3: Results

3.1 Determination of Vegetation Indices

The VIs were estimated using four different RS platforms for 44 stations at LIRF using different day of the year (DOY), as mentioned in Table 3. The VIs calculations were based on Equation 1 to Equation 4. The VIs results were compared and tested against the observed data obtained from MSR-5 proximal data dates mentioned in Table 2. Table 10 through Table 13 shows the average VIs obtained from the UAS, Planet-Dove, Sentinel-2, and Landsat platforms, respectively, for the deficit and full irrigation fields during the maize crop growth period.

Table 10: Average VIs values for each DOY for the UAS

		Full Irrigation stations			Deficit Irrigation stations		
Date	DOY	NDVI	OSAVI	SAVI	NDVI	OSAVI	SAVI
21-Jul	201	0.86	0.78	0.69	0.66	0.57	0.48
25-Jul	205	0.88	0.78	0.67	0.66	0.58	0.49
18-Aug	230	0.87	0.77	0.66	0.76	0.65	0.53
7-Sep	250	0.80	0.71	0.61	0.49	0.43	0.36

Table 11: Average VIs values for each DOY for the PlanetDove satellite

		Full Irrigation stations			Deficit Irrigation stations		
Date	DOY	NDVI	OSAVI	SAVI	NDVI	OSAVI	SAVI
12-Jul	193	0.77	0.65	0.55	0.44	0.37	0.32
16-Jul	197	0.82	0.71	0.60	0.59	0.51	0.44
17-Jul	198	0.80	0.69	0.58	0.64	0.54	0.46
26-Jul	207	0.87	0.76	0.64	0.77	0.64	0.55
30-Jul	211	0.85	0.75	0.64	0.79	0.68	0.58
1-Aug	213	0.82	0.73	0.62	0.77	0.67	0.57
4-Aug	216	0.81	0.69	0.59	0.77	0.64	0.55
5-Aug	217	0.82	0.71	0.59	0.77	0.65	0.55
10-Aug	222	0.83	0.71	0.61	0.75	0.63	0.53
18-Aug	230	0.81	0.71	0.61	0.78	0.66	0.56
24-Aug	236	0.79	0.69	0.59	0.76	0.65	0.55
2-Sep	245	0.78	0.68	0.57	0.66	0.56	0.47
7-Sep	250	0.79	0.69	0.59	0.61	0.52	0.44
11-Sep	254	0.74	0.64	0.55	0.58	0.48	0.41
26-Sep	269	0.69	0.59	0.50	0.39	0.33	0.28

Table 12: Average VIs values for each DOY for the Sentinel-2 satellite

		Full Irrigation stations			Deficit Irrigation stations		
Date	DOY	NDVI	OSAVI	SAVI	NDVI	OSAVI	SAVI
12-Jul	193	0.73	0.63	0.53	0.31	0.28	0.24
15-Jul	196	0.78	0.64	0.52	0.48	0.39	0.32
17-Jul	198	0.75	0.64	0.54	0.53	0.46	0.39
20-Jul	201	0.77	0.64	0.52	0.63	0.52	0.41
30-Jul	211	0.88	0.76	0.64	0.83	0.67	0.53
1-Aug	213	0.81	0.70	0.59	0.73	0.63	0.52
4-Aug	216	0.81	0.70	0.58	0.76	0.62	0.49
6-Aug	218	0.85	0.74	0.62	0.77	0.65	0.54
9-Aug	221	0.89	0.76	0.62	0.80	0.64	0.50
11-Aug	223	0.82	0.71	0.59	0.74	0.63	0.52
19-Aug	231	0.83	0.67	0.53	0.79	0.61	0.46
24-Aug	236	0.87	0.74	0.61	0.82	0.65	0.51
29-Aug	241	0.85	0.72	0.59	0.77	0.61	0.49
31-Aug	243	0.85	0.72	0.59	0.77	0.61	0.48
3-Sep	246	0.86	0.73	0.60	0.69	0.55	0.43
5-Sep	248	0.79	0.70	0.59	0.57	0.49	0.41
8-Sep	251	0.79	0.69	0.58	0.55	0.45	0.36
13-Sep	256	0.72	0.62	0.52	0.44	0.37	0.29
18-Sep	261	0.79	0.66	0.54	0.37	0.30	0.24
20-Sep	263	0.72	0.62	0.52	0.31	0.27	0.23
23-Sep	266	0.78	0.64	0.51	0.34	0.27	0.21
25-Sep	268	0.74	0.61	0.49	0.30	0.26	0.21
28-Sep	271	0.73	0.60	0.48	0.31	0.25	0.20

Table 13: Average VIs values for each DOY for the Landsat satellite

		Full Irrigation stations				Deficit Irrigation stations			
Date	DOY	NDVI	OSAVI	SAVI	NDWI	NDVI	OSAVI	SAVI	NDWI
8-Jul	189	0.66	0.55	0.47	0.39	0.42	0.35	0.30	0.27
9-Jul	190	0.67	0.57	0.49	0.41	0.37	0.32	0.28	0.27
16-Jul	197	0.80	0.67	0.57	0.47	0.61	0.51	0.43	0.36
17-Jul	198	0.75	0.64	0.54	0.47	0.59	0.49	0.42	0.37
25-Jul	206	0.83	0.69	0.59	0.52	0.74	0.58	0.49	0.41
1-Aug	213	0.82	0.71	0.59	0.54	0.79	0.66	0.56	0.48
2-Aug	214	0.78	0.68	0.58	0.53	0.75	0.64	0.54	0.47
10-Aug	222	0.83	0.72	0.61	0.54	0.76	0.63	0.54	0.45
17-Aug	229	0.83	0.71	0.61	0.54	0.83	0.68	0.58	0.47
18-Aug	230	0.81	0.69	0.59	0.53	0.79	0.66	0.56	0.46
2-Sep	245	0.79	0.68	0.58	0.52	0.69	0.57	0.49	0.41
3-Sep	246	0.79	0.68	0.58	0.52	0.68	0.56	0.48	0.42
11-Sep	254	0.78	0.66	0.56	0.50	0.57	0.47	0.40	0.37
18-Sep	261	0.76	0.64	0.54	0.48	0.41	0.35	0.29	0.28
19-Sep	262	0.72	0.62	0.53	0.47	0.39	0.34	0.29	0.28
27-Sep	270	0.65	0.55	0.47	0.44	0.36	0.30	0.26	0.23

Across all platforms, VIs for the full irrigation stations were consistently higher than the VIs for the deficit irrigation stations, which proved that higher water availability positively influences the canopy health and density. Moreover, VIs values varied significantly across different DOY, reflecting the dynamic nature of maize crop growth development stages. The peak VI values were observed around late June to early August.

The VIs values were then compared to the MSR-5 data to evaluate the performance of each RS platform in estimating the VIs throughout the dates shown in Table 2. The performance

of these indices was tested using Equation 6 to Equation 9. Table 14 shows the error analysis and performance of VI estimations.

As shown in below table, the estimated VIs' performance using the UAS platform was excellent and higher than that of all other RS platforms; this is likely due to the higher spatial resolution of the UAS and the fact that the system acquired RS data closer to the land surface thus minimizing atmospheric interference, which captures more detailed canopy information. The other RS platforms showed a relatively high performance in estimating VIs; they showed comparable trends in estimating VIs but with generally lower accuracies (higher MBE% and RMSE%) than the UAS, suggesting that they might be less sensitive to finer canopy details.

Table 14: Performance of VI estimations for each RS platform

RS platform	VI	MBE	MBE%	RMSE	RMSE%	Performance
UAS	NDVI	0.020	2.76	0.069	9.45	Excellent
	OSAVI	-0.0002	-0.03	0.044	6.78	Excellent
	SAVI	-0.026	-4.76	0.054	9.86	Excellent
PlanetDove	NDVI	0.009	1.40	0.084	12.84	Good
	OSAVI	0.034	5.98	0.078	13.53	Good
	SAVI	0.004	0.76	0.067	13.72	Good
Sentinel-2	NDVI	0.004	0.55	0.081	11.96	Good
	OSAVI	-0.064	-10.97	0.102	17.31	Good
	SAVI	-0.031	-6.34	0.081	16.43	Good
Landsat	NDVI	0.021	3.05	0.081	11.53	Good
	OSAVI	0.018	2.99	0.073	12.03	Good
	SAVI	-0.007	-1.43	0.068	13.45	Good
	NDWI	0.070	19.091	0.080	21.63	Fair

3.2 Median Absolute Deviation Analysis

The MADA was applied to the observed data for LAI, Hc, Fc, and ETa to estimate the outlier’s data from the resulting functions. Table 15 shows the MAD value for each observed data estimating CBPCs and ETa. Any resulting data that, when subtracted from the observed

data, has a higher or lower value than the reject value in Table 15 will be rejected from the analysis.

Table 15: MAD and used rejection values for each RS platform used to estimate CBPCs and ETa

			LAI		
RS platform	UAS	Planet	Landsat	Sentinel-2	MSR-5
MAD (m^2/m^2)	0.54	0.57	0.55	0.57	0.61
Reject value (m^2/m^2)	1.63	1.72	1.65	1.69	1.83
			Hc		
RS platform	UAS	Planet	Landsat	Sentinel-2	MSR-5
MAD (m)	0.19	0.22	0.19	0.21	0.22
Reject value (m)	0.59	0.65	0.59	0.64	0.65
			Fc		
RS platform	UAS	Planet	Landsat	Sentinel-2	MSR-5
MAD (%)	0.14	0.14	0.14	0.14	0.13
Reject value (%)	0.43	0.41	0.43	0.41	0.38
			ETa		
RS platform	UAS	Planet	Landsat	Sentinel-2	MSR-5
MAD (mm/day)	0.77	1.27	0.95	1.22	0.62
Reject value (mm/day)	2.31	3.80	2.85	3.66	1.84

3.3 Estimation of crop biophysical characteristics

3.3.1 Leaf Area Index Estimation

Based on Table 5, twelve models were selected to estimate the LAI; those models were based on different VIs. The estimated VIs from each RS platform result in section 3.1 were used as input values for these functions, and the MADA analysis was applied to reject some of the outliers in the resulting values. The MSR-5 sensor VI values were used in addition to the tested platforms. Figure 15 to Figure 19 and Tables in appendix A show the statistical analysis for each LAI function resulting from UAS, PlanetDove, Landsat, Sentinel-2, and MSR-5 RS platforms, respectively.

The error analysis, conducted across a diverse range of functions and VIs for LAI estimation using different RS datasets, provides a comprehensive understanding of the performance and reliability of these models. The selected VIs, each with its unique characteristics, demonstrate varying degrees of performance across different studies and datasets. The NDVI was the most utilized index; however, SAVI and OSAVI demonstrated similar performance compared to NDVI. The performance of LAI estimation models was slightly influenced by the type of RS reflectance data used or the high spatial resolution; a slightly better performance was noticed for the higher-resolution RS platforms. For instance, LAI results from models applied to PlanetDove, MSR-5, and UAS reflectance data showed relatively better performance compared to those applied to Landsat and Sentinel-2 data, which may provide evidence of how higher resolution RS platform can yield better estimations of LAI. The MBE values, which indicate providing insights into the overall bias of the LAI estimation models, were predominantly negative, suggesting an underestimation of LAI and VIs estimations.

The RMSE values reflect the accuracy of LAI estimation models throughout all the used models within all used RS platforms only. Mourad et al. (2022), Chavez et al. (2009), and Nguy-Robertson et al. (2012) models had a consistently high performance; these models were conducted in dry areas similar to LIRF, which shows the importance of selecting and applying LAI-functions done in arid or semi-arid areas. On the other hand, LAI models by Liu et al. (2012), Bastiaanssen (1998), and Anderson et al. (2004) showed lower performance throughout all RS platforms. In Bastiaanssen's (1998) study, an overall function used to estimate the LAI for multiple crop types and in multiple countries was used, which resulted in poor performance across all RS platforms. This highlights the need for more specific and localized LAI estimation models. Also, Both Liu et al. (2012) study, conducted in Ottawa, Ontario, and Anderson et al.

(2004), conducted in Walnut Creek Watershed, Iowa, had a humid site condition, which significantly impacted the results of LAI in this study. This emphasizes the importance of considering site conditions in future LAI estimation research.

Overall, higher-resolution RS platforms generally provide better performance, indicating that higher spatial resolution improves the accuracy of LAI estimation. Also, models developed in similar environmental conditions performed better, emphasizing the importance of site-specific calibration and the impact of differing site conditions on model accuracy. Moreover, the predominance of negative MBE values suggests a tendency for underestimation in LAI estimates across most of the models, which shows the need for further model calibration. In addition, model development localization is important, including the development of models with a specific crop type, crop variety, and sites. These key findings highlight the need for further research and development in the field of LAI estimation, particularly in the areas of model calibration and site-specific considerations.

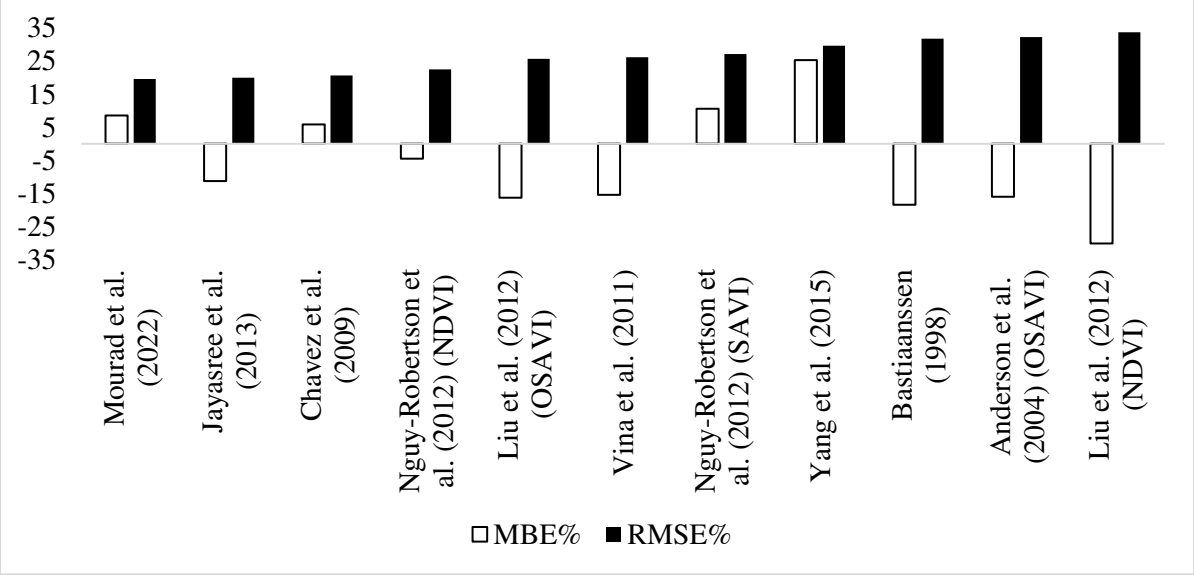

Figure 15: Error analysis for the UAS-based LAI estimation

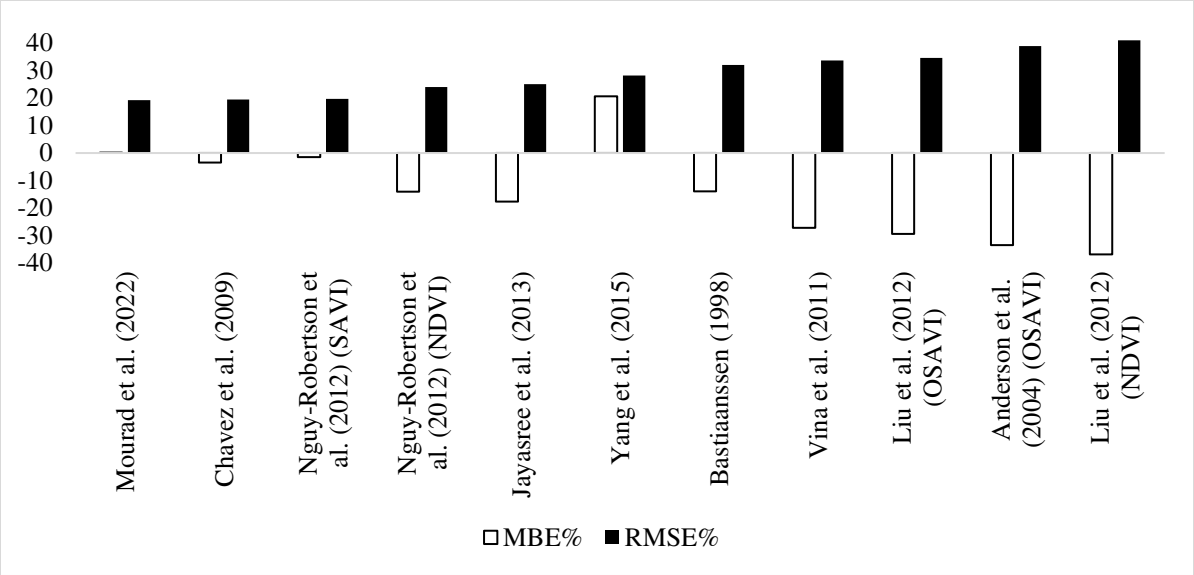

Figure 16: Error analysis for the Planet-based LAI estimation

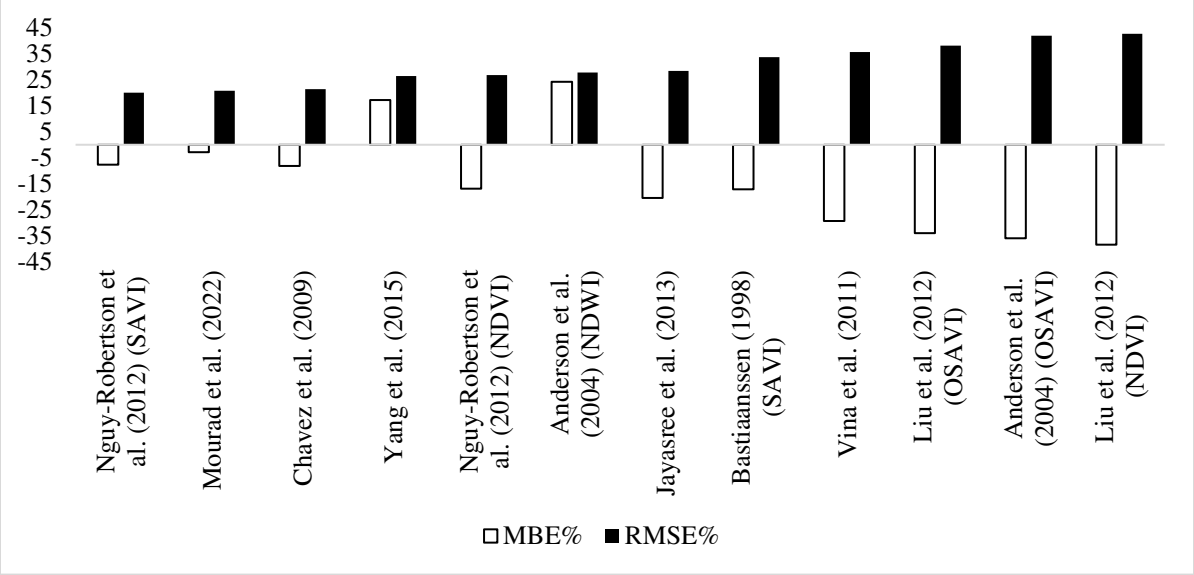

Figure 17: Error analysis for the Landsat-based LAI estimation

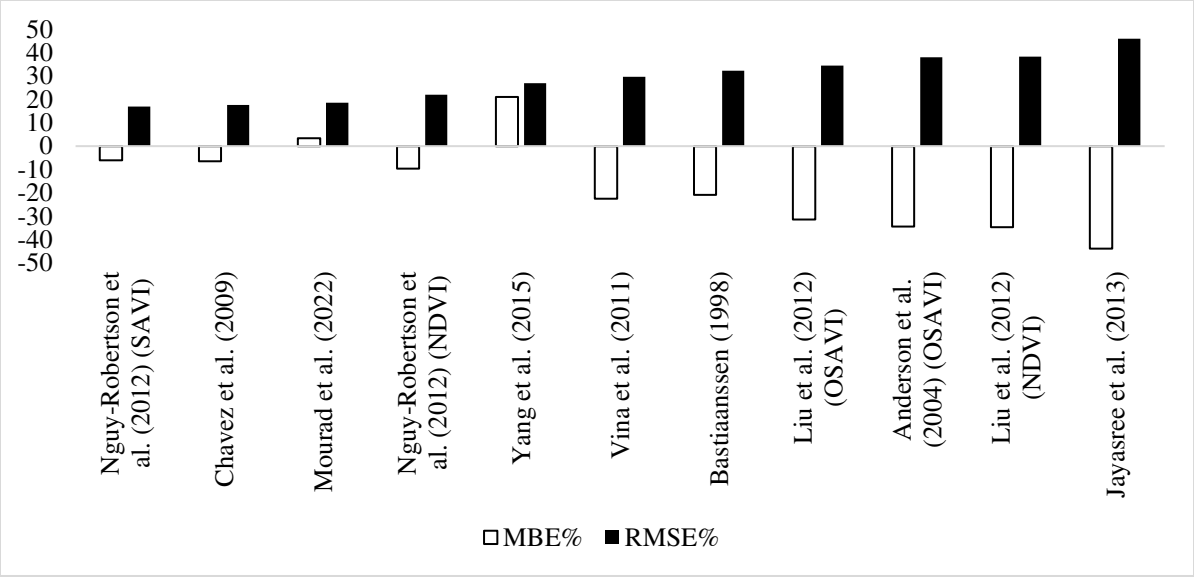

Figure 18: Error analysis for the Sentinel2-based LAI estimation

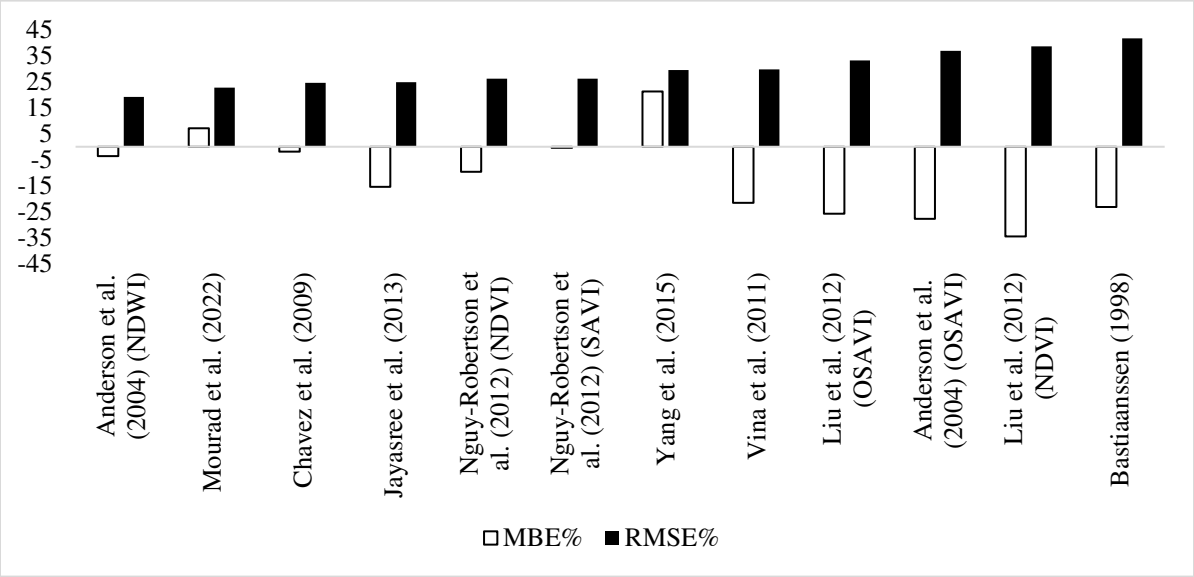

Figure 19: Error analysis for the MSR5-based LAI estimation

3.3.2 Crop Height Estimation

Based on Table 6, eight models were selected to estimate the Hc; those models were based on different VIs and observed LAI values. The estimated VIs from each RS platform result shown in section 3.1 and the observed LAI shown in Figure 4 were used as input values for these

functions; MADA was applied to reject some of the Hc data outliers throughout all the functions used. The MSR-5 sensor VI values were also used in addition to the tested platforms. Figure 20 to Figure 24 and Tables in Appendix B show the statistical analysis for each Hc function resulting from UAS, PlanetDove, Landsat, Sentinel-2, and MSR-5 RS platforms, respectively.

The findings of estimating Hc reveal that despite the variability of RS platform reflectance data, the relative performance of the used models to estimate Hc remained consistent. This consistency suggests that choosing a suitable function and VI- or LAI-based model is more critical than selecting a specific RS platform. As shown in the Figures below, the better performance functions were based on OSAVI, NDWI, and observed LAI, which are crucial factors to consider. Furthermore, these high-performance models have the same site conditions as LIRF, emphasizing the importance of choosing functions developed based on similar site conditions, including weather conditions, irrigation treatment, agricultural timing, and maize type. This understanding can significantly enhance the accuracy of canopy height estimations.

The highest performance of Hc estimation resulted from Costa-Filho et al. (2021) and Anderson et al. (2004) functions. Costa-Filho et al. (2021) model performed consistently well across all RS platforms with good performance and low RMSE%; this model appears to be the most reliable for estimating Hc in dry areas in Colorado or areas with similar weather conditions. The high performance in this study is interpreted by noting that the study was conducted in LIRF, showing the same weather conditions as this study. Anderson et al. (2004) functions that were based on using OSAVI- and NDWI to estimate the Hc showed higher performance across all RS platforms. On the other hand, the Hc estimation function by Khaliq et al. (2018), Arslan et al. (2022), and Yang et al. (2015) showed poor performance with an RMSE% exceeding 50%. The reason for the high error in these studies might be that the maize genetic varieties are

different from the one used in this research; different types of maize have different average canopy heights and structures. Also, different environmental conditions may result in different crop heights since soil type, moisture levels, temperature, and sunlight intensity influence maize height. In the Arslan et al. (2022) study, silage maize was planted, and the function in this study was built on the Hc observed data, which exceeded 2.5 m height. As for Khaliq et al. (2018), the Hc function was based on ground observed data, which averaged 2.46 m.

Overall, estimating Hc using different RS platforms and models demonstrates the critical importance of model selection and calibration. The Costa-Filho et al. (2021) model provided reliable estimates, making it a preferred choice for Hc estimation in conditions similar to LIRF. Conversely, models by Arslan et al. (2022) and Khaliq et al. (2018) showed poor performance, highlighting the need for site-specific models suitable to local conditions. This underscores the importance of considering environmental conditions and the specific characteristics of the RS platforms and models used in agricultural monitoring.

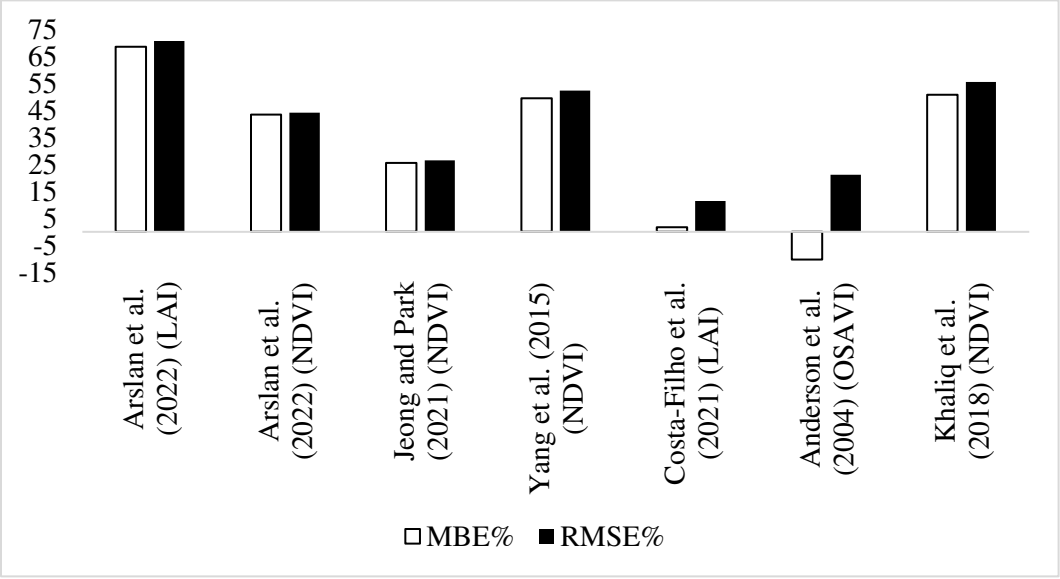

Figure 20: Error analysis for the UAS-based Hc estimation

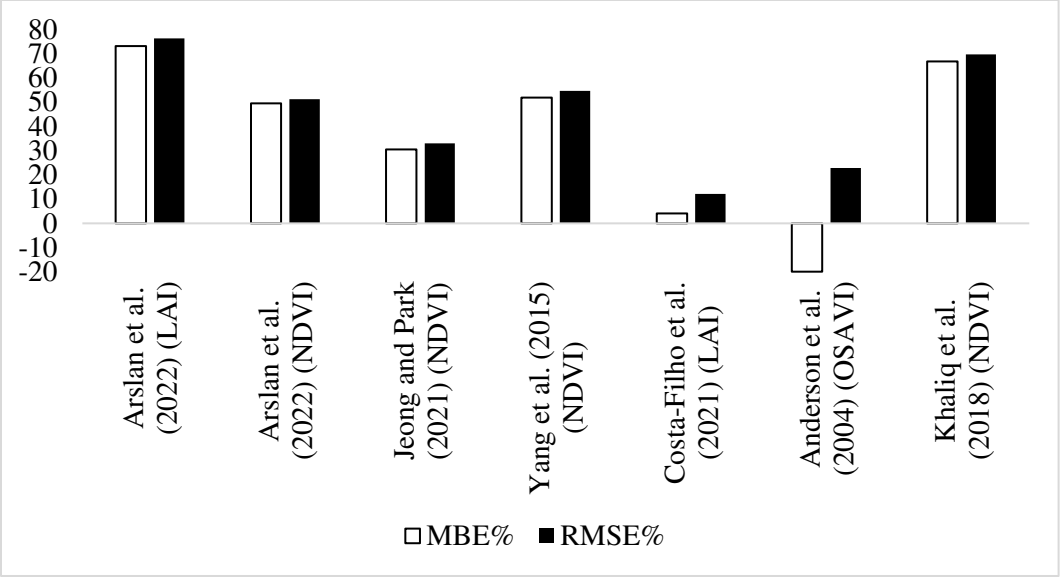

Figure 21: Error analysis for the Planet-based Hc estimation

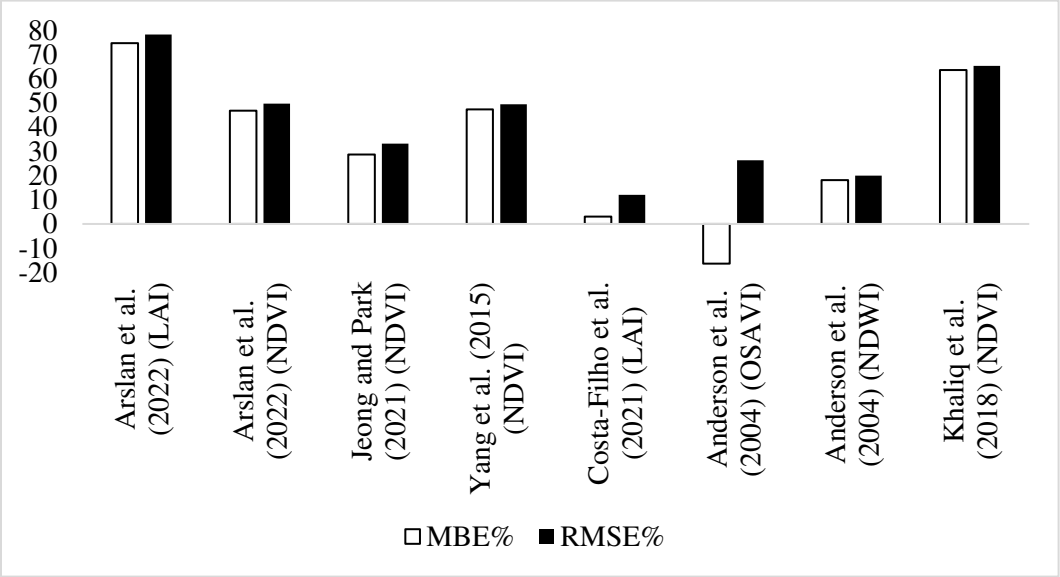

Figure 22: Error analysis for the Landsat-based Hc estimation

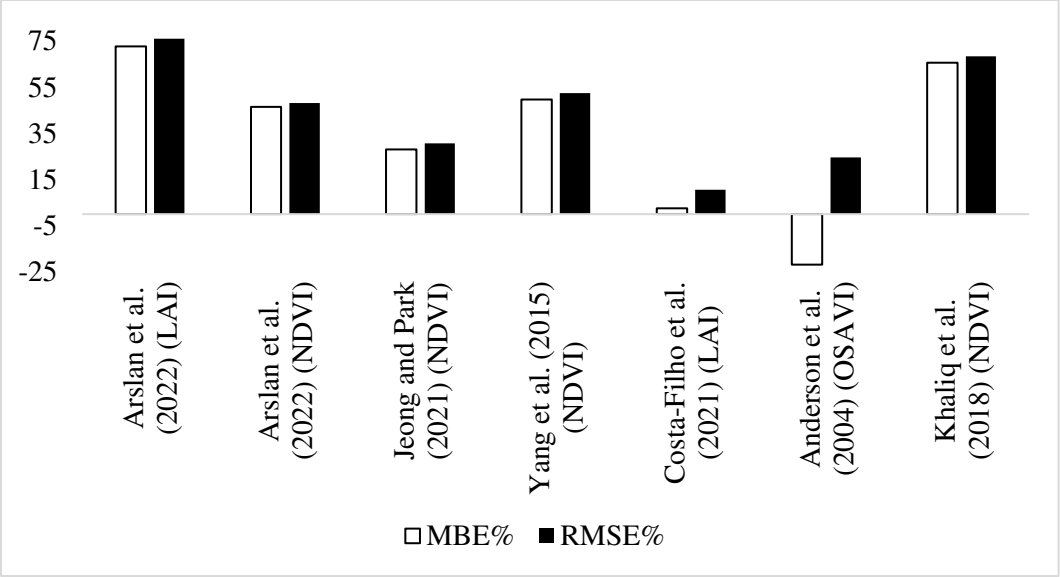

Figure 23: Error analysis for the Sentinel2-based Hc estimation

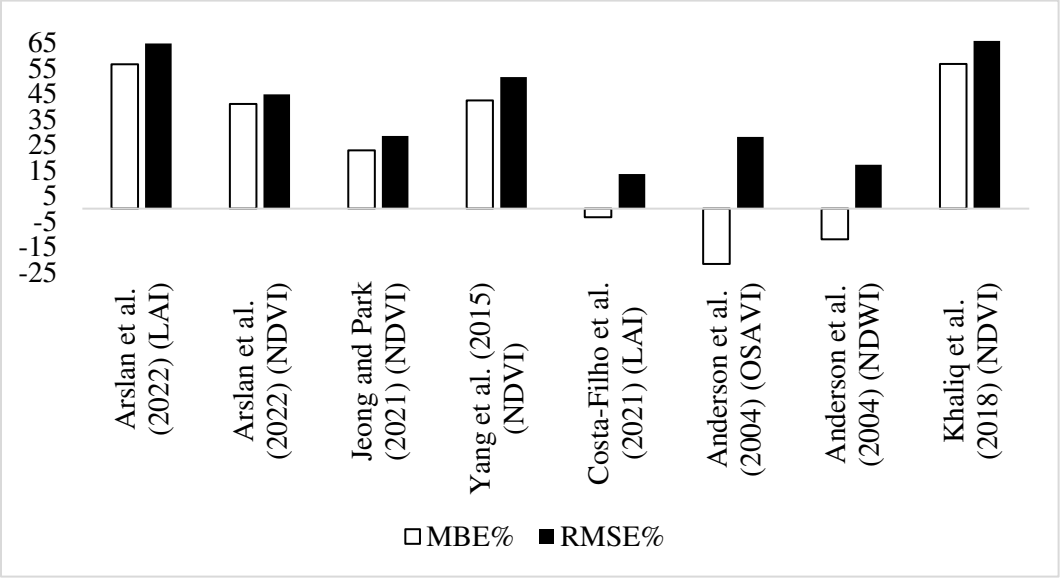

Figure 24: Error analysis for the MSR5-based Hc estimation

3.3.3 Crop Fractional Cover Estimation

Based on Table 7, three models were selected to estimate the Fc; those models were based on the NDVI. The estimated NDVI values resulting from each RS platform result shown in section 3.1 were used as input values for these functions and MADA was applied to the resulting

Fc data to reject the data outlier. The MSR-5 sensor NDVI values were also used in addition to the tested platforms. Figure 25 and Tables in Appendix C show the statistical analysis for each Fc function resulting from UAS, PlanetDove, Landsat, Sentinel-2, and MSR-5 RS platforms, respectively.

Consistent results and performance were noticed for all functions used to estimate Fc across all RS platforms. The UAS, which has the higher spatial resolution, showed a relatively higher performance in estimating Fc. However, Sentinel-2, which has a lower spatial resolution, did not show the lowest performance estimating Fc. This suggests that factors other than spatial resolution, such as specific characteristics of the Fc models and their calibration, may play a significant role in the accuracy of Fc estimation.

Across all platforms, the Gitelson (2013) model consistently demonstrated the lowest error values, indicating that it has more reliable results for estimating Fc. The model by Yang et al. (2015) showed relatively lower performance in estimating Fc than the other models, reflecting the importance of using models that developed in similar site areas, such as weather conditions, irrigation treatment, and maize type.

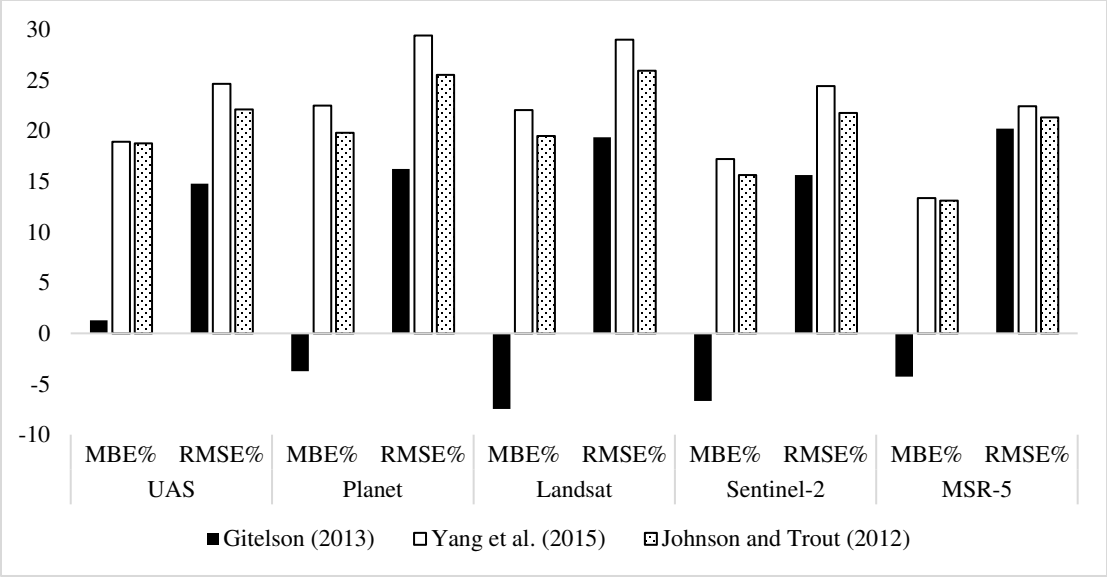

Figure 25: Error analysis for the Fc estimation

3.4 Estimation of actual crop coefficients and ETa

Based on Table 8, five models were selected to estimate the Kcb; those models were based on different VIs or the fractional values estimated by Johnson and Trout (2012). The MSR-5 sensor VI values were also used in addition to the tested RS platforms. After estimating the Kcb, the ETa was estimated using Equation 5. The ETr data were collected from COAGMET and shown in Table 16 below. Figure 26 to Figure 30 and Tables in Appendix D show the statistical analysis for each ETa function resulting from UAS, PlanetDove, Landsat, Sentinel-2, and MSR-5 RS platforms, respectively, compared to the ETgage 'measured' ETa values for the full irrigation field only. Just the fully irrigated field was instrumented with an ETgage atmometer.

All models performed well in estimating the ETa across all RS platforms. ETa estimations using the UAS and MSR-5 RS platforms showed the lowest RMSE%, showing that RS platforms with higher spatial resolution, and obtaining surface reflectance data closer to the ground, can perform better in estimating ETa. However, the results of PlanetDove functions

failed to perform better than those of Landsat and Sentinel-2 platforms in estimating ETa despite its higher spatial resolution, which indicates that other factors, such as imagery atmospheric calibration and ET model calibration and site conditions, are also essential to be considered.

The performance of models using inputs of VIs did not reveal a significant difference in estimating ETa. However, the model proposed by Trout and DeJonge, which utilized Fc as an input variable for ETa estimation, demonstrated a notably higher performance than other models, indicating a potential area for further research on the relationship between the Fc and ETa. The analysis also revealed that most models underestimated the ETa with negative MBE values. This shows the importance of continuous calibration of the models.

Table 16: ETr values collected from COAGMET

Date	ETr (mm)	Date	ETr (mm)	Date	ETr (mm)
14/Jul	7.40	05/Aug	7.66	05/Sep	6.48
15/Jul	8.40	06/Aug	7.99	07/Sep	5.84
16/Jul	6.76	09/Aug	7.36	08/Sep	4.00
17/Jul	8.76	10/Aug	8.50	11/Sep	4.15
20/Jul	7.66	11/Aug	5.96	13/Sep	6.42
21/Jul	6.16	17/Aug	5.23	18/Sep	5.67
25/Jul	7.61	18/Aug	6.29	19/Sep	5.73
26/Jul	8.44	19/Aug	7.13	20/Sep	5.95
27/Jul	7.41	24/Aug	6.15	23/Sep	3.75
30/Jul	6.91	29/Aug	4.97	25/Sep	3.70
01/Aug	6.62	31/Aug	5.19	26/Sep	4.65
02/Aug	6.52	02/Sep	7.72	27/Sep	3.84
04/Aug	7.09	03/Sep	6.85	28/Sep	4.26

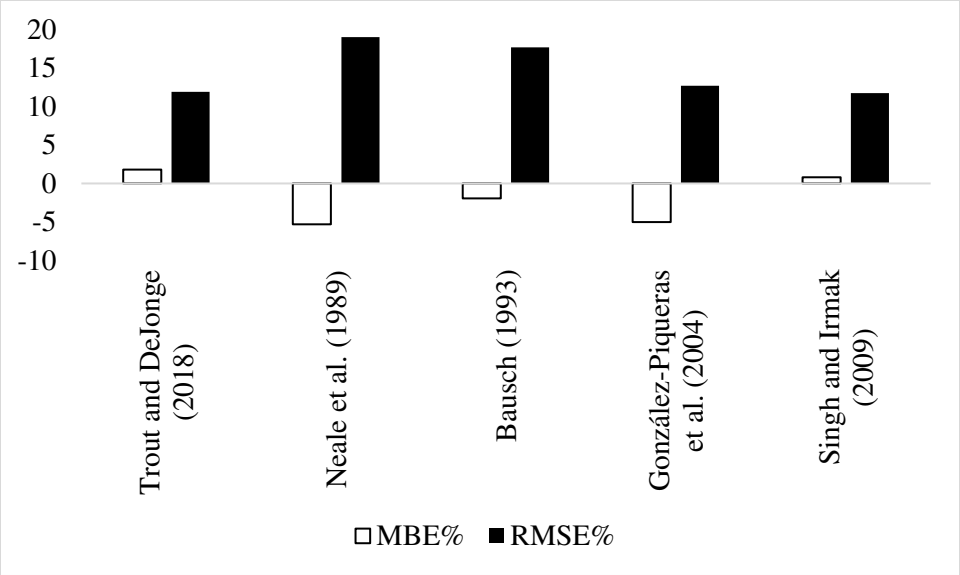

Figure 26: Error analysis for the UAS-based ETa estimation

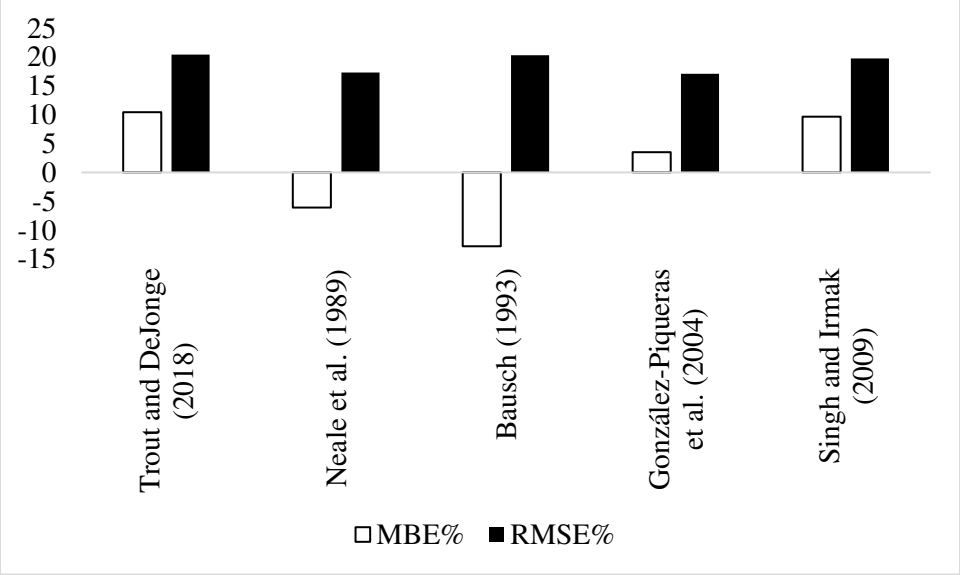

Figure 27: Error analysis for the Planet-based ETa estimation

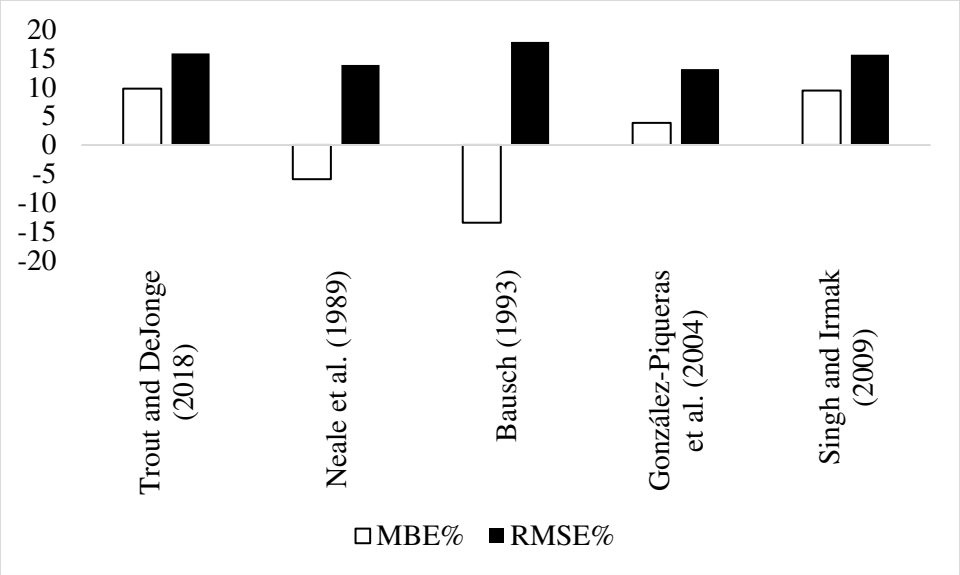

Figure 28: Error analysis for the Landsat-based ETa estimation

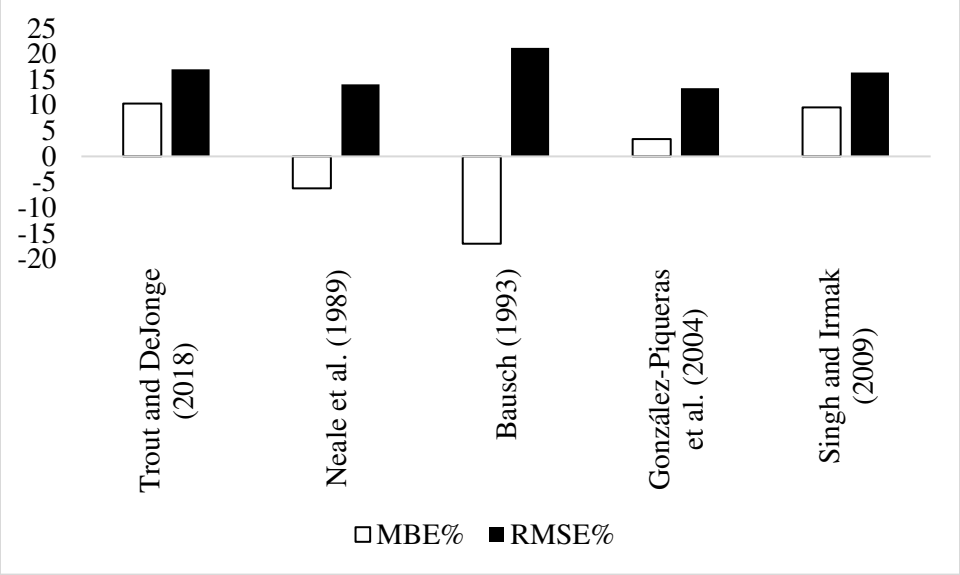

Figure 29: Error analysis for the Sentinel2-based ETa estimation

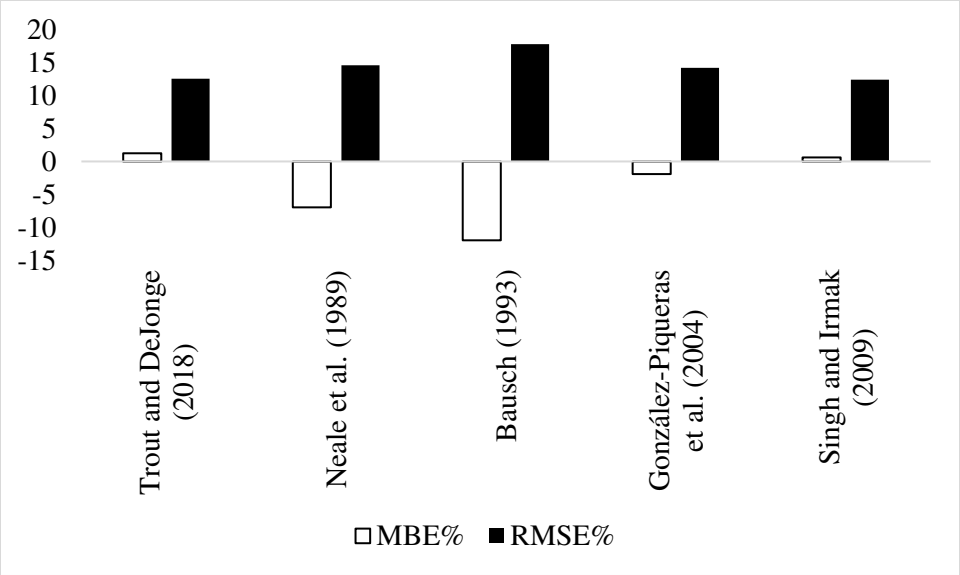

Figure 30: Error analysis for the MSR5-based ETa estimation

3.5 Balanced Analysis

3.5.1 Leaf Area Index Analysis

A new analysis was done to estimate the LAI using each RS platform with closely coinciding overpass dates. This new study was done to balance the comparison between each RS platform by having similar/close dates, number of data points (days in time) compared. Figure 31 to Figure 35 show the MBE% and RMSE% for the UAS, Planet, Landsat, Sentinel-2, and MSR-5 platforms, respectively, used to estimate the LAI.

The performance of different RS platforms in estimating the LAI varied considerably, as indicated by the MBE% and RMSE% metrics. The Landsat platform exhibited a wide range of performance across various models, suggesting that while Landsat can occasionally provide accurate LAI estimates, it has some limitations in accurately estimating the LAI for some models. Sentinel-2, on the other hand, demonstrated a slightly better overall performance than Landsat, indicating moderate reliability. Sentinel's ability to produce good performance metrics

in certain models highlights its potential for more accurate LAI estimation under specific conditions. The Planet platform generally produced a fair performance, suggesting a slightly higher accuracy level. However, like Landsat and Sentinel, Planet's data showed variability, with many models exhibiting poor performance.

UAS data consistently showed better performance across various models compared to other platforms. The best-performing models using UAS data achieved good performance levels with RMSE% values below 20%, and even the less accurate models generally fell within the fair range. This consistent performance underscores the higher accuracy and reliability of UAS for LAI estimation, likely due to its higher spatial resolution, flexibility in data acquisition, and its proximity. The MSR-5 platform displayed mixed results, depending on the model used, suggesting that while MSR-5 can be useful, its performance is less consistent and generally lower than that of UAS for some models. Attention should be given on the type of RS data used in the development of given CBPC models.

The UAS data provided the most reliable LAI estimates across different models, outperforming other RS platforms. Sentinel and Planet data showed moderate reliability, with potential for good performance in specific scenarios. Landsat generally exhibited higher variability and less reliability. MSR-5 demonstrated less consistent performance. These findings highlight the importance of choosing the appropriate RS platform based on the specific requirements and conditions of the study to ensure accurate LAI estimation.

The analysis of early and late crop growth stages reveals significant variations in the performance of the RS platforms in estimating LAI. By comparing the MBE% and RMSE% for each platform, this will allow showing the trends and identify which stages and platforms provide more accurate and stable results. Table 17 to Table 21 show the performance of UAS,

Planet, Landsat, Sentinel-2, and MSR-5 platforms in estimating the LAI during the early and late stages of the maize development.

During the early growth stages, the performance of RS platforms varied significantly. Generally, slightly higher RMSE% and MBE% values were observed, indicating less accuracy and greater bias in LAI estimates. For many RS platforms, the early-stage results exhibited considerable errors, reflecting the challenges associated with capturing accurate data during the initial phases of crop growth when the canopy is less developed and spectral signals are less accurate. Platforms like UAS, Planet, and MSR-5 demonstrated relatively better performance during the early stages compared to others. This suggests that in the early stages, with less dense canopies, the performance of higher spatial resolution RS platforms is higher, since they capture the less dense vegetation more accurately without including the soil background that will impact the results.

In the late growth stages, the RS platforms generally exhibited improved performance compared to the early stages. This trend of improved performance in the late stages was consistent, especially for the lower spatial resolution RS platforms. The improved performance during the late stages can be attributed to the more stable and developed canopy structure, which provides clearer spectral signals for the RS platforms to capture. The late growth stages generally provided better results across all RS platforms due to more stable canopy conditions. The UAS platform proved to be the most stable and reliable for LAI estimation, consistently showing moderate to good performance across both early and late stages. Sentinel also showed reasonable stability, particularly in the late stages, while platforms like Landsat and Planet exhibited higher variability and less consistent performance.

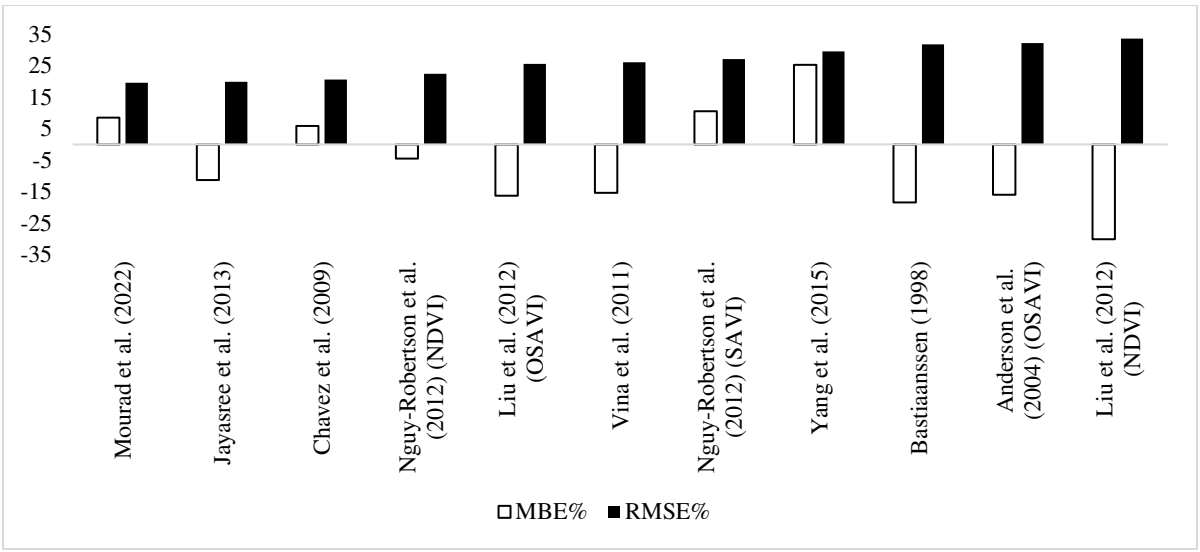

Figure 31: Error analysis for the UAS-based LAI balanced analysis

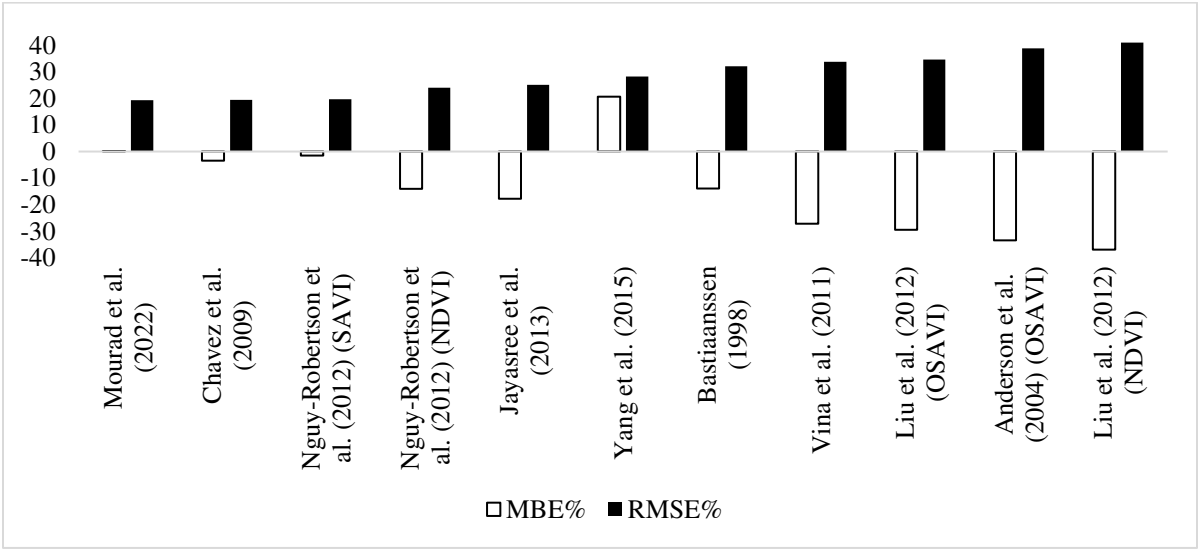

Figure 32: Error analysis for the Planet-based LAI balanced analysis

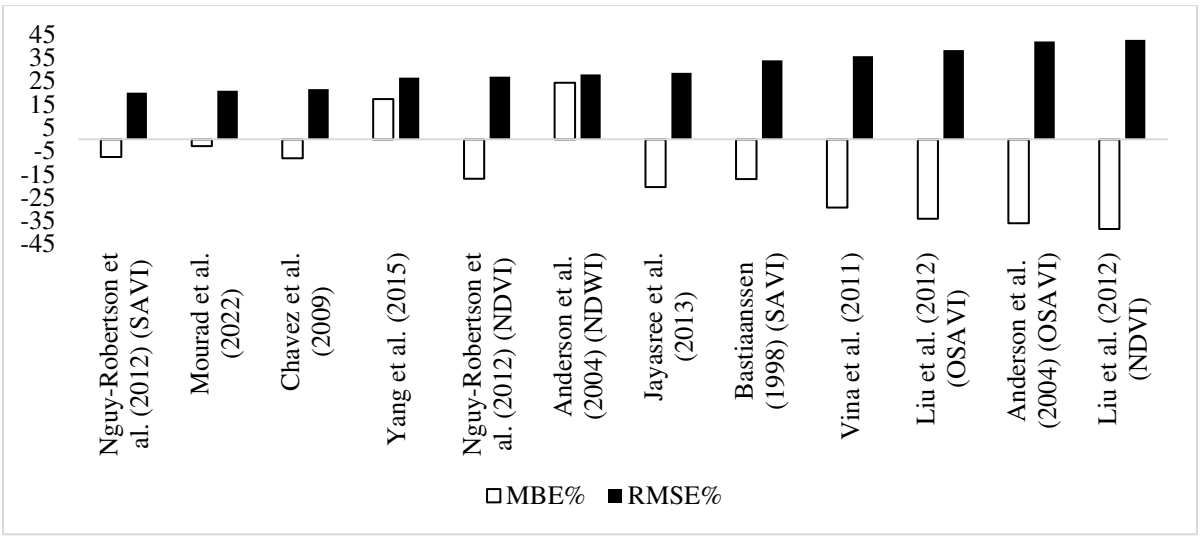

Figure 33: Error analysis for the Landsat-based LAI balanced analysis

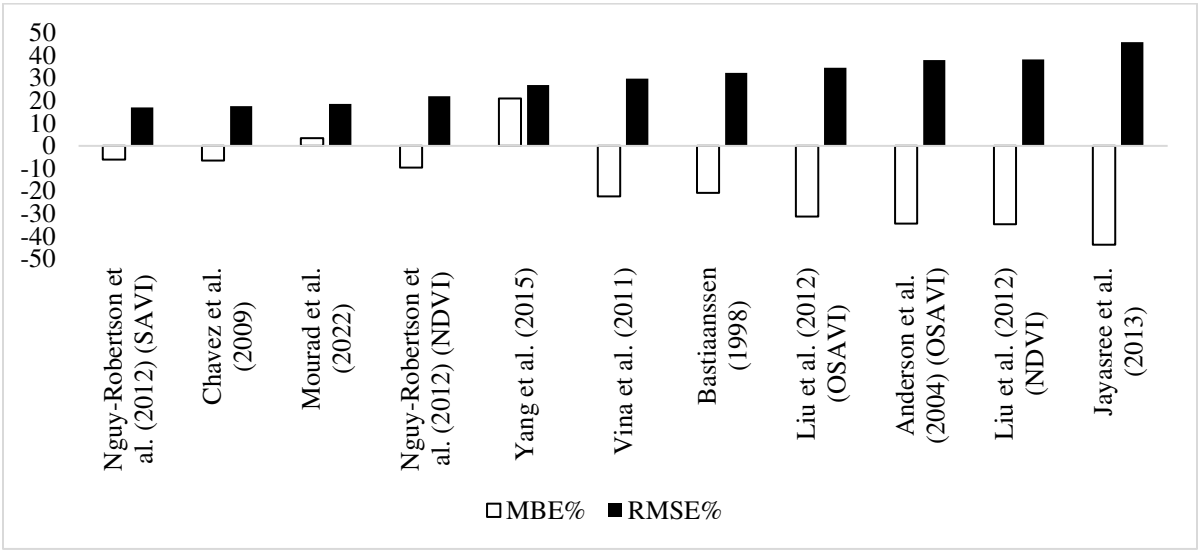

Figure 34: Error analysis for the Sentinel2-based LAI balanced analysis

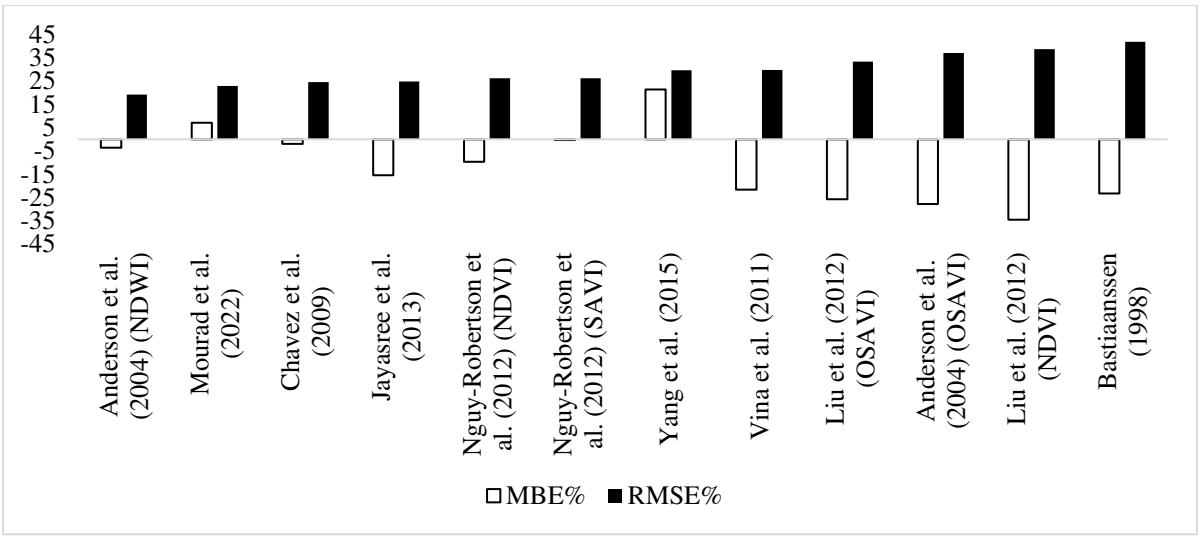

Figure 35: Error analysis for the MSR5-based LAI balanced analysis

Table 17: Early and late stages error analysis for the UAS-based LAI estimation

Reference	Early Stages				Late stages			
	MBE (m2/m2)	MBE %	RMSE (m2/m2)	RMSE%	MBE (m2/m2)	MBE%	RMSE (m2/m2)	RMSE%
Mourad et al. (2022) (NDVI)	0.6	18.6	0.9	27.4	0.0	-0.3	0.3	8.9
Jayasree et al. (2013) (NDVI)	-0.1	-2.2	0.6	17.4	-0.7	-20.2	0.8	22.0
Nguy-Robertson et al. (2012) (NDVI)	0.3	7.7	0.9	26.7	-0.6	-15.6	0.6	18.0
Nguy-Robertson et al. (2012) (SAVI)	0.8	24.3	1.3	37.9	0.0	-1.1	0.5	12.9
Vina et al. (2011) (NDVI)	-0.1	-2.3	0.7	22.5	-1.0	-28.0	1.0	29.0
Liu et al. (2012) (NDVI)	-0.7	-22.1	0.9	26.4	-1.4	-38.3	1.4	39.4
Liu et al. (2012) (OSAVI)	-0.1	-3.7	0.7	21.3	-1.0	-28.3	1.0	29.0
Yang et al. (2015) (NDVI)	1.1	33.3	1.2	36.7	0.6	18.1	0.8	21.9
Bastiaanssen (1998) (SAVI)	-0.1	-2.1	1.0	29.7	-1.1	-32.2	1.2	33.2
Chavez et al. (2009) (OSAVI)	0.5	16.2	1.0	29.8	-0.1	-1.9	0.3	9.6
Anderson et al. (2004) (OSAVI)	0.1	1.9	1.0	31.2	-1.1	-31.9	1.2	33.0

Table 18: Early and late stages error analysis for the Planet-based LAI estimation

Reference	Early Stages				Late stages			
	MBE (m2/m2)	MBE %	RMSE (m2/m2)	RMSE %	MBE (m2/m2)	MBE %	RMSE (m2/m2)	RMSE %
Mourad et al. (2022) (NDVI)	0.8	21.7	1.0	27.4	-0.1	-4.0	0.5	15.1
Jayasree et al. (2013) (NDVI)	0.0	-0.3	0.5	14.7	-0.8	-23.0	1.0	27.4
Nguy-Robertson et al. (2012) (NDVI)	0.3	7.4	0.7	21.4	-0.7	-20.9	0.9	25.2
Nguy-Robertson et al. (2012) (SAVI)	0.6	17.9	0.9	26.4	-0.2	-4.4	0.4	12.4
Vina et al. (2011) (NDVI)	-0.2	-6.2	0.6	18.4	-1.1	-32.9	1.3	36.1
Liu et al. (2012) (NDVI)	-0.7	-19.8	0.8	23.8	-1.5	-42.0	1.6	45.1
Liu et al. (2012) (OSAVI)	-0.4	-12.2	0.6	18.3	-1.1	-32.7	1.2	35.5
Yang et al. (2015) (NDVI)	1.4	39.1	1.4	41.6	0.6	18.7	0.8	23.9
Bastiaanssen (1998) (SAVI)	0.0	-0.2	1.0	31.2	0.3	8.5	1.1	34.6
Chavez et al. (2009) (OSAVI)	0.5	15.7	0.8	23.9	-0.2	-6.1	0.5	13.2
Anderson et al. (2004) (OSAVI)	-0.5	-13.6	0.8	21.9	-1.3	-38.5	1.4	40.9

Table 19: Early and late stages error analysis for the Landsat-based LAI estimation

Reference	Early Stages				Late stages			
	MBE (m2/m2)	MBE %	RMSE (m2/m2)	RMSE %	MBE (m2/m2)	MBE %	RMSE (m2/m2)	RMSE %
Mourad et al. (2022) (NDVI)	0.1	3.7	0.6	18.3	-0.2	-5.0	0.7	21.0
Jayasree et al. (2013) (NDVI)	-0.6	-15.9	0.8	23.3	-0.8	-24.1	1.1	31.2
Nguy-Robertson et al. (2012) (NDVI)	-0.5	-13.4	0.8	23.7	-0.7	-21.2	1.0	29.7
Nguy-Robertson et al. (2012) (SAVI)	-0.2	-6.6	0.7	20.1	-0.4	-10.9	0.7	20.7
Vina et al. (2011) (NDVI)	-0.9	-24.8	1.1	30.4	-1.2	-33.3	1.3	38.6
Liu et al. (2012) (NDVI)	-1.1	-33.0	1.3	36.3	-1.5	-42.5	1.6	46.2
Liu et al. (2012) (OSAVI)	-1.1	-30.4	1.2	34.1	-1.3	-38.6	1.5	42.0
Yang et al. (2015) (NDVI)	0.8	23.9	1.0	28.8	0.6	17.8	0.9	26.3
Bastiaanssen (1998) (SAVI)	-0.8	-24.5	1.1	33.5	-0.3	-8.1	1.0	31.4
Chavez et al. (2009) (OSAVI)	-0.3	-7.6	0.7	19.7	-0.4	-12.7	0.8	21.6
Anderson et al. (2004) (NDWI)	1.1	30.4	1.1	32.7	0.8	22.7	0.9	25.3
Anderson et al. (2004) (OSAVI)	-1.2	-35.7	1.4	39.0	-1.5	-44.1	1.6	46.9

Table 20: Early and late stages error analysis for the Sentinel2-based LAI estimation

Reference	Early Stages				Late stages			
	MBE (m2/m2)	MBE %	RMSE (m2/m2)	RMSE %	MBE (m2/m2)	MBE %	RMSE (m2/m2)	RMSE %
Mourad et al. (2022) (NDVI)	0.7	22.0	1.1	35.3	0.1	2.3	0.4	12.6
Jayasree et al. (2013) (NDVI)	-1.1	-34.8	1.2	37.5	-1.6	-46.3	1.7	48.1
Nguy-Robertson et al. (2012) (NDVI)	0.3	8.0	1.1	35.2	-0.5	-14.4	0.7	19.0
Nguy-Robertson et al. (2012) (SAVI)	0.0	-0.7	0.6	19.5	-0.4	-12.6	0.6	16.7
Vina et al. (2011) (NDVI)	-0.1	-3.3	1.0	32.0	-0.9	-26.3	1.0	28.7
Liu et al. (2012) (NDVI)	-0.7	-20.6	0.9	28.5	-1.3	-36.8	1.4	39.3
Liu et al. (2012) (OSAVI)	-0.6	-18.6	0.9	27.0	-1.3	-36.1	1.3	37.9
Yang et al. (2015) (NDVI)	1.0	32.4	1.2	36.6	0.8	22.4	0.9	26.1
Bastiaanssen (1998) (SAVI)	-0.4	-12.8	1.2	36.6	-0.9	-27.3	1.0	32.8
Chavez et al. (2009) (OSAVI)	0.3	9.2	0.9	28.4	-0.5	-13.6	0.6	17.3
Anderson et al. (2004) (OSAVI)	-0.6	-17.3	1.0	31.5	-1.5	-42.3	1.5	44.2

Table 21: Early and late stages error analysis for the MSR5-based LAI estimation

Reference	Early Stages				Late stages			
	MBE (m2/m2)	MBE %	RMSE (m2/m2)	RMSE %	MBE (m2/m2)	MBE %	RMSE (m2/m2)	RMSE %
Mourad et al. (2022) (NDVI)	0.6	20.5	0.9	27.9	0.3	8.4	0.7	19.4
Jayasree et al. (2013) (NDVI)	-0.2	-5.2	0.5	17.2	-0.5	-13.4	0.8	21.8
Nguy-Robertson et al. (2012) (NDVI)	0.1	3.7	0.8	24.9	-0.2	-6.9	0.7	21.0
Nguy-Robertson et al. (2012) (SAVI)	0.6	17.9	1.1	34.4	0.1	3.1	0.6	18.4
Vina et al. (2011) (NDVI)	-0.3	-10.9	0.7	22.6	-0.7	-19.6	0.9	25.9
Liu et al. (2012) (NDVI)	-0.8	-25.7	0.9	28.4	-1.2	-33.1	1.3	36.7
Liu et al. (2012) (OSAVI)	-0.3	-10.3	0.7	23.7	-0.9	-26.4	1.0	29.7
Yang et al. (2015) (NDVI)	1.1	36.9	1.3	40.5	0.9	24.4	1.1	30.8
Bastiaanssen (1998) (SAVI)	-0.7	-23.1	1.1	38.8	-0.2	-6.1	1.2	42.9
Chavez et al. (2009) (OSAVI)	0.5	17.4	1.0	32.6	0.0	1.4	0.6	16.6
Anderson et al. (2004) (NDWI)	0.1	3.2	0.7	22.1	0.0	0.1	0.4	11.0
Anderson et al. (2004) (OSAVI)	-0.3	-8.5	0.9	30.3	-1.0	-29.6	1.2	32.7

3.5.2 Crop Height Analysis

A new analysis was done to estimate the Hc using each RS platform with closely coinciding overpass dates. This new study was done to balance the comparison between each RS platform by having similar/close dates, number of data points (days in time) compared. Figure 36 to Figure 40 show the MBE% and RMSE% for the UAS, Planet, Landsat, Sentinel-2, and MSR-5 platforms, respectively, used to estimate the Hc.

The evaluation of various RS platforms for estimating Hc reveals distinct differences in performance and reliability. In this analysis, UAS showed a slightly better performance than the other platforms, with a generally lower RMSE%. However, the Landsat and Sentinel-2 platforms showed higher performances than the Planet and MSR-5 in estimating Hc.

The evaluation of various RS platforms for estimating Hc reveals distinct differences in performance and reliability. The UAS showed a slightly better performance than the other platforms, with generally lower RMSE% values, indicating that UAS data is more accurate and reliable for Hc estimation. This higher performance can be attributed to the higher spatial resolution and its proximity, which allows for more detailed and precise measurements. On the other hand, and despite having a lower spatial resolution, Landsat and Sentinel-2 platforms showed higher performances than the Planet and MSR-5 in estimating Hc. The lower performance of the Planet and MSR-5 can be interpreted by noting that the tested models were developed using lower spatial resolution, such as ASTER images (15-meter spatial resolution), Sentinel-2 (10-meter spatial resolution).

The analysis of early and late crop growth stages reveals significant variations in the performance of the RS platforms in estimating the Hc. By comparing the MBE% and RMSE%

for each platform, this will allow showing the trends and identify which stages and platforms provide more accurate and stable results. Table 22 to Table 26 show the performance of UAS, Planet, Landsat, Sentinel-2, and MSR-5 platforms in estimating the LAI during the early and late stages of the maize development.

During the early stages of crop growth, all the RS platforms had a similar trend, and their performance had a slight difference. In the late stages, the performance of the RS platforms did not significantly change except for the UAS which demonstrated a significantly higher performance in estimating Hc during the late stages. Also, a slightly better performance for most utilized RS platforms was noticed.

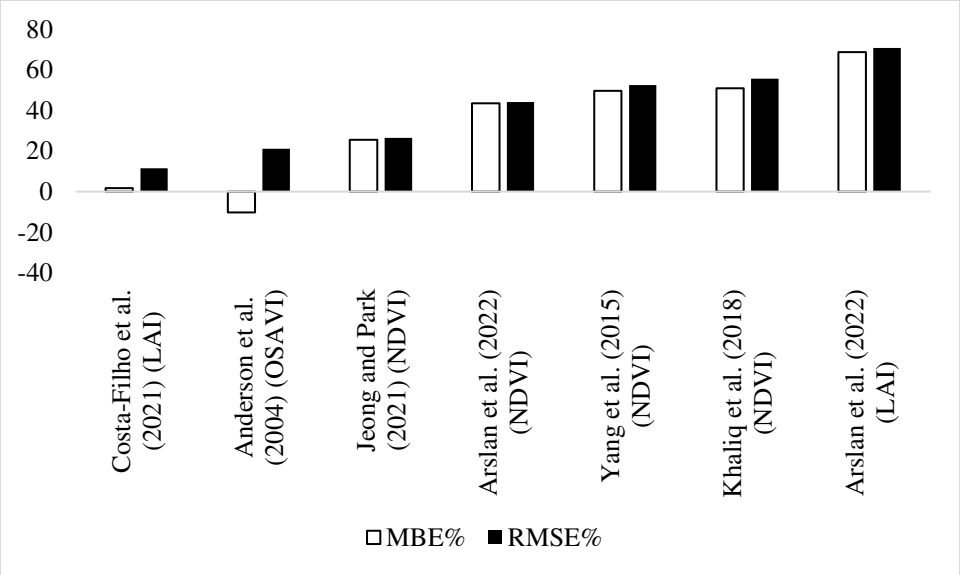

Figure 36: Error analysis for the UAS-based balanced analysis for Hc estimation

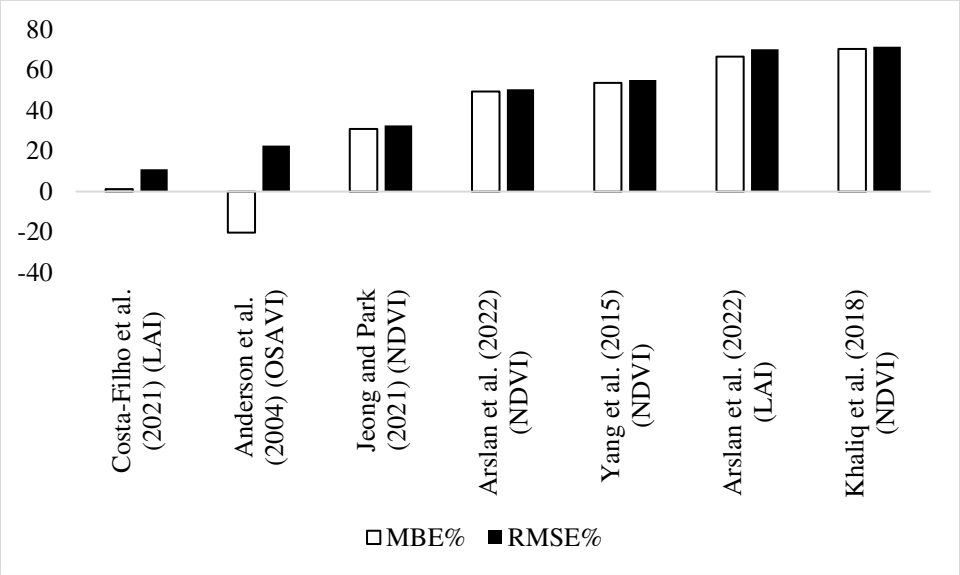

Figure 37: Error analysis for the Planet-based balanced analysis for Hc estimation

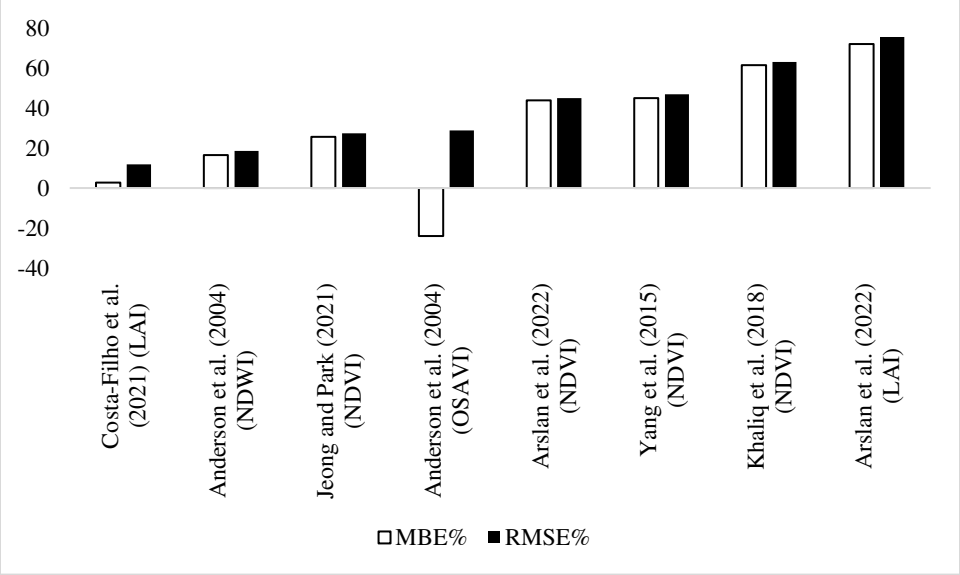

Figure 38: Error analysis for the Landsat-based balanced analysis for Hc estimation

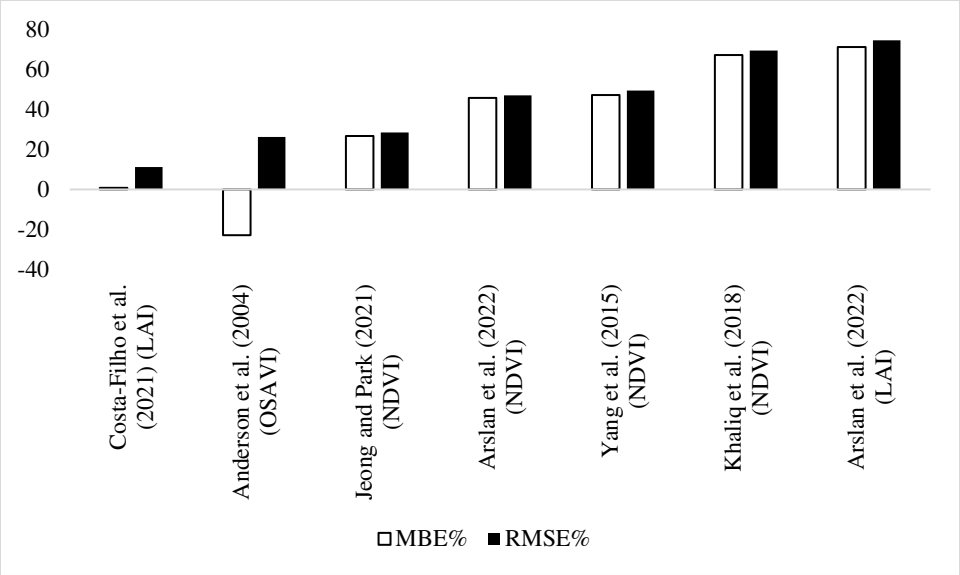

Figure 39: Error analysis for the Sentinel2-based balanced analysis for Hc estimation

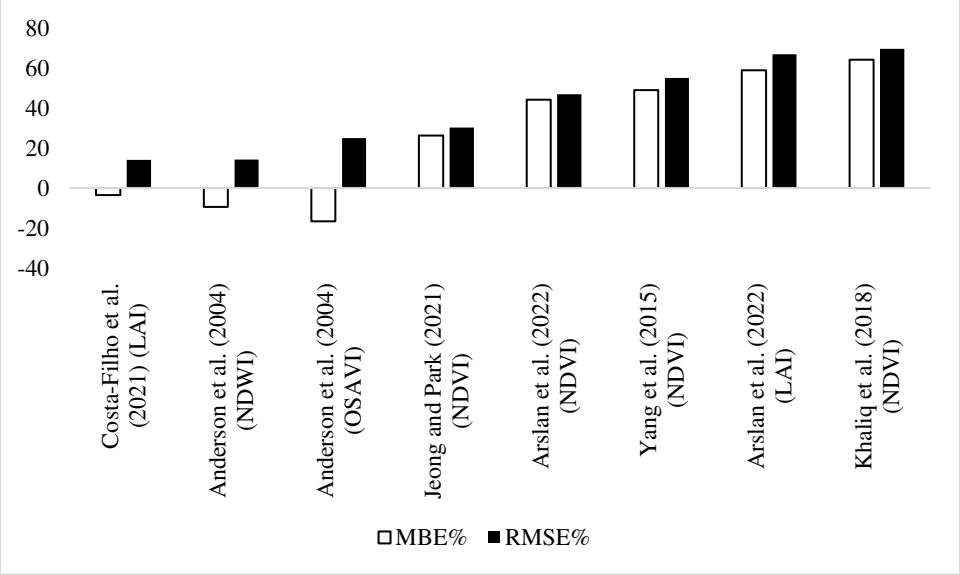

Figure 40: Error analysis for the MSR5-based balanced analysis for Hc estimation

Table 22: Early and late stages error analysis for the UAS-based Hc estimation

Reference	Early Stages				Late Stages			
	MBE (m)	MBE %	RMSE (m)	RMSE %	MBE (m)	MBE %	RMSE (m)	RMSE %
Arslan et al. (2022) (LAI)	1.0	68.7	1.1	71.8	1.2	78.0	1.2	82.0
Arslan et al. (2022) (NDVI)	0.7	48.8	0.7	49.8	0.6	35.8	0.6	36.9
Jeong and Park (2021) (NDVI)	0.4	29.3	0.4	30.9	0.3	19.3	0.4	21.2
Yang et al. (2015) (NDVI)	0.6	47.1	0.7	49.3	0.7	41.5	0.7	42.7
Costa-Filho et al. (2021) (LAI)	0.0	2.6	0.2	11.9	0.0	2.9	0.2	12.0
Anderson et al. (2004) (OSAVI)	-0.3	-21.3	0.4	28.3	-0.5	-28.7	0.5	29.2
Anderson et al. (2004) (NDWI)	0.3	19.5	0.3	21.6	0.2	11.5	0.2	13.0
Khaliq et al. (2018) (NDVI)	0.9	64.1	0.9	66.2	0.9	56.7	1.0	57.6

Table 23: Early and late stages error analysis for the Planet-based Hc estimation

Reference	Early Stages				Late Stages			
	MBE (m)	MBE %	RMSE (m)	RMSE %	MBE (m)	MBE %	RMSE (m)	RMSE %
Arslan et al. (2022) (LAI)	1.0	67.9	1.1	70.8	1.2	77.8	1.2	81.4
Arslan et al. (2022) (NDVI)	0.7	50.5	0.8	51.8	0.6	37.5	0.6	38.2
Jeong and Park (2021) (NDVI)	0.4	30.2	0.5	32.0	0.3	20.9	0.4	22.2
Yang et al. (2015) (NDVI)	0.7	48.8	0.8	52.0	0.7	44.3	0.8	45.1
Costa-Filho et al. (2021) (LAI)	0.0	-0.2	0.2	11.1	0.0	2.7	0.2	11.2
Anderson et al. (2004) (OSAVI)	-0.3	-18.8	0.3	22.1	-0.6	-33.8	0.6	33.9
Khaliq et al. (2018) (NDVI)	1.0	71.6	1.1	74.6	1.0	59.4	1.0	60.0

Table 24: Early and late stages error analysis for the Landsat-based Hc estimation

Reference	Early Stages				Late Stages			
	MBE (m)	MBE %	RMSE (m)	RMSE %	MBE (m)	MBE %	RMSE (m)	RMSE %
Arslan et al. (2022) (LAI)	1.0	62.0	1.0	65.0	1.2	75.2	1.2	79.1
Arslan et al. (2022) (NDVI)	0.8	58.3	0.8	58.8	0.6	34.9	0.6	35.6
Jeong and Park (2021) (NDVI)	0.5	38.4	0.5	39.2	0.3	18.4	0.3	19.7
Yang et al. (2015) (NDVI)	0.9	61.9	0.9	63.2	0.7	39.9	0.7	40.5
Costa-Filho et al. (2021) (LAI)	0.0	0.4	0.2	10.7	0.0	2.7	0.2	11.6
Anderson et al. (2004) (OSAVI)	-0.2	-15.9	0.2	17.9	-0.5	-27.7	0.5	28.1
Khaliq et al. (2018) (NDVI)	1.1	79.5	1.1	80.6	0.9	55.2	0.9	55.7

Table 25: Early and late stages error analysis for the Sentinel2-based Hc estimation

Reference	Early Stages				Late Stages			
	MBE (m)	MBE %	RMSE (m)	RMSE %	MBE (m)	MBE %	RMSE (m)	RMSE %
Arslan et al. (2022) (LAI)	1.0	70.9	1.1	73.2	0.9	62.8	0.9	63.8
Arslan et al. (2022) (NDVI)	0.7	46.5	0.7	47.4	0.6	38.7	0.6	38.9
Jeong and Park (2021) (NDVI)	0.4	27.7	0.4	29.0	0.4	22.1	0.4	22.4
Yang et al. (2015) (NDVI)	0.7	51.4	0.8	55.4	0.8	46.5	0.8	47.5
Costa-Filho et al. (2021) (LAI)	0.0	1.0	0.2	11.0	0.0	2.9	0.2	12.3
Anderson et al. (2004) (OSAVI)	-0.1	-6.6	0.3	21.5	-0.3	-16.8	0.3	20.6
Khaliq et al. (2018) (NDVI)	0.9	64.5	1.0	67.8	0.5	30.0	0.5	31.9

Table 26: Early and late stages error analysis for the MSR5-based Hc estimation

Reference	Early Stages				Late Stages			
	MBE (m)	MBE %	RMSE (m)	RMSE %	MBE (m)	MBE %	RMSE (m)	RMSE %
Arslan et al. (2022) (LAI)	0.9	61.6	1.0	68.5	0.8	53.1	0.9	63.4
Arslan et al. (2022) (NDVI)	0.6	43.9	0.7	47.9	0.7	44.4	0.7	44.9
Jeong and Park (2021) (NDVI)	0.4	25.3	0.5	31.4	0.5	27.6	0.5	28.4
Yang et al. (2015) (NDVI)	0.7	45.0	0.8	54.0	0.9	56.0	0.9	56.2
Costa-Filho et al. (2021) (LAI)	0.0	0.5	0.2	12.1	-0.2	-11.4	0.3	17.4
Anderson et al. (2004) (OSAVI)	-0.2	-16.9	0.4	29.1	-0.3	-16.1	0.3	17.1
Anderson et al. (2004) (NDWI)	-0.2	-12.8	0.3	17.8	-0.1	-3.6	0.1	6.0
Khaliq et al. (2018) (NDVI)	0.9	60.2	1.0	68.4	1.2	70.7	1.2	70.9

3.5.3 Crop fractional cover Analysis

A new analysis was done to estimate the Fc using each RS platform with closely coinciding overpass dates. This new study was done to balance the comparison between each RS platform by having similar/close dates, number of data points (days in time) compared. Figure 41 show the MBE% and RMSE% for the UAS, Planet, Landsat, Sentinel-2, and MSR-5 platforms used to estimate the Fc.

The UAS platform exhibited the highest performance in Fc estimation, characterized by consistently low MBE and RMSE values across different models, underscoring the reliability of UAS data, likely attributed to its high spatial resolution enabling detailed vegetation monitoring. Landsat data, while not as precise as UAS, showed moderate to good performance in Fc estimation, suggesting that Landsat is a reliable option for Fc estimation. Sentinel-2 results also demonstrated strong performance, highlighting Sentinel-2's capability to provide consistent and accurate Fc estimates.

In contrast, Planet and MSR-5 results showed more variability in Fc estimation. The higher RMSE values and greater variability in MBE% suggest that both Planet and MSR-5 results are less reliable for Fc estimation using the suggested models, potentially due to the models being developed using data from different RS platforms, leading to potential mismatches in sensor characteristics and data quality.

The analysis of early and late crop growth stages reveals significant variations in the performance of the RS platforms in estimating Fc. By comparing the MBE% and RMSE% for each platform, this will allow showing the trends and identify which stages and platforms provide more accurate and stable results. Table 27 shows the performance of UAS, Planet, Landsat, Sentinel-2, and MSR-5 platforms in estimating the Fc during the early and late stages of the maize development.

During the early growth stages, the higher spatial resolution platforms exhibited higher performance than the Landsat and Sentinel-2. However, all RS platforms showed higher error resulted during the early growth stages compared to the late stages. Platforms like UAS, Planet, and MSR-5 demonstrated relatively better performance during the early stages, suggesting that in early stages, the performance of higher spatial resolution RS platforms are better when the

canopy cover is less dense, since they capture the less dense vegetation more accurately without including the soil background that will impact the results.

In the late growth stages, all RS platforms exhibited better performance compared to the early stages. The improved performance during the late stages can be attributed to the more stable and developed canopy, which provides clearer spectral signals for the RS platforms to capture. The UAS platform proved to be the most stable and reliable for Fc estimation, which consistently showed higher performance across both stages. The Fc models using Sentinel-2 and Landsat platforms showed a high improvement in the late stages, and slightly better performance using Planet and MSR-5 platforms.

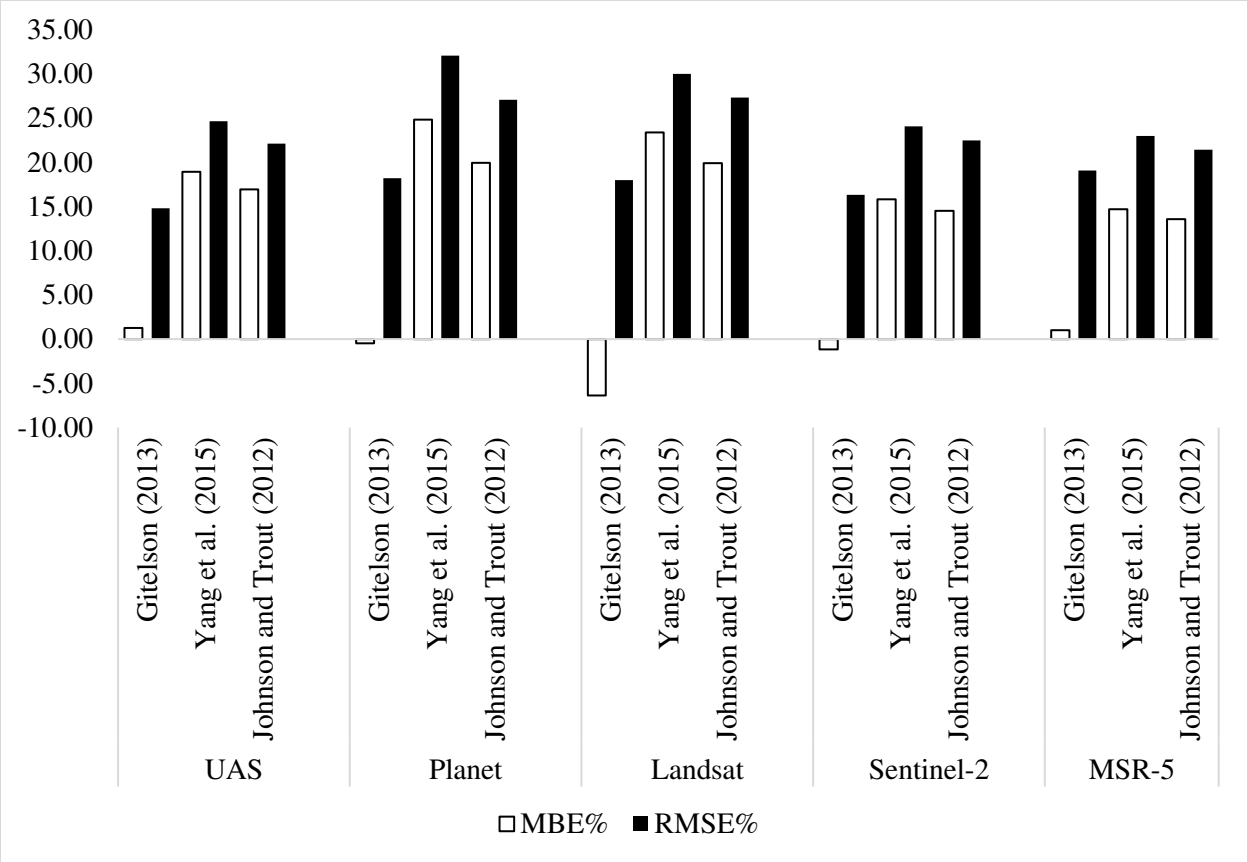

Figure 41: Error analysis for the balanced analysis for Fc estimation

Table 27: Early and late stages error analysis for Fc estimation

RS platform	Stage	Reference	Gitelson (2013)	Yang et al. (2015)	Johnson and Trout (2012)
UAS	Early Stages	MBE	0.0	0.2	0.1
		MBE%	7.5	26.8	25.3
		RMSE	0.1	0.2	0.2
		RMSE%	17.7	29.9	27.5
	Late Stages	MBE	-0.1	0.1	0.0
		MBE%	-8.1	7.4	5.2
		RMSE	0.1	0.1	0.1
		RMSE%	10.1	16.2	13.3
Planet	Early Stages	MBE	0.1	0.2	0.2
		MBE%	10.4	36.7	31.4
		RMSE	0.1	0.2	0.2
		RMSE%	15.7	41.0	35.2
	Late Stages	MBE	-0.1	0.1	0.0
		MBE%	-16.3	8.8	5.6
		RMSE	0.2	0.1	0.1
		RMSE%	20.1	18.0	14.9
Landsat	Early Stages	MBE	0.0	0.2	0.2
		MBE%	-2.3	33.8	30.2
		RMSE	0.1	0.2	0.2
		RMSE%	16.0	37.6	34.1
	Late Stages	MBE	-0.1	0.1	0.0
		MBE%	-12.5	8.9	5.8
		RMSE	0.2	0.1	0.1
		RMSE%	19.5	18.4	17.1
Sentinel-2	Early Stages	MBE	0.0	0.1	0.1
		MBE%	3.3	20.9	20.1
		RMSE	0.1	0.2	0.2
		RMSE%	18.9	27.8	26.6
	Late Stages	MBE	-0.1	0.1	0.1
		MBE%	-8.7	8.9	6.6
		RMSE	0.1	0.1	0.1
		RMSE%	11.8	18.4	16.0
MSR-5	Early Stages	MBE	0.0	0.1	0.1
		MBE%	-0.3	18.1	16.4
		RMSE	0.1	0.2	0.1
		RMSE%	23.7	25.7	23.2
	Late Stages	MBE	0.0	0.1	0.1
		MBE%	2.8	9.7	9.5
		RMSE	0.1	0.1	0.1
		RMSE%	11.3	18.8	18.6

3.5.4 Actual Crop Evapotranspiration Analysis

A new analysis was done to estimate the ETa using each RS platform with closely coinciding overpass dates. This new study was done to balance the comparison between each RS platform by having similar/close dates, number of data points (days in time) compared. Figure 42 to Figure 46 show the MBE% and RMSE% for the UAS, Planet, Landsat, Sentinel-2, and MSR-5 platforms, respectively used to estimate the ETa.

Using the new balanced analysis, the UAS performance was slightly better than the other RS platforms in estimating ETa, highlighting the UAS's accuracy and higher spatial resolution. The Landsat and MSR-5 platforms also showed a high performance compared to the Sentinel-2 and Planet platforms, which showed lower performance in estimating ETa. The variations in performance among different RS platforms in estimating ETa can be attributed to differences in spatial resolution, sensor calibration, and the sensors used to develop the tested models. The UAS and MSR-5 were the most reliable platforms due to their high spatial resolution and proximity. Landsat showed higher performance due to the development of the models were done using low spatial resolution sensors such as Landsat 5 and Landsat 7.

The analysis of early and late crop growth stages showed significant variations in the performance of the RS platforms in estimating ETa when comparing the MBE% and RMSE% for each platform in different stages. Table 28 to Table 32 show the performance of UAS, Planet, Landsat, Sentinel-2, and MSR-5 platforms in estimating the LAI during the early and late stages of the maize development.

During the early growth stages, the performance of RS platforms varied significantly. Higher spatial resolution platforms showed higher performance in the early stages, highlighting the importance of capturing accurate data during the initial phases of crop growth when the canopy is less developed and spectral signals are less accurate, with less dense canopies, the performance of higher spatial resolution RS platforms are higher, since they capture the less dense vegetation more accurately without including the soil background that will impact the results.

In the late growth stages, the Landsat and Sentinel-2 RS platforms exhibited improved performance compared to the early stages, while other RS platforms did not show a significant change in the performance. The higher performance during the late stages compared to the early stages can be attributed to the more stable and developed canopy, which provides clearer spectral signals for the RS platforms to capture. The UAS and Planet platforms had more stability in estimating ETa, showing moderate to good performance across both early and late stages. Sentinel-2 and Landsat showed lower stability.

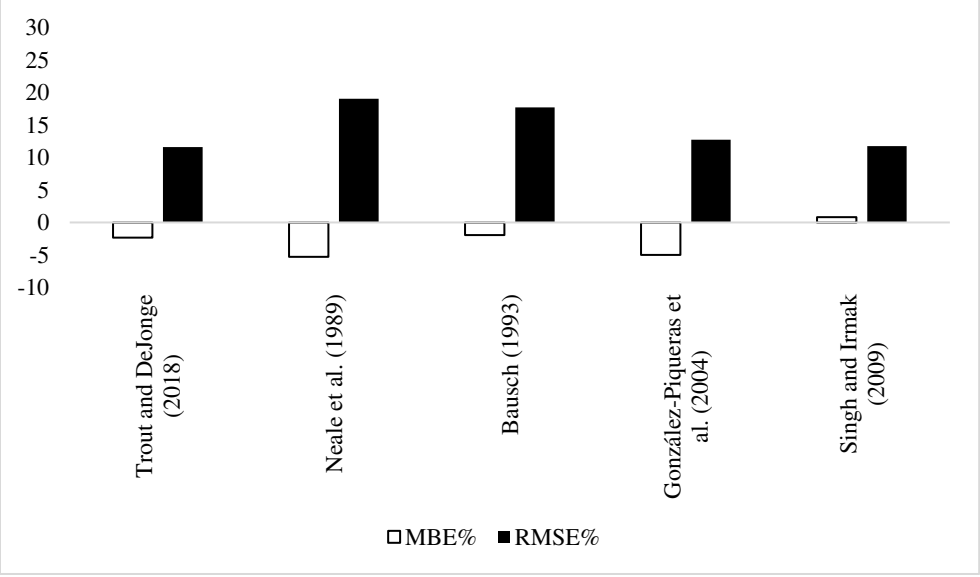

Figure 42: Error analysis for the UAS-based ETa balanced analysis

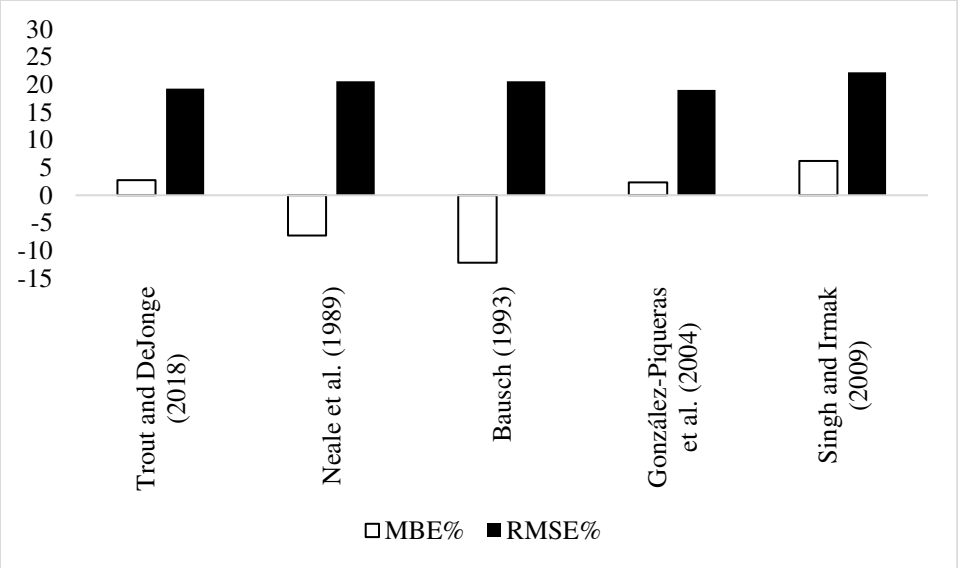

Figure 43: Error analysis for the Planet-based ETa balanced analysis

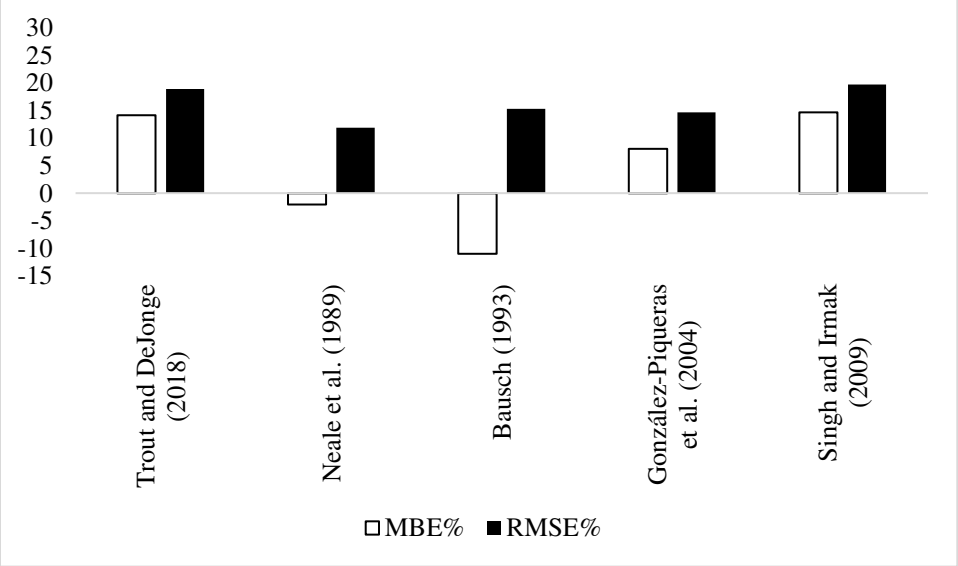

Figure 44: Error analysis for the Landsat-based ETa balanced analysis

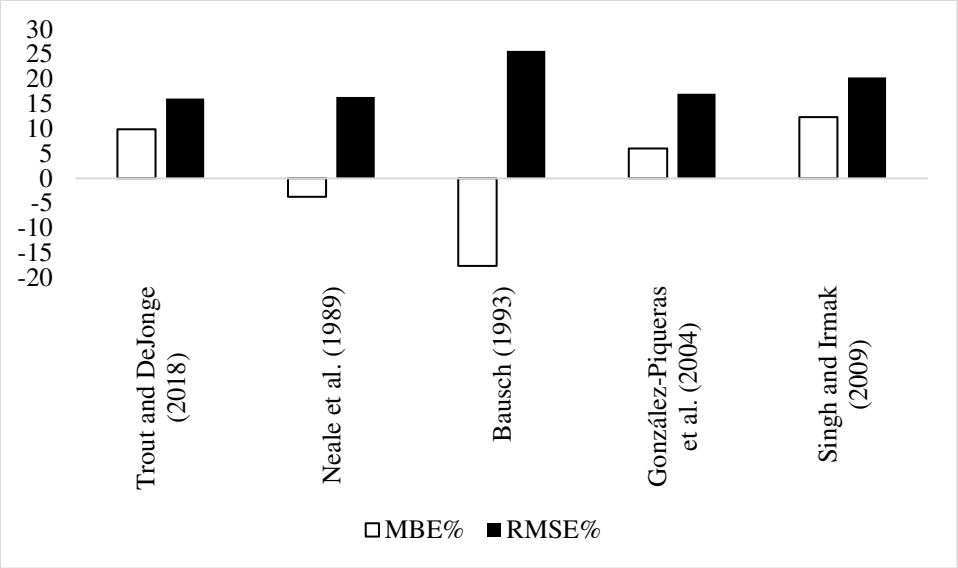

Figure 45: Error analysis for the Sentinel2-based ETa balanced analysis

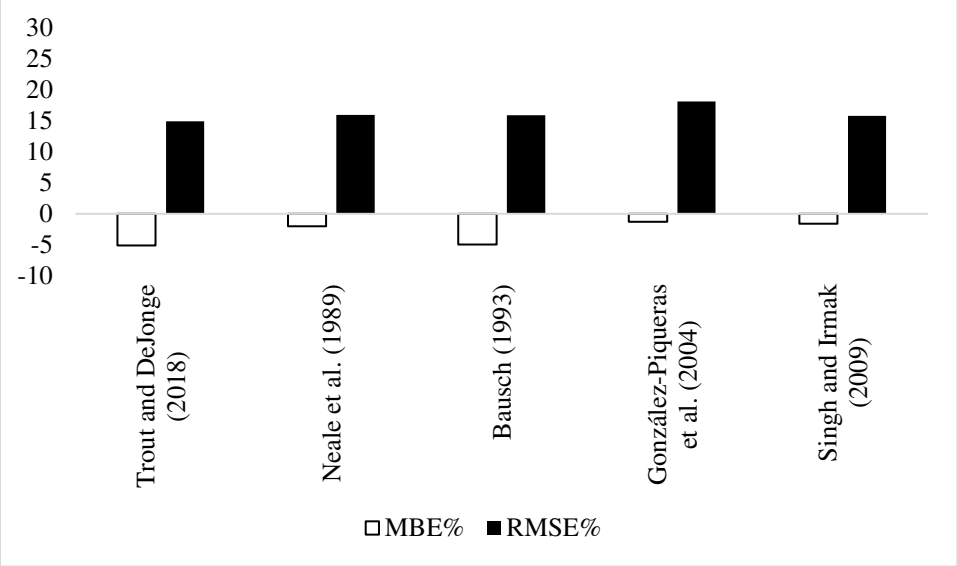

Figure 46: Error analysis for the MSR5-based ETa balanced analysis

Table 28: Early and late stages error analysis for the UAS-based ETa estimation

Early Stages					
Reference	Trout and DeJonge (2018)	Neale et al. (1989)	Bausch (1993)	González-Piqueras et al. (2004)	Singh and Irmak (2009)
MBE	0.89	0.81	0.68	0.80	1.20
MBE%	14.55	13.26	11.07	13.16	19.70
RMSE	0.89	1.02	0.82	0.82	1.21
RMSE%	12.44	16.76	12.40	11.48	17.02
Late Stages					
Reference	Trout and DeJonge (2018)	Neale et al. (1989)	Bausch (1993)	González-Piqueras et al. (2004)	Singh and Irmak (2009)
MBE	-0.68	-1.54	-1.62	-0.92	-0.52
MBE%	-8.82	-19.92	-20.91	-11.90	-6.66
RMSE	0.79	1.56	1.63	0.95	0.56
RMSE%	11.12	20.12	24.62	13.29	7.88

Table 29: Early and late stages error analysis for the Planet-based ETa estimation

Early Stages					
Reference	Trout and DeJonge (2018)	Neale et al. (1989)	Bausch (1993)	González-Piqueras et al. (2004)	Singh and Irmak (2009)
MBE	1.77	0.73	0.09	1.56	1.98
MBE%	26.07	10.84	1.30	20.78	29.18
RMSE	1.81	0.86	0.46	1.63	2.03
RMSE%	26.55	12.63	6.83	21.62	29.93
Late Stages					
Reference	Trout and DeJonge (2018)	Neale et al. (1989)	Bausch (1993)	González-Piqueras et al. (2004)	Singh and Irmak (2009)
MBE	-0.79	-1.78	-2.03	-1.21	-0.82
MBE%	-11.60	-26.27	-30.15	-15.57	-12.02
RMSE	0.88	1.79	2.05	1.26	0.90
RMSE%	12.91	26.39	30.46	16.28	13.22

Table 30: Early and late stages error analysis for the Landsat-based ETa estimation

Early Stages					
Reference	Trout and DeJonge (2018)	Neale et al. (1989)	Bausch (1993)	González-Piqueras et al. (2004)	Singh and Irmak (2009)
MBE	1.53	0.33	-0.36	1.09	1.57
MBE%	23.84	4.71	-5.73	15.60	24.50
RMSE	1.67	0.80	0.74	1.30	1.73
RMSE%	26.08	11.52	11.65	18.69	27.01
Late Stages					
Reference	Trout and DeJonge (2018)	Neale et al. (1989)	Bausch (1993)	González-Piqueras et al. (2004)	Singh and Irmak (2009)
MBE	0.28	-0.60	-1.04	-0.04	0.31
MBE%	4.41	-9.98	-16.33	-0.73	4.86
RMSE	0.38	0.74	1.16	0.33	0.43
RMSE%	5.93	12.34	18.21	5.57	6.80

Table 31: Early and late stages error analysis for the Sentinel2-based ETa estimation

Early Stages					
Reference	Trout and DeJonge (2018)	Neale et al. (1989)	Bausch (1993)	González-Piqueras et al. (2004)	Singh and Irmak (2009)
MBE	1.29	0.44	-0.39	1.14	1.59
MBE%	20.05	6.90	-5.86	17.70	24.70
RMSE	1.58	1.28	1.38	1.65	2.00
RMSE%	24.55	19.92	20.67	25.70	31.10
Late Stages					
Reference	Trout and DeJonge (2018)	Neale et al. (1989)	Bausch (1993)	González-Piqueras et al. (2004)	Singh and Irmak (2009)
MBE	0.12	-0.98	-1.96	-0.28	0.17
MBE%	1.48	-12.50	-29.36	-3.61	2.12
RMSE	0.34	1.04	1.99	0.47	0.42
RMSE%	4.31	13.36	29.78	5.96	5.34

Table 32: Early and late stages error analysis for the MSR5-based ETa estimation

Early Stages					
Reference	Trout and DeJonge (2018)	Neale et al. (1989)	Bausch (1993)	González-Piqueras et al. (2004)	Singh and Irmak (2009)
MBE	1.07	0.58	0.28	1.24	1.44
MBE%	14.63	8.11	3.96	17.16	19.70
RMSE	1.08	0.72	0.42	1.29	1.46
RMSE%	14.73	10.09	5.90	17.96	19.91
Late Stages					
Reference	Trout and DeJonge (2018)	Neale et al. (1989)	Bausch (1993)	González-Piqueras et al. (2004)	Singh and Irmak (2009)
MBE	-1.09	-1.72	-2.09	-1.30	-0.93
MBE%	-14.96	-24.26	-29.46	-18.03	-12.71
RMSE	1.10	1.72	2.02	1.31	0.96
RMSE%	15.02	24.27	28.59	18.25	13.14

3.6 Sensitivity Analysis

3.6.1 Leaf Area Index Analysis

A sensitivity analysis for the estimation of LAI was done using four different scenarios including +2.5%, +5%, -2.5%, -5% variation of the values of the independent variables, which in this case refers to VIs. The analysis was done for all RS platforms to indicate how different VI values will impact the dependent LAI value. Figure 47 to Figure 51 show the RMSE% for the

base models and how changes in VI values impact the RMSE% of the models for the UAS, PlanetDove, Landsat, Sentinel-2, and MSR-5 platforms, respectively.

The sensitivity analysis for the UAS platform in estimating LAI shows that the models are relatively stable, with RMSE% ranging from 15.95% to 39.62%. The slight increase in RMSE% under positive scenarios indicates that the model tends to overestimate LAI slightly when VIs increase. Conversely, the models show less deviation in RMSE% under negative scenarios, suggesting better performance in estimating lower LAI values. The PlanetDove platform, however, exhibits a broader range of RMSE%, indicating a higher sensitivity to changes in VI values, particularly under negative scenarios, where the RMSE% increases significantly. The results suggest that while PlanetDove can effectively estimate LAI, it is more susceptible to inaccuracies when there is a decrease in VI values.

The sensitivity analysis for Landsat shows RMSE% variations similar to those of the UAS platform, exhibiting moderate sensitivity to VI changes, with slightly higher RMSE% under positive scenarios. Sentinel-2, on the other hand, demonstrates a more comprehensive RMSE% range, indicating higher sensitivity than the UAS and the Landsat platforms. The analysis shows significant variations under both positive and negative scenarios, suggesting that Sentinel-2 is sensitive to both increases and decreases in VI values, impacting the accuracy of LAI estimates. The MSR-5 platform shows the highest sensitivity; the significant variation in RMSE% indicates that MSR-5 is highly sensitive to changes in VI values, particularly under negative scenarios, where the RMSE% increases drastically.

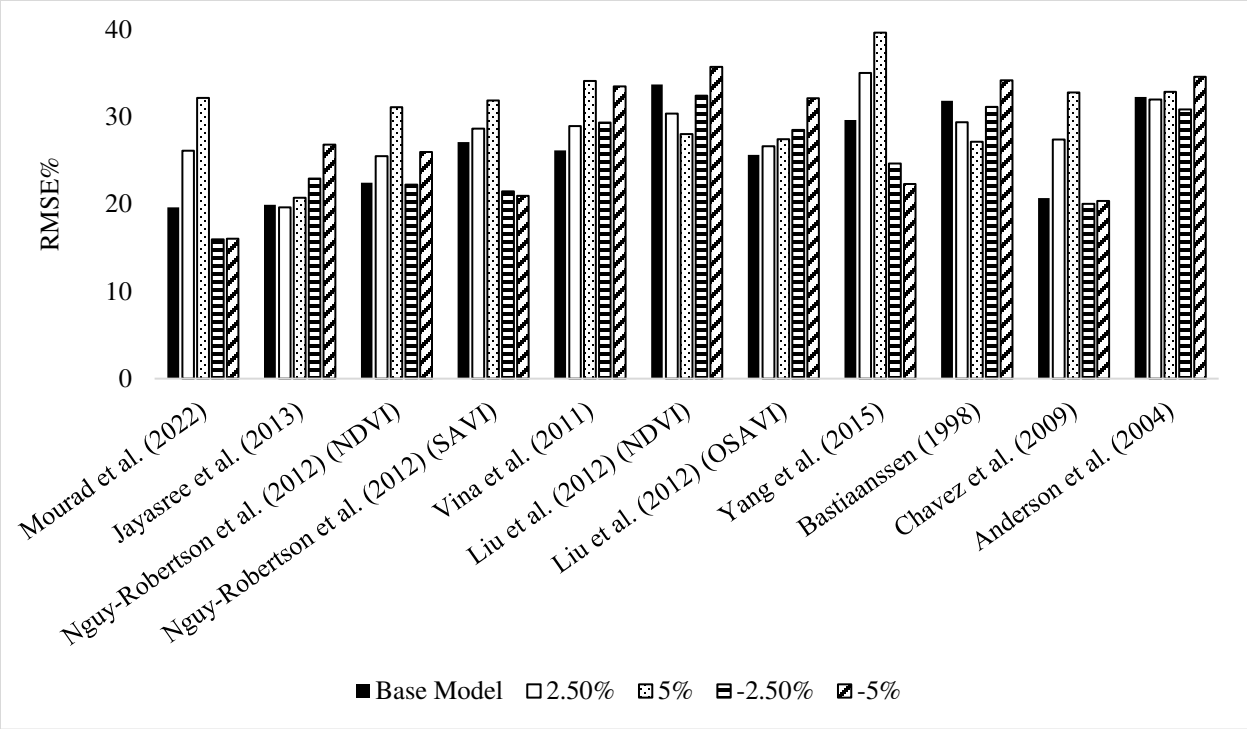

Figure 47: RMSE% for all scenarios used in sensitivity analysis estimating LAI using the UAS platform

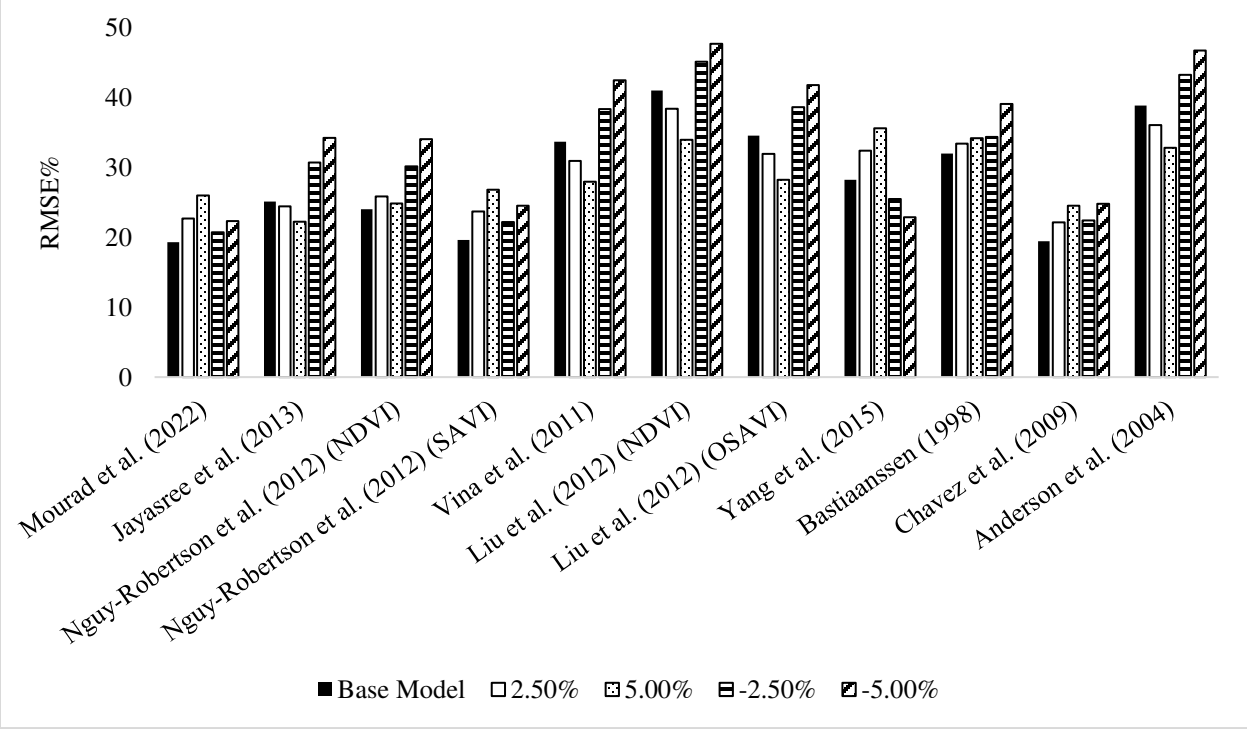

Figure 48: RMSE% for all scenarios used in sensitivity analysis estimating LAI using Planet platform

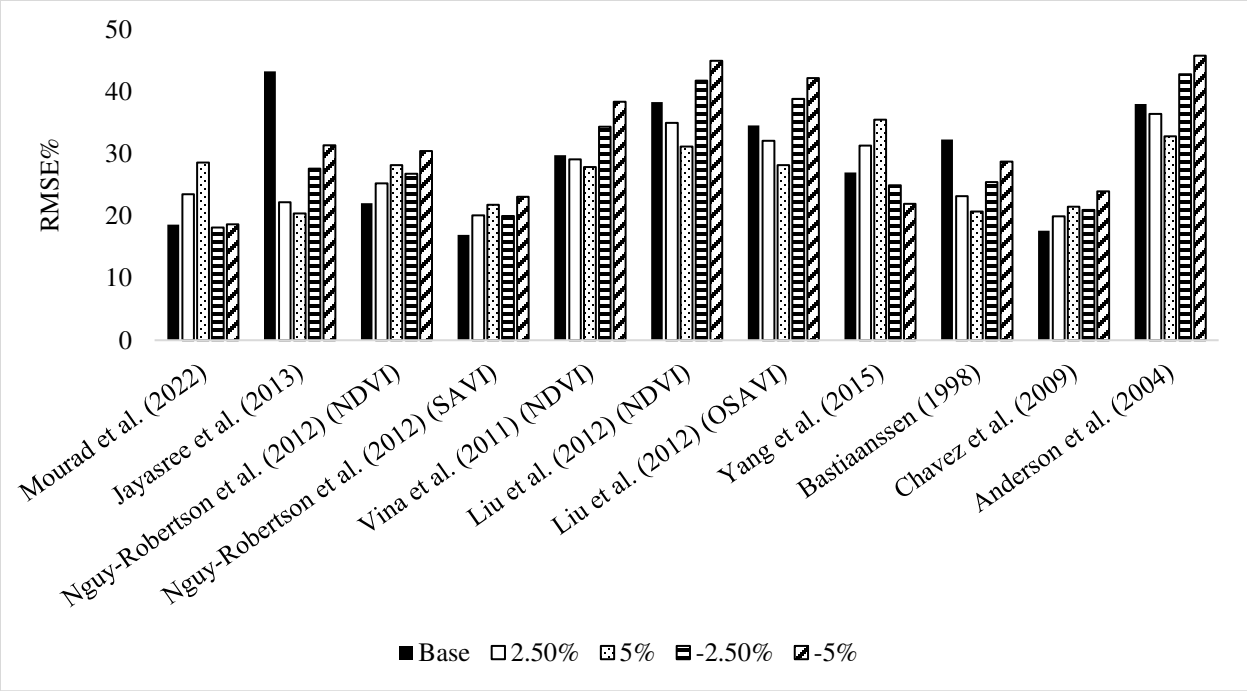

Figure 49: RMSE% for all scenarios used in sensitivity analysis estimating LAI using Landsat platform

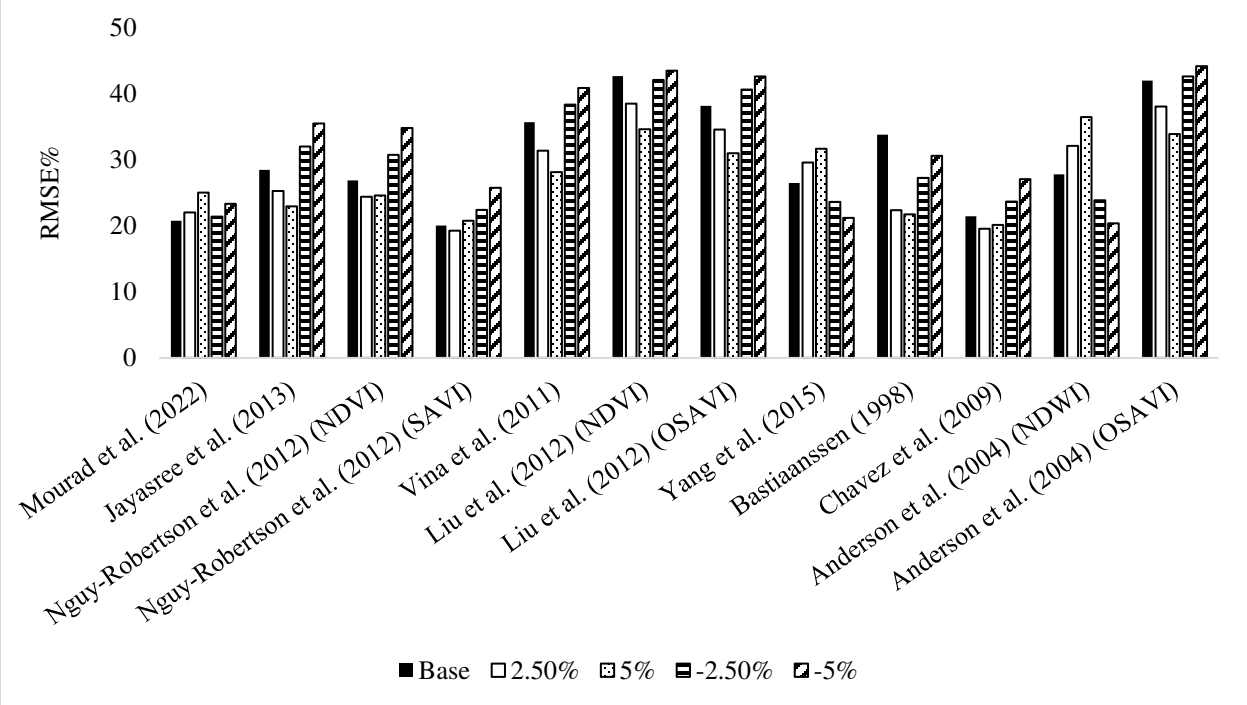

Figure 50: RMSE% for all scenarios used in sensitivity analysis estimating LAI using Sentinel-2 platform

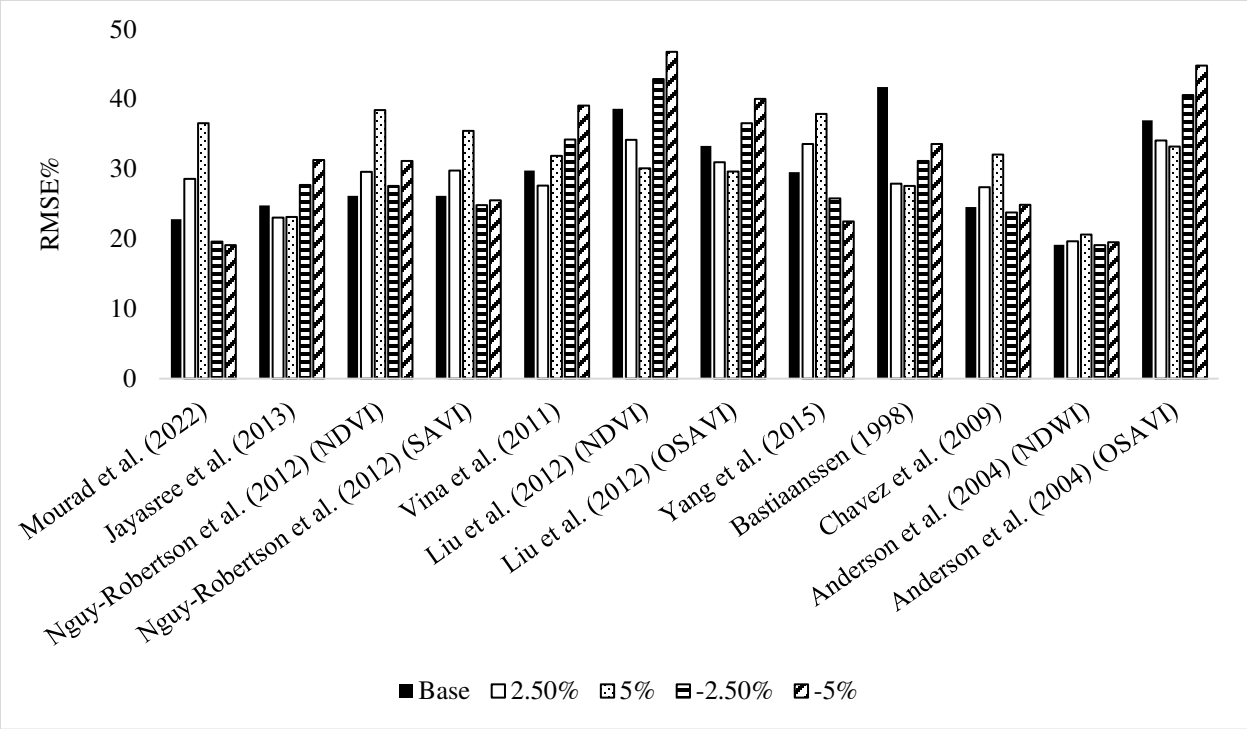

Figure 51: RMSE% for all scenarios used in sensitivity analysis estimating LAI using MSR-5 platform

3.6.2 Canopy Height Analysis

A sensitivity analysis for the estimation of Hc was done using the same scenarios used to estimate the LAI, which included +2.5%, +5%, -2.5%, -5% changes or variations of the values of independent variables, which are the VIs and the LAI in this case. The analysis was done for all RS platforms to indicate how changes in VI and LAI values will impact the dependent Hc value. Figure 52 to Figure 56 show the RMSE% for the base models and four different change scenarios of the models used to estimate Hc using the UAS, PlanetDove, Landsat, Sentinel-2, and MSR-5 platforms, respectively.

The RMSE% change for Hc estimation using all RS platforms, as shown in the below figures, shows a high sensitivity for most of the models, excluding the models by Costa-Filho et al. (2021) and Anderson et al. (2004). The relatively same changes in RMSE% (same sensitivity)

were noticed in all RS platforms, where the trend of the changes suggested a better performance when the independent variables were decreased and lower performance when the independent variables were increased. This indicates that the independent variables (VIs and LAI) were overestimated.

The RMSE% for Hc estimation using the UAS platform models showed a higher sensitivity to positive changes, suggesting a tendency to overestimate Hc when VIs increase. The analysis indicates that UAS-based Hc models are more accurate under negative scenarios. Other platforms, like the UAS, showed a broad range of RMSE%. The results highlight significant sensitivity to both positive and negative changes, with models showing increased errors, particularly under positive scenarios.

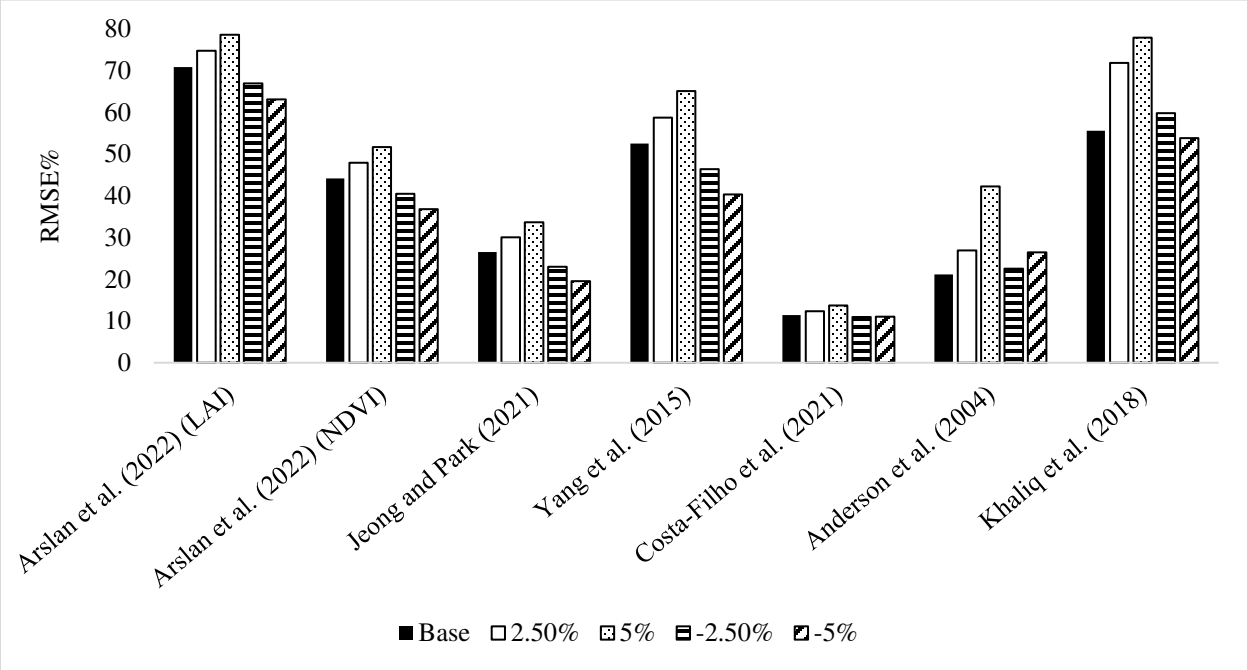

Figure 52: RMSE% for all scenarios used in sensitivity analysis estimating Hc using the UAS platform

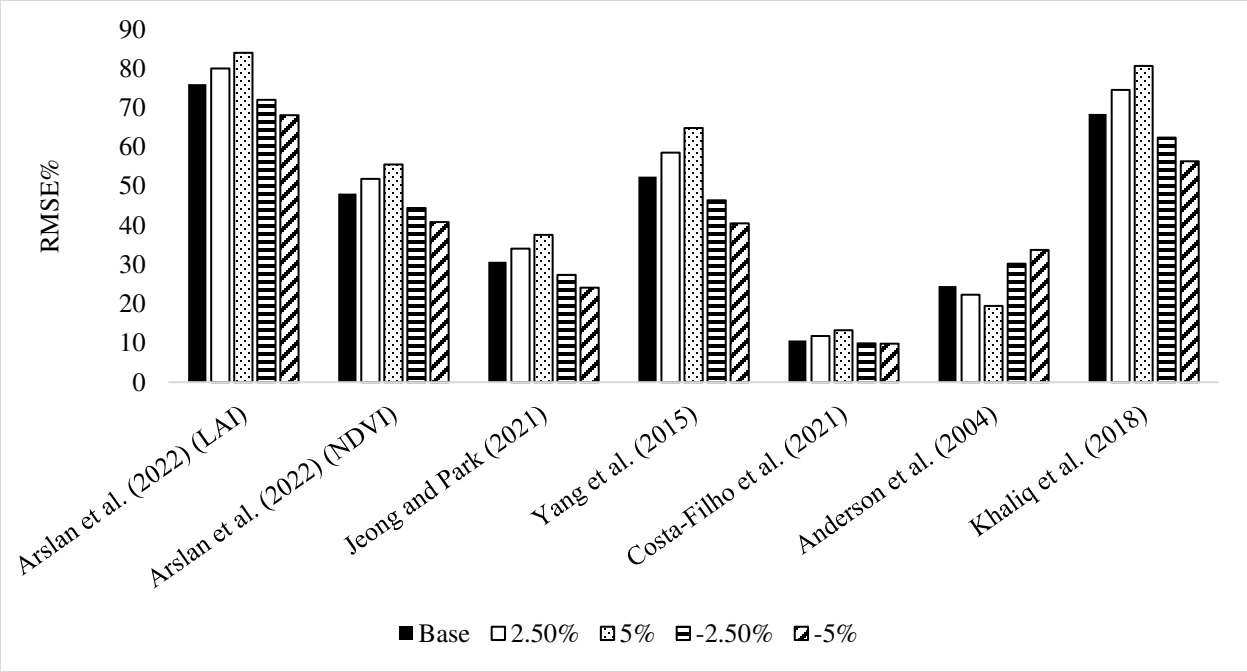

Figure 53: RMSE% for all scenarios used in sensitivity analysis estimating Hc using Planet platform

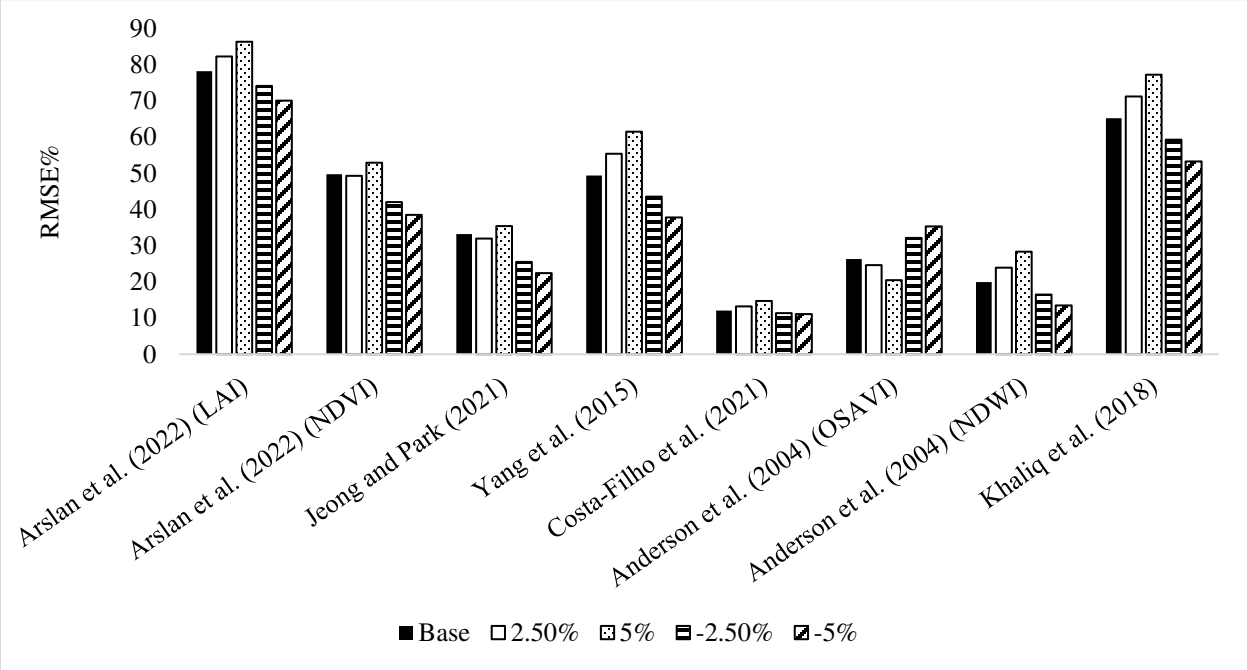

Figure 54: RMSE% for all scenarios used in sensitivity analysis estimating Hc using Landsat platform

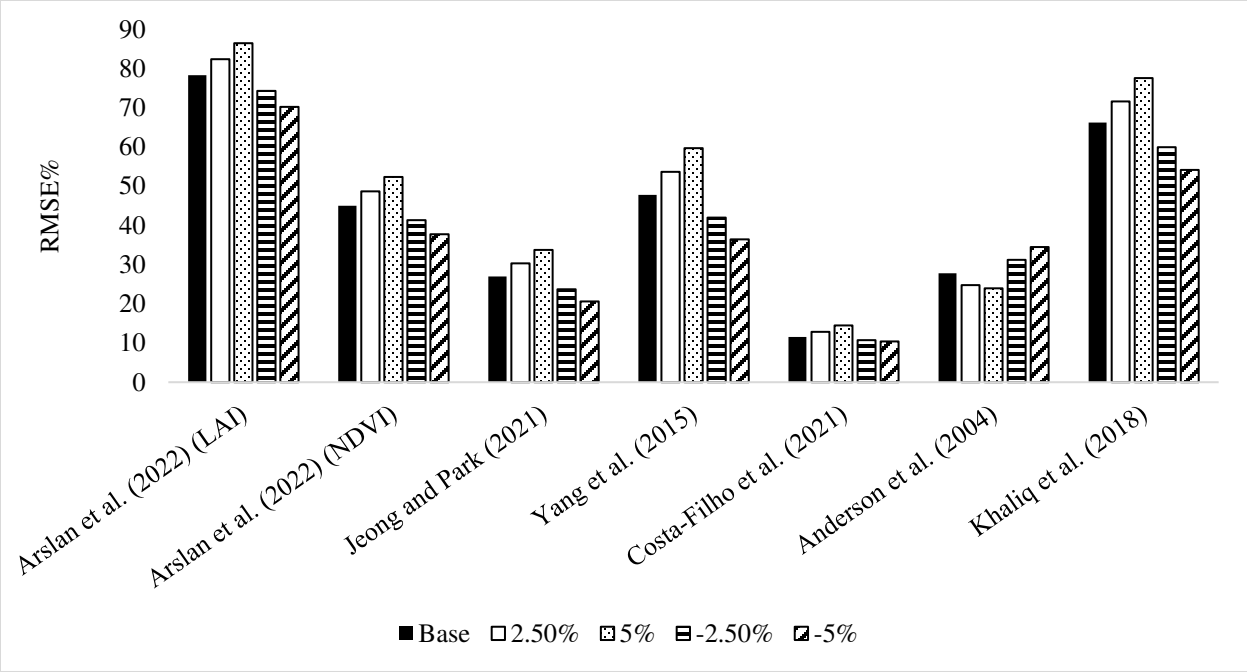

Figure 55: RMSE% for all scenarios used in sensitivity analysis estimating Hc using Sentinel-2 platform

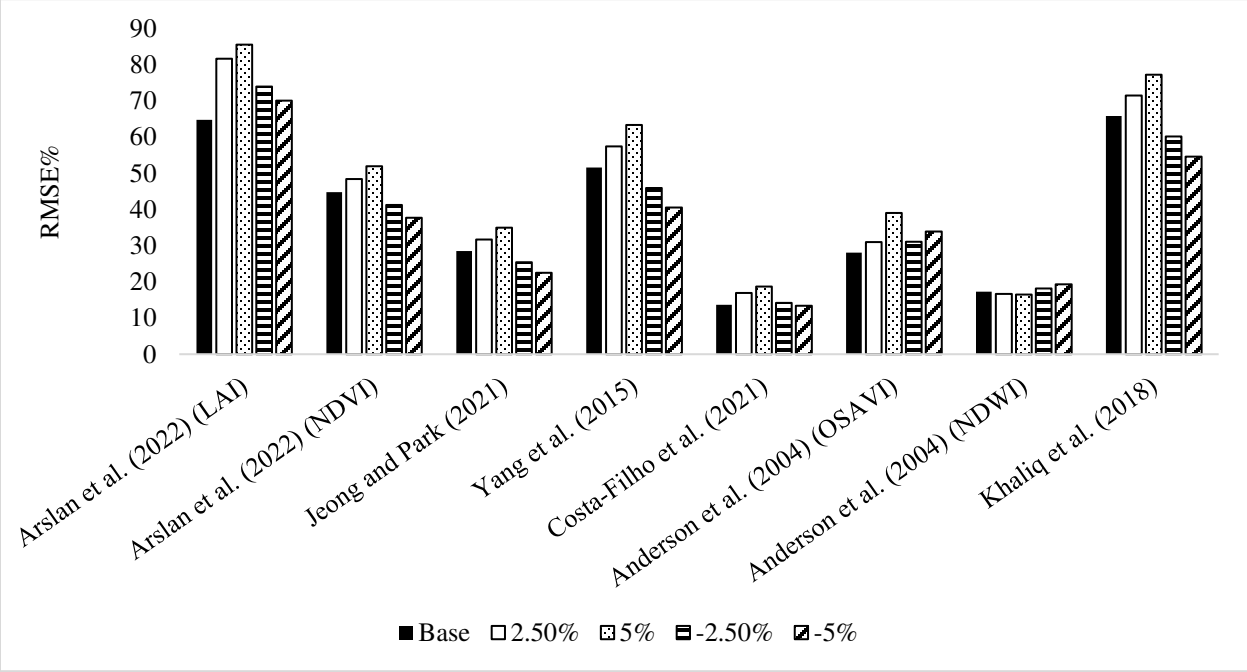

Figure 56: RMSE% for all scenarios used in sensitivity analysis estimating Hc using MSR-5 platform

3.6.3 Canopy fractional cover Analysis

A sensitivity analysis for the estimation of Fc was done using the same scenarios used in the analysis of LAI, including +2.5%, +5%, -2.5%, -5% change of the values of the independent variables, which are the NDVI values in the Fc case. The analysis was done for all RS platforms to indicate how a change in NDVI values will impact the dependent Fc value. Figure 57 to Figure 61 show the RMSE% for the base models and the RMSE% for the four different change scenarios of the models used to estimate Fc using the UAS, PlanetDove, Landsat, Sentinel-2, and MSR-5 platforms, respectively.

The models used with the UAS platform show moderate sensitivity with RMSE%, showing slight increases in RMSE% under both positive and negative scenarios, indicating stable performance but a tendency to overestimate Fc when NDVI increases. PlanetDove exhibits higher sensitivity with RMSE%, indicating a significant sensitivity to changes in NDVI values, particularly under positive scenarios. This suggests that PlanetDove's Fc estimation models are less robust compared to UAS.

Landsat shows a wide range of RMSE%, indicating higher sensitivity to changes in NDVI values. The results suggest that Landsat's Fc models are highly sensitive, particularly under negative scenarios, where RMSE% increases significantly. Sentinel-2 demonstrates moderate sensitivity with RMSE%, indicating more stable performance but a tendency to overestimate Fc under positive scenarios. The results suggest that Sentinel-2 provides relatively accurate Fc estimates but requires careful calibration. MSR-5, on the other hand, shows the highest sensitivity with RMSE%. The large variation in RMSE% indicates that MSR-5 models estimating the Fc are highly sensitive to changes in NDVI values, particularly under negative scenarios, suggesting the need for further calibration.

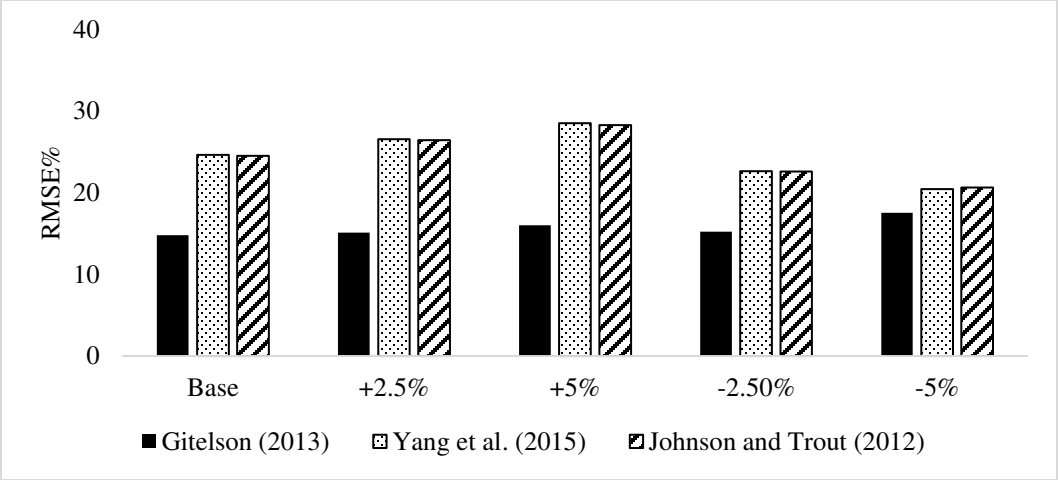

Figure 57: RMSE% for all scenarios used in sensitivity analysis estimating Fc using the UAS platform

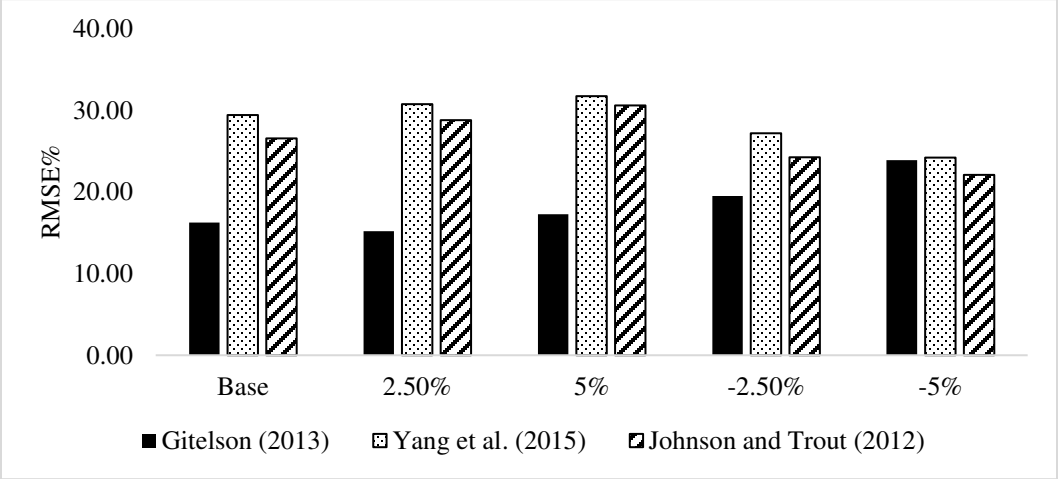

Figure 58: RMSE% for all scenarios used in sensitivity analysis estimating Fc using Planet platform

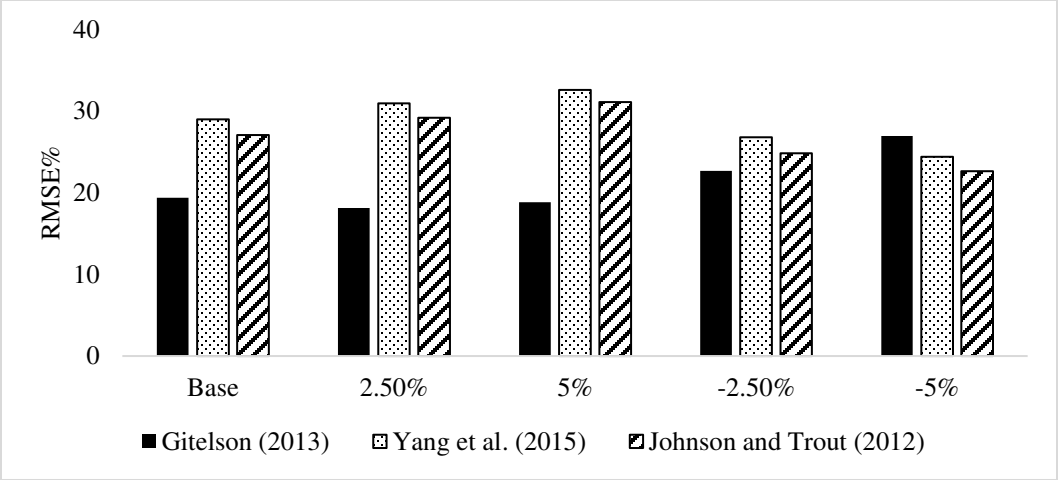

Figure 59: RMSE% for all scenarios used in sensitivity analysis estimating Fc using Landsat platform

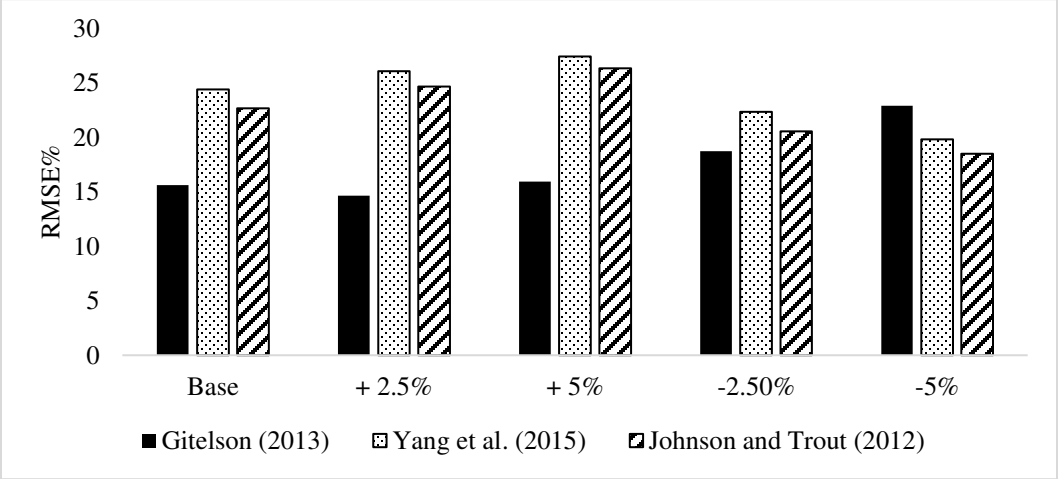

Figure 60: RMSE% for all scenarios used in sensitivity analysis estimating Fc using Sentinel-2 platform

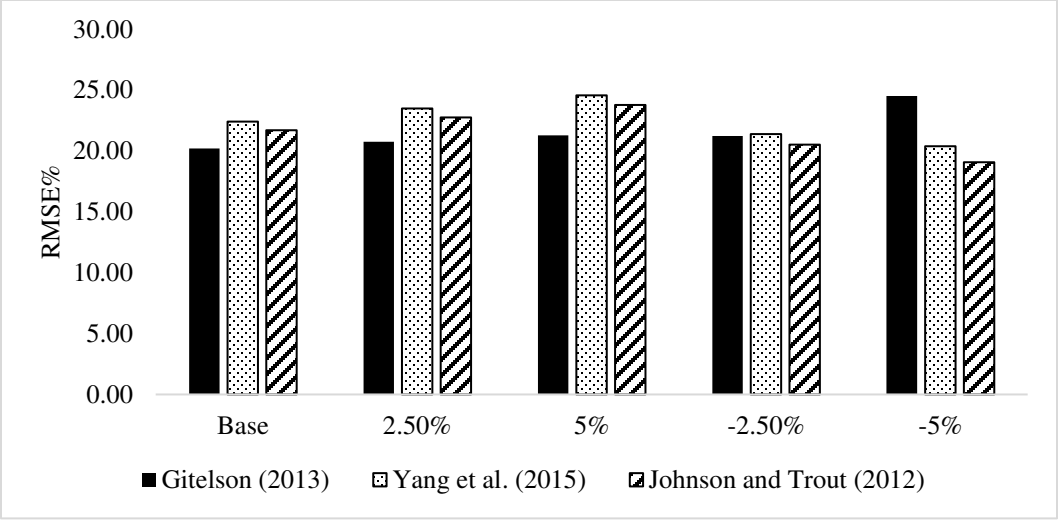

Figure 61: RMSE% for all scenarios used in sensitivity analysis estimating Fc using MSR-5 platform

3.6.4 Actual Crop Evapotranspiration Analysis

A sensitivity analysis for the estimation of ETa was done using the same scenarios used in the analysis of LAI, including (+2.5%, +5%, -2.5%, -5%) changes of the independent variables, which are the NDVI, SAVI, and Fc values. The analysis was done for all RS platforms to indicate how changes in the values of the independent variables will impact the dependent ETa value. Figure 62 to Figure 66 show the RMSE% for the base models and the RMSE% for the four different change scenarios of the models used to estimate ETa using the UAS, PlanetDove, Landsat, Sentinel-2, and MSR-5 platforms, respectively.

As shown in the figures below, most models showed relatively low sensitivity when either increasing or decreasing the independent variable values throughout all RS platforms. The general trend of the performance indicated by the RMSE% varies depending on the model and the RS platform used to estimate the ETa. Models by Trout and DeJonge (2018) and Neale et al. (1989) showed lower sensitivity compared to other models.

The models used in the UAS platform show low sensitivity, indicating a slight increase in RMSE% under both positive and negative scenarios, indicating stable performance and accurate ETa estimates. PlanetDove exhibited higher sensitivity compared to the UAS, and the results indicate significant sensitivity to changes in VI values, particularly under positive scenarios, suggesting that PlanetDove's ETa imagery needs further calibration to be effectively used in ETa models based on surface reflectance. Landsat showed moderate sensitivity, and the results suggest stable ETa estimates from Landsat, but careful calibration is required under positive scenarios to avoid overestimation. Sentinel-2 demonstrates high sensitivity, indicating that Sentinel-2's ETa models are highly sensitive to changes in VI values, particularly under positive scenarios, suggesting the need for further calibration. MSR-5 shows moderate sensitivity, and the results indicate that MSR-5's ETa estimation models are highly sensitive to changes in VI values, particularly under negative scenarios.

The sensitivity analysis across different RS platforms underscores the varying degrees of robustness and accuracy in estimating LAI, Hc, Fc, and ETa. It is important to note that high-resolution platforms like UAS generally demonstrate more stable and accurate estimates, while lower-resolution platforms like PlanetDove and Landsat show higher sensitivity to changes in VI values. This analysis underscores the importance of selecting appropriate RS platforms and calibrating models carefully to ensure accurate agricultural monitoring and water management.

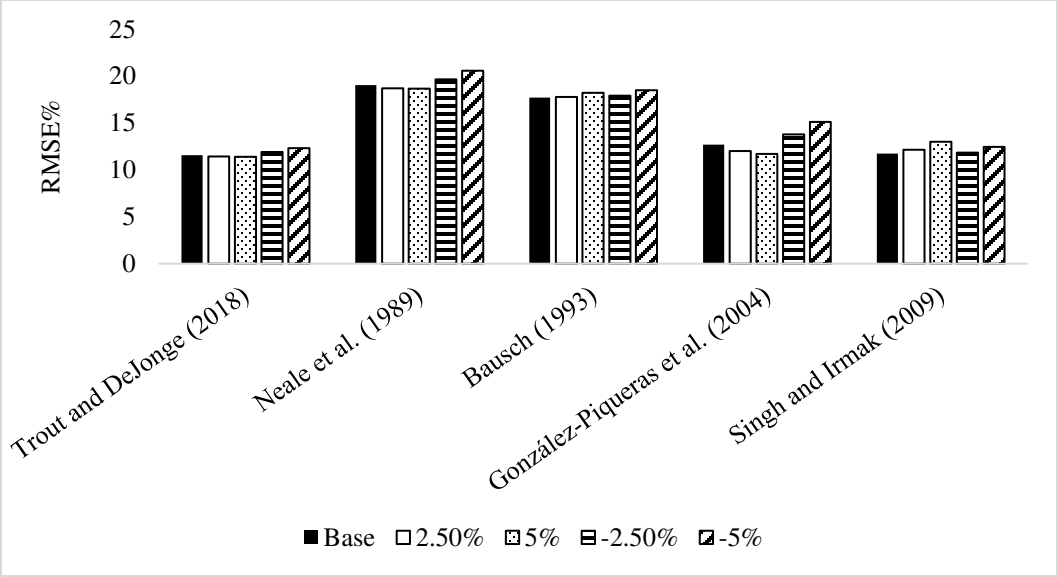

Figure 62: RMSE% for all scenarios used in sensitivity analysis estimating ETa using the UAS platform

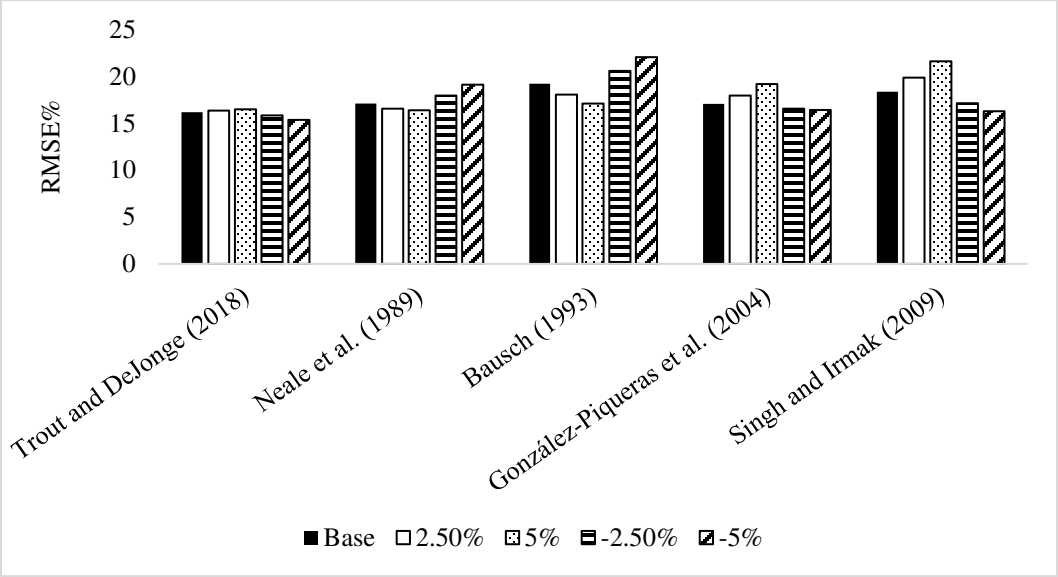

Figure 63: RMSE% for all scenarios used in sensitivity analysis estimating ETa using Planet platform

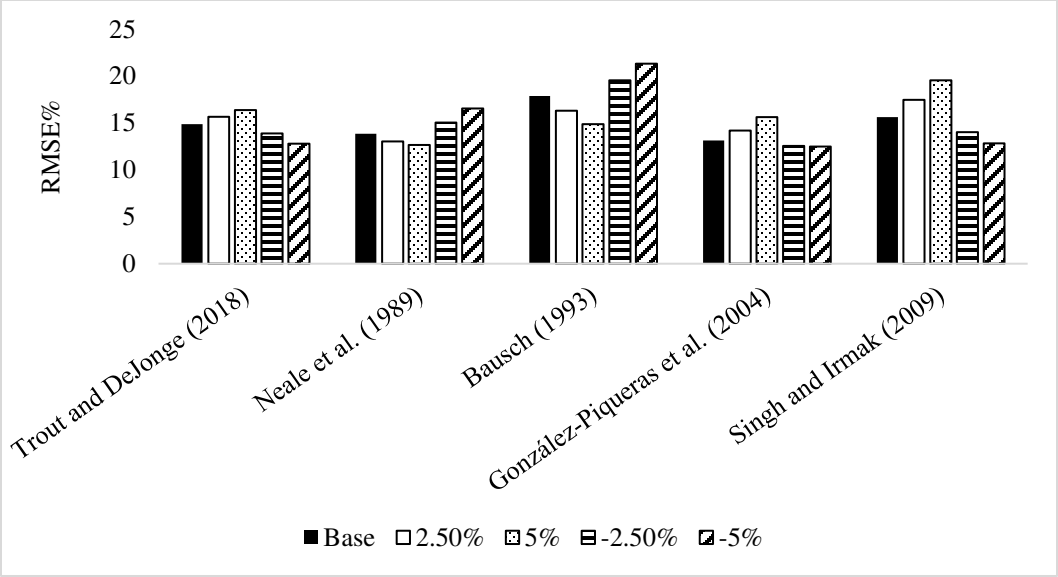

Figure 64: RMSE% for all scenarios used in sensitivity analysis estimating ETa using Landsat platform

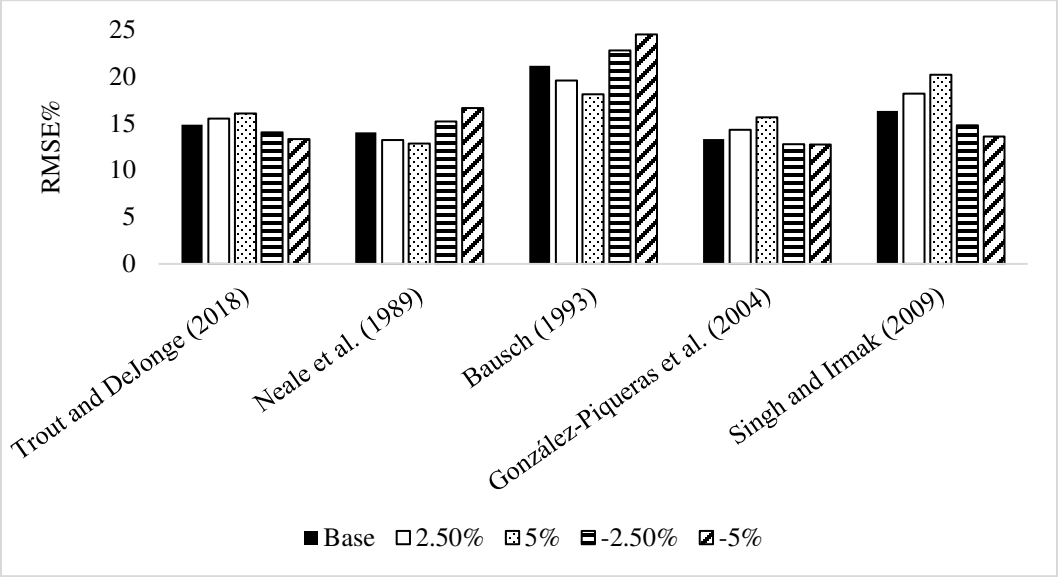

Figure 65: RMSE% for all scenarios used in sensitivity analysis estimating ETa using Sentinel-2 platform

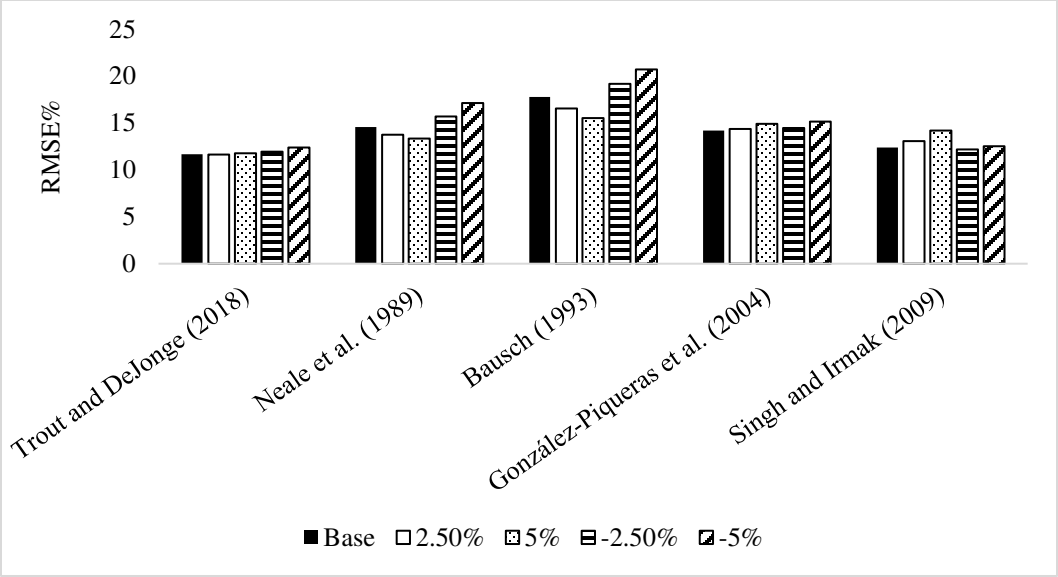

Figure 66: RMSE% for all scenarios used in sensitivity analysis estimating ETa using MSR-5 platform

Chapter 4: Conclusions and Recommendations

This study provided a comprehensive analysis of various RS platforms in estimating CBPCs and ETa for maize fields in northeastern Colorado. The findings of this research highlight several key points.

Firstly, the accuracy of VIs estimation varied significantly among the RS platforms. The UAS platform showed the highest accuracy in estimating VIs such as NDVI, OSAVI, and SAVI. The high spatial resolution of UAS, and the fact that surface reflectance values were acquired closer to the ground surface, allowed for detailed canopy assessments, which contributed to its high performance. Other satellite platforms, including PlanetDove, Sentinel-2, and Landsat, showed slightly less accuracy, still providing valuable insights with relatively high performance. These platforms offer broader coverage and frequent revisit times, making them practical for regional-scale monitoring and long-term agricultural assessments.

Secondly, the estimation of CBPCs, including LAI, Hc, and Fc, demonstrated that models developed using VIs from the UAS platform provided the most accurate estimates. The high-resolution data captured by UAS proved to be more sensitive to variations in crop canopy structure and health. Other platforms followed in accuracy, with each showing strengths depending on specific conditions and crop stages. The influence of environmental conditions on the performance of RS models was significant. Locally calibrated models, which consider the specific environmental conditions of the study area, performed better than those developed in different environmental contexts. These results underscore the importance of site-specific calibration for improving model accuracy. The MSR-5 radiometer, despite being a standard for

evaluating vegetation indices, showed suboptimal performance in estimating CBPCs and ETa in this study. This could be attributed to the type of model used, which were developed using different RS senors/platforms, predominantly space-borne and airborne satellites with different spectral and spatial resolutions.

Thirdly, the estimation of Kcb and ETa revealed that the accuracy varied among the different RS data from platforms used, with UAS-based models again showing higher performance. However, satellite-based estimates were also within acceptable error margins, demonstrating their utility in providing reliable data for large-scale agricultural management. Sensitivity analysis indicated that slight variations in VIs could lead to significant changes in CBPCs and ETa estimates. This result highlights the need for local accurate calibration and validation of RS models to ensure their reliability and accuracy.

Fourthly, the study underscores the potential of advanced remote sensing technologies, particularly UAS, in enhancing agriculture practices and water use. The accurate estimation of CBPCs and ETa can inform better irrigation scheduling, leading to optimized water use and improved crop yields. This has significant implications for water resource management in agriculture, particularly in regions facing water scarcity and climatic variability. The analysis of LAI, Hc, Fc, and ETa across various RS platforms reveals distinct performance variations. UAS consistently provided more accurate and reliable estimates across all parameters. Sentinel-2 and Planet platforms showed moderate reliability and potential for good performance under specific conditions. Landsat had the highest variability and generally less reliable estimates, while MSR-5's performance was less consistent and lower than UAS. The results highlight the importance of selecting appropriate RS platforms based on specific study requirements to ensure accurate estimations.

The performance of RS platforms improved significantly during the late crop growth stages compared to the early stages for all parameters. This improvement is attributed to the more stable and developed canopy structure in the late stages, providing clearer spectral signals for the RS platforms to capture. Higher spatial resolution platforms like UAS, Planet, and MSR-5 demonstrated better performance during the early stages when the canopy was less dense. However, all platforms showed improved accuracy in the late stages, with UAS remaining the most reliable and stable across both growth stages.

In summary, the choice of an RS platform for agricultural monitoring depends on different characteristics of the RS platform, including spatial, spectral and temporal resolutions. The UAS, with its very high spatial resolution, is ideal for detailed field-level analysis, capturing fine-scale variability in VIs. However, its limited temporal resolution necessitates frequent flights, which may not be feasible for large-scale applications. On the other hand, Planet provides daily revisit times, making it suitable for monitoring rapid changes in crop conditions, although its lower spatial resolution compared to UAS might miss finer details. Sentinel-2 offers a balance between spatial and temporal resolution, suitable for regional-scale studies, while Landsat's longer revisit time and broader coverage make it ideal for large-scale environmental monitoring.

Agricultural stakeholders should consider integrating high-resolution UAS data into their monitoring systems for more accurate and reliable results. The higher accuracy of UAS in estimating VIs and CBPCs can lead to more accurate and timely agricultural management decisions. Despite their slightly lower accuracy compared to UAS, other platforms are important to be used due to their broad coverage and frequent revisit times. These platforms are particularly useful for regional-scale monitoring.

Models for estimating CBPCs and ETa should be calibrated using local data to account for specific environmental conditions. This will enhance the accuracy and applicability of the models across different regions. Future studies should focus on the comprehensive validation of RS models across different crop types and environmental conditions. This will help in developing robust models that can be generalized to various agricultural settings.

References

Acharya, T. D., & Yang, I. (2015). Exploring landsat 8. International Journal of IT, Engineering and Applied Sciences Research (IJIEASR), 4(4), 4-10.

Adams, J. E., & Arkin, G. F. (1977). A light interception method for measuring row crop ground cover. Soil Science Society of America Journal, 41(4), 789-792.

Anderson, K., & Gaston, K. J. (2013). Lightweight unmanned aerial vehicles will revolutionize spatial ecology. Frontiers in Ecology and the Environment, 11(3), 138-146.

Anderson, M. C., Neale, C. M. U., Li, F., Norman, J. M., Kustas, W. P., Jayanthi, H., & Chavez, J. (2004). Upscaling ground observations of vegetation water content, canopy height, and leaf area index during SMEX02 using aircraft and Landsat imagery. Remote sensing of environment, 92(4), 447-464.

Arslan, İ., Topakcı, M., & Demir, N. (2022). Monitoring maize growth and calculating plant heights with Synthetic Aperture Radar (SAR) and optical satellite images. Agriculture, 12(6), 800.

Baret, F., & Guyot, G. (1991). Potentials and limits of vegetation indices for LAI and APAR assessment. Remote sensing of environment, 35(2-3), 161-173.

Basso, B., Cammarano, D., & De Vita, P. (2004). Remotely sensed vegetation indices: Theory and applications for crop management. Rivista Italiana di Agrometeorologia, 1(5), 36-53.

Bastiaanssen, W. G. M. (1998). Remote sensing in water resources management: The state of the art. International Irrigation Management Institute.

Bausch, W. C. (1993). Soil background effects on reflectance-based crop coefficients for corn. Remote Sensing of Environment, 46(2), 213-222.

Bruinsma, J. (2017). World agriculture: towards 2015/2030: an FAO study. Routledge.

Chávez, J. L., Gowda, P. H., Howell, T. A., Neale, C. M. U., & Copeland, K. S. (2009). Estimating hourly crop ET using a two-source energy balance model and multispectral airborne imagery. Irrigation science, 28, 79-91.

Chávez, J. L., Zhang, H., Brown, A. J., Andales, A., & Costa-Filho, E. (2024). Maize Evapotranspiration Estimates Using Planet Dove Mini-Satellites and Field-Level InfraRed Thermometers. Applied Engineering in Agricultural, 40(1): 69-78

Costa-Filho, E., Chávez, J. L., Zhang, H., & Andales, A. A. (2021). An optimized surface aerodynamic temperature approach to estimate maize sensible heat flux and evapotranspiration. Agricultural and Forest Meteorology, 311, 108683.

European Space Agency (ESA). Sentinel-2 Spectral Response Functions (S2-SRF), Version: 3.0. (Dec. 19, 2017).

Galán-Martín, Á., Vaskan, P., Antón, A., Esteller, L. J., & Guillén-Gosálbez, G. (2017). Multi-objective optimization of rainfed and irrigated agricultural areas considering production and environmental criteria: a case study of wheat production in Spain. Journal of Cleaner Production, 140, 816-830.

Gao, B. C. (1996). NDWI—A normalized difference water index for remote sensing of vegetation liquid water from space. Remote sensing of environment, 58(3), 257-266.

Gitelson, A. A. (2013). Remote estimation of crop fractional vegetation cover: the use of noise equivalent as an indicator of performance of vegetation indices. International journal of remote sensing, 34(17), 6054-6066.

Gleason, D. J., Andales, A. A., Bauder, T. A., & Chávez, J. L. (2013). Performance of atmometers in estimating reference evapotranspiration in a semi-arid environment. Agricultural water management, 130, 27-35.

Gonzalez-Piqueras, J., Calera, A., Gilabert, M. A., Cuesta, A., & De la Cruz Tercero, F. (2004, February). Estimation of crop coefficients by means of optimized vegetation indices for corn. In Remote Sensing for Agriculture, Ecosystems, and Hydrology V (Vol. 5232, pp. 110-118). SPIE.

Huete, A. R. (1988). A soil-adjusted vegetation index (SAVI). Remote sensing of environment, 25(3), 295-309.

Jamieson, P. D., Porter, J. R., & Wilson, D. R. (1991). A test of the computer simulation model ARCWHEAT1 on wheat crops grown in New Zealand. Field crops research, 27(4), 337-350.

Jayasree, G., Lingaiah, D., Reddy, D. R., & Rao, S. N. (2013). Relationship between biophysical parameters and normalized difference vegetation index in maize. Journal of Agrometeorology, 15(2), 120-125.

Jeong, C.H. & Park, J.H (2021). Analysis of Growth Characteristics Using Plant Height and NDVI of Four Waxy Corn Varieties Based on UAV Imagery. Korean J. Remote Sens. 37(4), 733–745.

Johnson, L. F., & Trout, T. J. (2012). Satellite NDVI assisted monitoring of vegetable crop evapotranspiration in California's San Joaquin Valley. Remote Sensing, 4(2), 439-455.

Kamble, B., Irmak, A., Hubbard, K., & Gowda, P. (2013). Irrigation scheduling using remote sensing data assimilation approach. Advances in Remote Sensing, 2(03), 258.

Karthikeyan, L., Chawla, I., & Mishra, A. K. (2020). A review of remote sensing applications in agriculture for food security: Crop growth and yield, irrigation, and crop losses. Journal of Hydrology, 586, 124905.

Khaliq, A., Musci, M. A., & Chiaberge, M. (2018, October). Analyzing relationship between maize height and spectral indices derived from remotely sensed multispectral imagery. In 2018 IEEE Applied imagery pattern recognition workshop (AIPR) (pp. 1-5). IEEE.

Leys, C., Ley, C., Klein, O., Bernard, P., & Licata, L. (2013). Detecting outliers: Do not use standard deviation around the mean, use absolute deviation around the median. Journal of experimental social psychology, 49(4), 764-766.

Liu, J., Pattey, E., & Jégo, G. (2012). Assessment of vegetation indices for regional crop green LAI estimation from Landsat images over multiple growing seasons. Remote Sensing of Environment, 123, 347-358.

Micasense. 2015. MicaSense RedEdge TM 3 Multispectral Camera User Manual: 1–27

Miller, J. (1991). Reaction time analysis with outlier exclusion: Bias varies with sample size. The Quarterly Journal of Experimental Psychology Section A, 43(4), 907-912.

Moran, M. S., Inoue, Y., & Barnes, E. M. (1997). Opportunities and limitations for image-based remote sensing in precision crop management. Remote sensing of Environment, 61(3), 319-346.

Mourad, R., Jaafar, H., Anderson, M., & Gao, F. (2020). Assessment of leaf area index models using harmonized landsat and sentinel-2 surface reflectance data over a semi-arid irrigated landscape. Remote Sensing, 12(19), 3121.

Neale, C. M., Bausch, W. C., & Heermann, D. F. (1990). Development of reflectance-based crop coefficients for corn. Transactions of the ASAE, 32(6), 1891-1900.

Nguy-Robertson, A., Gitelson, A., Peng, Y., Viña, A., Arkebauer, T., & Rundquist, D. (2012). Green leaf area index estimation in maize and soybean: Combining vegetation indices to achieve maximal sensitivity. Agronomy journal, 104(5), 1336-1347.

Planet Team. (2017). Planet Application Program Interface: In Space for Life on Earth. San Francisco, CA. Retrieved from https://api.planet.com

Rondeaux, G., Steven, M., & Baret, F. (1996). Optimization of soil-adjusted vegetation indices. Remote sensing of environment, 55(2), 95-107.

Rouse, J. W., Haas, R. H., Schell, J. A., & Deering, D. W. (1974). Monitoring vegetation systems in the Great Plains with ERTS. NASA Spec. Publ, 351(1), 309.

Saadi, S. (2018). Spatial estimation of actual evapotranspiration and irrigation volumes using water and energy balance models forced by optical remote sensing data (VIS/NIR/TIR) (Doctoral dissertation, Université Paul Sabatier-Toulouse III; Université de Carthage (Tunisie)).

Shanmugapriya, P., Rathika, S., Ramesh, T., & Janaki, P. (2019). Applications of remote sensing in agriculture-A Review. Int. J. Curr. Microbiol. Appl. Sci, 8(01), 2270-2283.

Singh, R. K., & Irmak, A. (2009). Estimation of crop coefficients using satellite remote sensing. Journal of irrigation and drainage engineering, 135(5), 597-608.

Sishodia, R. P., Ray, R. L., & Singh, S. K. (2020). Applications of remote sensing in precision agriculture: A review. Remote sensing, 12(19), 3136.

Skakun, S., Kalecinski, N. I., Brown, M. G., Johnson, D. M., Vermote, E. F., Roger, J. C., & Franch, B. (2021). Assessing within-field corn and soybean yield variability from WorldView-3, Planet, Sentinel-2, and Landsat 8 satellite imagery. Remote Sensing, 13(5), 872.

Thenkabail, P. S., Lyon, J. G., & Huete, A. (2018). Advances in hyperspectral remote sensing of vegetation and agricultural crops. In Fundamentals, Sensor Systems, Spectral Libraries, and Data Mining for Vegetation (pp. 3-37). CRC press.

Trout, T. J., & DeJonge, K. C. (2018). Crop water use and crop coefficients of maize in the great plains. Journal of Irrigation and Drainage Engineering, 144(6), 04018009.

Vanhellemont, Q. (2019). Daily metre-scale mapping of water turbidity using CubeSat imagery. Optics express, 27(20), A1372-A1399.

Viña, A., Gitelson, A. A., Nguy-Robertson, A. L., & Peng, Y. (2011). Comparison of different vegetation indices for the remote assessment of green leaf area index of crops. Remote sensing of environment, 115(12), 3468-3478.

Wardlow, B. D., Egbert, S. L., & Kastens, J. H. (2007). Analysis of time-series MODIS 250 m vegetation index data for crop classification in the US Central Great Plains. Remote sensing of environment, 108(3), 290-310.

Xue, J., & Su, B. (2017). Significant remote sensing vegetation indices: A review of developments and applications. Journal of sensors, 2017.

Yang, Y., Long, D., Guan, H., Liang, W., Simmons, C., & Batelaan, O. (2015). Comparison of three dual-source remote sensing evapotranspiration models during the MUSOEXE-12 campaign: Revisit of model physics. Water resources research, 51(5), 3145-3165.

Zhu, Z., & Woodcock, C. E. (2014). Continuous change detection and classification of land cover using all available Landsat data. Remote sensing of Environment, 144, 152-171.

APPENDICES

Appendix A: Leaf Area Index Error Analysis Tables

Table A 1: Error analysis for UAS-based LAI estimation models

Reference	VI Based	MBE (m^2/m^2)	MBE%	RMSE (m^2/m^2)	RMSE %	Performance	n
Mourad et al. (2022)	NDVI	0.29	8.50	0.67	19.60	Good	123
Jayasree et al. (2013)	NDVI	-0.39	-11.31	0.68	19.91	Good	128
Nguy-Robertson et al. (2012)	NDVI	-0.15	-4.49	0.77	22.45	Fair	122
	SAVI	0.36	10.56	0.93	27.09	Fair	121
Vina et al. (2011)	NDVI	-0.53	-15.39	0.89	26.14	Fair	125
Liu et al. (2012)	NDVI	-1.03	-30.17	1.16	33.69	Poor	126
	OSAVI	-0.56	-16.29	0.88	25.63	Fair	125
Yang et al. (2015)	NDVI	0.87	25.29	1.02	29.61	Fair	124
Bastiaanssen (1998)	SAVI	-0.63	-18.46	1.09	31.80	Poor	121
Chavez et al. (2009)	OSAVI	0.20	5.86	0.71	20.66	Fair	113
Anderson et al. (2004)	OSAVI	-0.55	-16.05	1.11	32.25	Poor	124

Table A 2: Error analysis for Planet-based LAI estimation models

Reference	VI Based	MBE (m^2/m^2)	MBE%	RMSE (m^2/m^2)	RMSE %	Performance	n
Mourad et al. (2022)	NDVI	0.01	0.17	0.67	19.29	Good	501
Jayasree et al. (2013)	NDVI	-0.62	-17.72	0.87	25.11	Fair	485
Nguy-Robertson et al. (2012)	NDVI	-0.49	-14.09	0.84	24.04	Fair	481
	SAVI	-0.05	-1.47	0.68	19.65	Good	492
Vina et al. (2011)	NDVI	-0.95	-27.17	1.17	33.71	Poor	498
Liu et al. (2012)	NDVI	-1.28	-36.86	1.43	41.01	Poor	489
	OSAVI	-1.02	-29.44	1.20	34.58	Poor	499
Yang et al. (2015)	NDVI	0.72	20.58	0.98	28.23	Fair	503
Bastiaanssen (1998)	SAVI	-0.44	-13.89	1.01	32.02	Poor	297
Chavez et al. (2009)	OSAVI	-0.12	-3.46	0.68	19.46	Good	494
Anderson et al. (2004)	OSAVI	-1.16	-33.45	1.35	38.86	Poor	494

Table A 3: Error analysis for Landsat-based LAI estimation models

Reference	VI Based	MBE (m^2/m^2)	MBE%	RMSE (m^2/m^2)	RMSE %	Performance	n
Mourad et al. (2022)	NDVI	-0.10	-2.87	0.72	20.78	Fair	439
Jayasree et al. (2013)	NDVI	-0.71	-20.47	0.99	28.50	Fair	428
Nguy-Robertson et al. (2012)	NDVI	-0.59	-16.96	0.94	26.89	Fair	418
	SAVI	-0.26	-7.63	0.70	20.05	Fair	422
Vina et al. (2011)	NDVI	-1.02	-29.32	1.24	35.69	Poor	424
Liu et al. (2012)	NDVI	-1.34	-38.46	1.49	42.68	Poor	419
	OSAVI	-1.19	-34.05	1.33	38.18	Poor	428
Yang et al. (2015)	NDVI	0.60	17.25	0.92	26.49	Fair	428
Bastiaanssen (1998)	SAVI	-0.57	-17.10	1.12	33.79	Poor	306
Chavez et al. (2009)	OSAVI	-0.29	-8.20	0.75	21.45	Fair	413
Anderson et al. (2004)	NDWI	0.84	24.26	0.97	27.80	Fair	413
	OSAVI	-1.25	-36.03	1.46	41.99	Poor	417

Table A 4: Error analysis for Sentinel2-based LAI estimation models

Reference	VI Based	MBE (m^2/m^2)	MBE%	RMSE (m^2/m^2)	RMSE %	Performance	n
Mourad et al. (2022)	NDVI	0.12	3.46	0.65	18.58	Good	712
Jayasree et al. (2013)	NDVI	-1.54	-43.80	1.62	45.97	Poor	694
Nguy-Robertson et al. (2012)	NDVI	-0.34	-9.60	0.77	22.02	Fair	682
	SAVI	-0.21	-6.01	0.59	16.97	Good	709
Vina et al. (2011)	NDVI	-0.79	-22.43	1.05	29.73	Fair	706
Liu et al. (2012)	NDVI	-1.22	-34.73	1.35	38.37	Poor	716
	OSAVI	-1.10	-31.35	1.21	34.52	Poor	710
Yang et al. (2015)	NDVI	0.74	21.05	0.95	26.97	Fair	703
Bastiaanssen (1998)	SAVI	-0.66	-20.85	1.02	32.28	Poor	470
Chavez et al. (2009)	OSAVI	-0.23	-6.50	0.62	17.61	Good	707
Anderson et al. (2004)	OSAVI	-1.21	-34.38	1.34	37.98	Poor	692

Table A 5: Error analysis for MSR5-based LAI estimation models

Reference	VI Based	MBE (m^2/m^2)	MBE %	RMSE (m^2/m^2)	RMSE %	Performance	n
Mourad et al. (2022)	NDVI	0.23	7.15	0.74	22.83	Fair	211
Jayasree et al. (2013)	NDVI	-0.50	-15.42	0.80	24.81	Fair	206
Nguy-Robertson et al. (2012)	NDVI	-0.31	-9.61	0.85	26.18	Fair	205
	SAVI	-0.01	-0.34	0.85	26.19	Fair	201
Vina et al. (2011)	NDVI	-0.70	-21.65	0.97	29.77	Fair	200
Liu et al. (2012)	NDVI	-1.12	-34.51	1.25	38.64	Poor	207
	OSAVI	-0.83	-25.75	1.08	33.29	Poor	209
Yang et al. (2015)	NDVI	0.69	21.30	0.96	29.54	Fair	198
Bastiaanssen (1998)	SAVI	-0.74	-23.26	1.16	41.73	Poor	85
Chavez et al. (2009)	OSAVI	-0.06	-1.92	0.80	24.58	Fair	203
Anderson et al. (2004)	NDWI	-0.12	-3.62	0.62	19.16	Good	211
	OSAVI	-0.90	-27.73	1.20	36.96	Poor	205

Appendix B: Crop Height Error Analysis Tables

Table B 1: Error analysis for UAS-based Hc estimation models

Reference	Model-Based	MBE (m)	MBE %	RMSE (m)	RMSE %	Performance	n
Arslan et al. (2022)	LAI	1.00	68.81	1.03	70.86	Poor	85
Arslan et al. (2022)	NDVI	0.67	43.56	0.68	44.21	Poor	120
Jeong and Park (2021)	NDVI	0.39	25.57	0.41	26.54	Fair	119
Yang et al. (2015)	NDVI	0.76	49.63	0.80	52.50	Poor	128
Costa-Filho et al. (2021)	LAI	0.02	1.65	0.17	11.43	Good	99
Anderson et al. (2004)	OSAVI	-0.16	-10.31	0.32	21.16	Fair	126
Khaliq et al. (2018)	NDVI	0.78	50.93	0.85	55.63	Poor	120

Table B 2: Error analysis for Planet-based Hc estimation models

Reference	Model-Based	MBE (m)	MBE%	RMSE (m)	RMSE %	Performance	n
Arslan et al. (2022)	LAI	1.13	73.21	1.18	76.42	Poor	319
Arslan et al. (2022)	NDVI	0.71	49.50	0.74	51.24	Poor	438
Jeong and Park (2021)	NDVI	0.44	30.46	0.48	33.07	Poor	435
Yang et al. (2015)	NDVI	0.75	51.86	0.79	54.70	Poor	425
Costa-Filho et al. (2021)	LAI	0.06	4.05	0.19	12.12	Good	324
Anderson et al. (2004)	OSAVI	-0.29	-19.93	0.33	22.90	Fair	420
Khaliq et al. (2018)	NDVI	0.97	66.83	1.01	69.70	Poor	405

Table B 3: Error analysis for Landsat-based Hc estimation models

Reference	Model-Based	MBE (m)	MBE%	RMSE (m)	RMSE %	Performance	n
Arslan et al. (2022)	LAI	1.11	74.62	1.16	78.21	Poor	272
Arslan et al. (2022)	NDVI	0.71	46.73	0.75	49.72	Poor	352
Jeong and Park (2021)	NDVI	0.43	28.61	0.50	33.21	Poor	352
Yang et al. (2015)	NDVI	0.71	47.25	0.75	49.39	Poor	352
Costa-Filho et al. (2021)	LAI	0.05	3.07	0.18	12.04	Good	272
Anderson et al. (2004)	OSAVI	-0.25	-16.36	0.40	26.34	Fair	334
Anderson et al. (2004)	NDWI	0.27	18.04	0.30	19.96	Fair	346
Khaliq et al. (2018)	NDVI	0.96	63.48	0.99	65.22	Poor	352

Table B 4: Error analysis for Sentinel2-based Hc estimation models

Reference	Model-Based	MBE (m)	MBE%	RMSE (m)	RMSE %	Performance	n
Arslan et al. (2022)	LAI	1.12	72.65	1.17	76.03	Poor	327
Arslan et al. (2022)	NDVI	0.69	46.45	0.71	48.14	Poor	440
Jeong and Park (2021)	NDVI	0.41	28.02	0.45	30.69	Poor	440
Yang et al. (2015)	NDVI	0.73	49.62	0.77	52.41	Poor	440
Costa-Filho et al. (2021)	LAI	0.04	2.49	0.16	10.61	Good	327
Anderson et al. (2004)	OSAVI	-0.32	-21.88	0.36	24.55	Fair	423
Khaliq et al. (2018)	NDVI	0.97	65.61	1.01	68.45	Poor	440

Table B 5: Error analysis for MSR5-based Hc estimation models

Reference	Model-Based	MBE (m)	MBE %	RMSE (m)	RMSE %	Performance	n
Arslan et al. (2022)	LAI	0.84	56.65	0.96	64.74	Poor	220
Arslan et al. (2022)	NDVI	0.60	41.09	0.66	44.77	Poor	220
Jeong and Park (2021)	NDVI	0.34	22.81	0.42	28.47	Fair	220
Yang et al. (2015)	NDVI	0.62	42.40	0.76	51.58	Poor	220
Costa-Filho et al. (2021)	LAI	-0.05	-3.31	0.20	13.62	Good	220
Anderson et al. (2004)	OSAVI	-0.32	-21.68	0.41	28.09	Fair	211
Anderson et al. (2004)	NDWI	-0.18	-11.98	0.25	17.27	Good	220
Khaliq et al. (2018)	NDVI	0.83	56.72	0.97	65.80	Poor	220

Appendix C: Crop Fractional Cover Error Analysis Tables

Table C 1: Error analysis for UAS-based Fc estimation models

Reference	MBE (%)	MBE%	RMSE (%)	RMSE%	Performance	n
Gitelson (2013)	0.01	1.28	0.10	14.78	Good	132
Yang et al. (2015)	0.12	18.91	0.16	24.63	Fair	127
Johnson and Trout (2012)	0.12	18.75	0.16	22.09	Fair	124

Table C 2: Error analysis for Planet-based Fc estimation models

Reference	MBE (%)	MBE%	RMSE (%)	RMSE%	Performance	n
Gitelson (2013)	-0.02	-3.74	0.10	16.23	Good	438
Yang et al. (2015)	0.14	22.49	0.19	29.40	Fair	428
Johnson and Trout (2012)	0.13	19.80	0.17	25.50	Fair	419

Table C 3: Error analysis for Landsat-based Fc estimation models

Reference	MBE (%)	MBE%	RMSE (%)	RMSE%	Performance	n
Gitelson (2013)	-0.04	-7.45	0.12	19.36	Good	436
Yang et al. (2015)	0.13	22.02	0.17	28.99	Fair	436
Johnson and Trout (2012)	0.12	19.47	0.16	25.93	Fair	424

Table C 4: Error analysis for Sentinel2-based Fc estimation models

Reference	MBE (%)	MBE%	RMSE (%)	RMSE%	Performance	n
Gitelson (2013)	-0.04	-6.68	0.10	15.63	Good	475
Yang et al. (2015)	0.11	17.21	0.16	24.41	Fair	466
Johnson and Trout (2012)	0.10	15.61	0.14	21.76	Fair	468

Table C 5: Error analysis for MSR5-based Fc estimation models

Reference	MBE (%)	MBE%	RMSE (%)	RMSE%	Performance	n
Gitelson (2013)	-0.03	-4.26	0.13	20.21	Fair	210
Yang et al. (2015)	0.08	13.34	0.14	22.42	Fair	208
Johnson and Trout (2012)	0.08	13.10	0.14	21.30	Fair	209

Appendix D: Actual Evapotranspiration Error Analysis Tables

Table D 1: Error analysis for UAS-based ETa estimation models

Reference	Function-based	MBE (mm)	MBE%	RMSE (mm)	RMSE %	n
Trout and DeJonge (2018)	Fc	-0.16	-2.31	0.83	11.58	66
Neale et al. (1989)	NDVI	-0.37	-5.30	1.32	19.04	88
Bausch (1993)	SAVI	-0.13	-1.94	1.17	17.70	68
González-Piqueras et al. (2004)	NDVI	-0.35	-5.01	0.91	12.71	66
Singh and Irmak (2009)	NDVI	0.06	0.82	0.84	11.74	66

Table D 2: Error analysis for Planet-based ETa estimation models

Reference	Function-based	MBE (mm)	MBE%	RMSE (mm)	RMSE %	n
Trout and DeJonge (2018)	Fc	0.44	6.47	1.10	16.18	283
Neale et al. (1989)	NDVI	-0.40	-5.90	1.16	17.10	307
Bausch (1993)	SAVI	-0.79	-11.73	1.29	19.23	296
González-Piqueras et al. (2004)	NDVI	0.24	3.50	1.16	17.08	308
Singh and Irmak (2009)	NDVI	0.56	8.21	1.25	18.37	300

Table D 3: Error analysis for Landsat-based ETa estimation models

Reference	Function-based	MBE (mm)	MBE%	RMSE (mm)	RMSE %	n
Trout and DeJonge (2018)	Fc	0.56	8.75	0.95	14.90	299
Neale et al. (1989)	NDVI	-0.38	-5.95	0.89	13.86	308
Bausch (1993)	SAVI	-0.85	-13.45	1.14	17.88	303
González-Piqueras et al. (2004)	NDVI	0.24	3.81	0.84	13.16	308
Singh and Irmak (2009)	NDVI	0.60	9.43	1.00	15.62	302

Table D 4: Error analysis for Sentinel2-based ETa estimation models

Reference	Function-based	MBE (mm)	MBE%	RMSE (mm)	RMSE %	n
Trout and DeJonge (2018)	Fc	0.51	7.62	1.00	14.86	484
Neale et al. (1989)	NDVI	-0.42	-6.21	0.94	14.03	484
Bausch (1993)	SAVI	-1.14	-17.03	1.41	21.13	482
González-Piqueras et al. (2004)	NDVI	0.23	3.39	0.89	13.31	484
Singh and Irmak (2009)	NDVI	0.64	9.54	1.09	16.32	484

Table D 5: Error analysis for MSR-based ETa estimation models

Reference	Function-based	MBE (mm)	MBE%	RMSE (mm)	RMSE %	n
Trout and DeJonge (2018)	Fc	-0.12	-1.61	0.85	11.66	132
Neale et al. (1989)	NDVI	-0.49	-6.96	1.04	14.56	130
Bausch (1993)	SAVI	-0.85	-11.94	1.26	17.77	126
González-Piqueras et al. (2004)	NDVI	-0.14	-1.93	1.02	14.22	148
Singh and Irmak (2009)	NDVI	0.05	0.63	0.91	12.40	133